

2

AD-A196 962

NAVAL POSTGRADUATE SCHOOL Monterey, California

DTIC FILE COPY



S DTIC
ELECTE
AUG 16 1988
CD
D

THESIS

THE CLIMATOLOGICAL SEASONAL RESPONSE
OF THE OCEAN MIXED LAYER IN THE
EQUATORIAL
AND TROPICAL PACIFIC OCEAN

by
Harry J. Ries, Jr.

March 1988

Thesis Advisor Roland W. Garwood, Jr.

Approved for public release; distribution is unlimited.

UNCLAS

SECURITY CLASSIFICATION OF THIS PAGE

REPORT DOCUMENTATION PAGE

1a. REPORT SECURITY CLASSIFICATION UNCLAS		1b. RESTRICTIVE MARKINGS	
2a. SECURITY CLASSIFICATION AUTHORITY		3. DISTRIBUTION/AVAILABILITY OF REPORT Approved for public release; distribution is unlimited.	
2b. DECLASSIFICATION/DOWNGRADING SCHEDULE		5. MONITORING ORGANIZATION REPORT NUMBER(S)	
4. PERFORMING ORGANIZATION REPORT NUMBER(S)		6a. NAME OF PERFORMING ORGANIZATION Department of Oceanography Naval Postgraduate School	
6a. NAME OF PERFORMING ORGANIZATION		6b. OFFICE SYMBOL (If applicable) Code 68	7a. NAME OF MONITORING ORGANIZATION Naval Postgraduate School
6c. ADDRESS (City, State, and ZIP Code) Monterey, CA 93943		7b. ADDRESS (City, State, and ZIP Code) Monterey, CA 93943	
8a. NAME OF FUNDING/SPONSORING ORGANIZATION		8b. OFFICE SYMBOL (If applicable)	9. PROCUREMENT INSTRUMENT IDENTIFICATION NUMBER
8c. ADDRESS (City, State, and ZIP Code)		10. SOURCE OF FUNDING NUMBERS	
		PROGRAM ELEMENT NO.	PROJECT NO.
		TASK NO.	WORK UNIT ACCESSION NO.
11. TITLE (Include Security Classification) THE CLIMATOLOGICAL SEASONAL RESPONSE OF THE OCEAN MIXED LAYER IN THE EQUATORIAL AND TROPICAL PACIFIC OCEAN			
12. PERSONAL AUTHOR(S) Ries, Harry J.			
13a. TYPE OF REPORT Master's Thesis	13b. TIME COVERED FROM TO	14. DATE OF REPORT (Year, Month, Day) 1988 March	15. PAGE COUNT 97
16. SUPPLEMENTARY NOTATION			
17. COSATI CODES		18. SUBJECT TERMS (Continue on reverse if necessary and identify by block number)	
FIELD	GROUP	SUB-GROUP	
		Ocean Mixed Layer	
		Equatorial and Tropical Pacific Ocean	
19. ABSTRACT (Continue on reverse if necessary and identify by block number) The seasonal changes of mixed layer depth (MLD) can be related to the forcing by the net surface heating and wind speed. This is shown in this study by comparing the monthly mixed layer depth from temperature profiles in the Bauer-Robinson Numerical Atlas with monthly net surface heating and wind speed obtained from the Weare Marine Climatic Atlas of the Tropical Pacific Ocean. Using a conceptual model based on mixed layer physics, ocean response and atmospheric forcing are examined using the Obukhov mixing length. A pattern in the seasonal variation of upwelling along the Equator is also examined. The model links the atmospheric and oceanic climatologies through the derived MLD (oceanic data) and Obukhov mixing lengths (forcing data). The results show a high degree of pattern similarity between the seasonal response of the ocean and the seasonal changes in atmospheric forcing. The pattern of			
20. DISTRIBUTION/AVAILABILITY OF ABSTRACT <input checked="" type="checkbox"/> UNCLASSIFIED/UNLIMITED <input type="checkbox"/> SAME AS RPT <input type="checkbox"/> DTIC USERS		21. ABSTRACT SECURITY CLASSIFICATION UNCLAS	
22a. NAME OF RESPONSIBLE INDIVIDUAL R. W. Garwood, Code 68Cd		22b. TELEPHONE (Include Area Code) 408-646-3260	22c. OFFICE SYMBOL 68Cd

DD FORM 1473, 84 MAR

83 APR edition may be used until exhausted.

All other editions are obsolete

SECURITY CLASSIFICATION OF THIS PAGE

U.S. Government Printing Office: 1986-606-24.

19. Continued:

seasonal influence on MLD at the Equator is very weak in comparison to that of the tropics and sub-tropics.

Handwritten notes:
The seasonal influence on MLD at the Equator is very weak in comparison to that of the tropics and sub-tropics.
(This is due to the fact that the seasonal variation in solar radiation is very small at the Equator.)

+

Approved for public release; distribution is unlimited.

The Climatological Seasonal Response
of the Ocean Mixed Layer in the Equatorial
and Tropical Pacific Ocean

by

Harry J. Ries, Jr.
Lieutenant, United States Navy
B.A., Pennsylvania State University
University Park, Pennsylvania, 1979

Submitted in partial fulfillment of the
requirements for the degree of

MASTER OF SCIENCE IN METEOROLOGY AND OCEANOGRAPHY

from the

NAVAL POSTGRADUATE SCHOOL
March 1988

Author:

Harry J. Ries, Jr.

Harry J. Ries, Jr.

Approved by:

Roland W. Garwood, Jr.

Roland W. Garwood, Jr., Thesis Advisor

Mary L. Batteen

Mary L. Batteen, Second Reader

Curtis A. Collins

Curtis A. Collins, Chairman,
Department of Oceanography

Gordon E. Schacher

Gordon E. Schacher,
Dean of Science and Engineering

TABLE OF CONTENTS

I.	INTRODUCTION	10
II.	CLIMATOLOGICAL DATA AND MIXED LAYER DYNAMICS	11
A.	THE CLIMATOLOGICAL DATA SOURCES	11
1.	The Bauer-Robinson Numerical Atlas	11
2.	The Weare Marine Climatic Atlas	12
B.	METHODS OF DETERMINING MIXED LAYER DEPTH	16
C.	A ONE-DIMENSIONAL MODEL OF THE MIXED LAYER	17
1.	The Temperature Equation	18
2.	The Structure Equation	20
3.	The Equilibrium Solution	22
4.	The Equilibrium Solution in the Presence of Vertical Advection	22
D.	SUMMARY OF EQUATIONS IN THE CONCEPTUAL MODEL	23
III.	RESULTS: SEASONALLY CHANGING CLIMATOLOGICAL ASPECTS OF MIXED LAYER DEPTH	24
A.	LARGE AREA CONTOURS OF MIXED LAYER DEPTH	24
1.	The Slope of the Equatorial Thermocline	24
2.	Seasonal Changes of Mixed Layer Depth Contours in the Eastern Pacific Ocean	26
B.	SMALL AREA ANALYSIS OF ATMOSPHERIC FORCING AND MIXED	30
1.	Atmospheric Forcing	30
2.	The Oceanic Response	35
C.	THE FLUCTUATION FIELDS	41
1.	The Derivation of Fluctuating Quantities	41

2. Statistical Analysis	42
D. THE VERTICAL INTEGRAL OF TEMPERATURE WITHIN THE SURFACE LAYER	51
E. THE OBUKHOV MIXING LENGTH	51
IV. CONCLUSIONS	60
APPENDIX A: MERIDIONAL SECTIONS OF TEMPERATURE	62
APPENDIX B: MONTHLY MLD CONTOURS	70
APPENDIX C: ENHANCEMENT OF DEEPENING AND SHALLOWING OF MLD	83
APPENDIX D: MODIFIED MIXING SCALE	87
LIST OF REFERENCES	91
INITIAL DISTRIBUTION LIST	93

LIST OF FIGURES

2.1	Numbers of Temperature Profiles for the North Pacific Ocean from the Robinson Atlas (1976)	13
2.2	Zonal Sections of Temperature ($^{\circ}\text{C}$) at 1°N for (a) February and (b) August	14
2.3	Density of Atmospheric Data from Weare, et. al.(1980)	15
2.4	A Conceptual Model of the Ocean Mixed Layer	18
3.1	Yearly Average Mixed Layer Depth Contour Interval is 15 meters	25
3.2	Maximum and Minimum Westward Extent of the 30m MLD Contour	27
3.3	Annual Cycle of North-South Movement of 30m MLD Contour	28
3.4	Annual Cycle of Movement of 30m MLD Contour	29
3.5	Meridians Cross-secting the Area of Study	31
3.6	Net Surface Heating for the Area of Study	32
3.7	Net Surface Heating at 155°E Contour Interval is $30\text{ W}\cdot\text{m}^2$	36
3.8	Wind Speed at 155°E Contour Interval is $0.5\text{ m}\cdot\text{s}$	37
3.9	Pattern of Seasonal Influence	38
3.10	Mixed Layer Depth at 155°E Contour Interval is 15 m	39
3.11	Time Rate of Change of Mixed Layer Depth at 155°E Contour Interval is $10\text{m}\cdot\text{month}$	40
3.12	Fluctuation in Wind Speed at 155°E Contour Interval is $0.5\text{m}\cdot\text{s}$	43
3.13	Fluctuation in Net Surface Heating at 155°E Contour Interval is $20\text{ W}\cdot\text{m}^2$	44
3.14	Fluctuation in Mixed Layer Depth at 155°E Contour Interval is 10m	45
3.15	A Seasonal Pattern of (a) Wind Speed and (b) Net Surface Heating in the Equatorial Pacific Ocean	46
3.16	A Seasonal Pattern of (a) Mixed Layer Depth and the (b) Time Rate of Mixed Layer Depth	47
3.17	Correlation Coefficients vs. Latitude along 155°E (a) Net Surface Heating and (b) Wind Speed with MLD	48

3.18	Correlation Coefficients vs. Latitude along 155°W (a) Net Surface Heating and (b) Wind Speed with MLD	49
3.19	Correlation Coefficients vs. Latitude along 105°W (a) Net Surface Heating and (b) Wind Speed with MLD	50
3.20	Time Rate of Change of Heat in the Water Column at 155 °E Contour Interval is 35W m ²	52
3.21	Difference of Net Surface Heating and Heat in the Water Column at 155 °E Contour Interval is 35 W m ²	53
3.22	Obukhov Mixing Length at 155 °E Contour Interval is 15m	55
3.23	Ratio of Mixed Layer Depth and Obukhov Mixing Length at 155 °E	56
3.24	Ratio of Mixed Layer Depth and Obukhov Mixing Length at 155 °W	57
3.25	Ratio of Mixed Layer Depth and Obukhov Mixing Length at 105 °W	58
3.26	Ratio of Mixed Layer Depth and Obukhov Mixing Length at the Equator	59
A.1	Meridional Sections of Temperature (°C) at 90 °W for (a) February and (b) August	63
A.2	Meridional Sections of Temperature (°C) at 100 °W for (a) February and (b) August	64
A.3	Meridional Sections of Temperature (°C) at 120 °W for (a) February and (b) August	65
A.4	Meridional Sections of Temperature (°C) at 140 °W for (a) February and (b) August	66
A.5	Meridional Sections of Temperature (°C) at 170 °W for (a) February and (b) August	67
A.6	Meridional Sections of Temperature (°C) at 170 °E for (a) February and (b) August	68
A.7	Meridional Sections of Temperature (°C) at 140 °E for (a) February and (b) August	69
B.1	January Mixed Layer Depth	71
B.2	February Mixed Layer Depth	72
B.3	March Mixed Layer Depth	73
B.4	April Mixed Layer Depth	74
B.5	May Mixed Layer Depth	75
B.6	June Mixed Layer Depth	76

B.7	July Mixed Layer Depth	77
B.8	August Mixed Layer Depth	78
B.9	September Mixed Layer Depth	79
B.10	October Mixed Layer Depth	80
B.11	November Mixed Layer Depth	81
B.12	December Mixed Layer Depth	82
C.1	(a) Areas of Upwelling and Downwelling and Lines of Zero Surface Heat Flux (b) and Enhanced Deepening and Shallowing at 155°E	84
C.2	Same as Fig. C.1 but at 155°W.....	85
C.3	Same as Fig. C.1 but at 105°W.....	86
D.1	Modified Mixing Scale at 155 °E	89
D.2	Ratio of Mixed Layer Depth and Modified Mixing Scale at the Equator	90

I. INTRODUCTION

Numerical modeling of the oceanic planetary boundary layer (OPBL) has been advancing steadily since the pioneering work of Kraus and Turner (1967). All numerical models must be able to accurately reproduce the mean state of the phenomenon under study to give the predicted variations geophysical relevance. An understanding of the actual mean state of a fully turbulent OPBL (for a given geographical region and time scale) is quite often gained from the many climatic atlases and environmental data sets available to the researcher. The resolution, density, and quality of these atlases and data sets are highly variant from one region of the world's oceans to another and from one time scale to another.

This study focuses on the mean seasonal response of the OPBL in the equatorial and tropical Pacific Ocean on a seasonal time scale. The study has been carried out to provide the numerical modeler with a more definite depiction of the mean state and seasonal variations of the OPBL in the equatorial and tropical Pacific Ocean.

Several climatic information sources have been examined and evaluated for their suitability for integration into this study. The Bauer-Robinson Numerical Atlas (containing oceanic data) and the Weare Marine Climatic Atlas (containing atmospheric data) were both available in a digitized format on microcomputer hard-disk storage. All of the computationally derived data were produced and processed by microcomputer.

A one dimensional conceptual model is utilized to relate the seasonal variations of atmospheric forcing on the OPBL to the variations of the ocean boundary layer. These seasonal variations are related using the Obukhov length scale (a modeling approach) and statistically based correlation coefficients.

The thesis is organized as follows. First, the sources of climatological ocean and atmospheric forcing data are reviewed, in light of the understanding of mixed layer dynamics and how mixed layer physics should influence determination of climatological or average values of mixed layer depth. Next, climatological ocean data are analyzed to determine the climatological mixed layer depth in the tropical Pacific Ocean. Finally, seasonal changes in atmospheric forcing are related to the seasonal changes in the of mixed layer depth.

II. CLIMATOLOGICAL DATA AND MIXED LAYER DYNAMICS

A. THE CLIMATOLOGICAL DATA SOURCES

1. The Bauer-Robinson Numerical Atlas

The Bauer-Robinson Numerical Atlas provides monthly temperature profiles from the ocean surface down to a typical depth of 150 meters at 30 meter intervals. These monthly temperature profiles represent an average profile for a one degree (of latitude by longitude) quadrangle. Coverage of the atlas includes all of the world ocean basins except the Arctic Ocean. A secondary set of data contains the annual mean temperature and salinity at 30 meter intervals from the ocean surface to the bottom (or to a 7000 meter depth). Data for the Pacific Ocean portion of the atlas, the geographical area germane to this thesis, have two categorical differences. Data for the North Pacific portion was derived from hand digitized mechanical bathythermograph (MBT) files, prior to 1967. At the present time, the MBT files are a part of the Master Oceanographic Observation Data Set (MOODS) maintained at the Fleet Numerical Oceanography Center. Data for the Southern Pacific portion were compiled up to 1981, and were utilized in assembling the atlas.

Each of the individual observations was interpolated to the 30 meter interval levels. Then, a mean profile was computed for each of the one degree quadrangle for each month and level. For the Northern Pacific data, it was necessary to use a slightly different technique. Mechanical bathythermograph data have good relative accuracy, but limited absolute accuracy. A system of an average difference mean was employed, whereby the mean at the surface was used as a starting point. Then, average temperature differences in each interval were successively added to this starting point. By this method, false-positive temperature gradients were not produced. The density of observations contributing to the mean of a particular one degree quadrangle could vary by as much as two orders of magnitude. This variation of the density of observations is largely contiguous for particular regions within the equatorial and tropical areas of study (as charted in Bauer and Robinson 1976).

The data densities for the North Pacific Ocean are displayed in Fig. 2.1. The data density is lowest along the Equator and increases significantly in subtropical latitudes. It is clear that high data densities occur along the major shipping routes.

For detailed analysis, three meridians were selected: 155E, 155W, and 105W. The data density along these meridians is highly variant. This variation will be considered later in the results section.

Zonal sections of temperature in the surface layer at 1°N are presented in Fig. 2.2. Of particular note is the westward deepening of the thermocline between 110W and 150W. This westward deepening is steeper in August than in February. The pool of water warmer than 28°C in the western Pacific is greater in August as is the volume of water cooler than 14°C and above 150m in the Eastern Pacific. Selected meridional cross-sections are presented and discussed in Appendix A.

2. The Weare Marine Climatic Atlas

The atmospheric forcing data (e.g. wind speed, zonal wind stress, and the components for net surface heating) were obtained from the numerical version of the Marine Climate Atlas of the Tropical Pacific Ocean, by Weare, *et. al.* (1980). The area covered by this atlas is the same as the area of study for this thesis (i.e. 40S to 30N and from 110E to 75W). All of the atmospheric data was obtained either directly or indirectly, using bulk formula, and derived from five million individual marine weather reports for the years 1957 to 1976. Data from this 240 month period are condensed into an average climatic year. The data is resolved on five degree quadrangles. Long term monthly means, and standard deviations for variables such as wind speed were calculated and examined for gross errors. Bulk formulas, which are discussed in detail in Weare *et. al.* (1980), were applied to each report to obtain the flux quantities which were then averaged and evaluated. A detailed error analysis is presented in a companion paper, Weare (1981), for the principal flux quantities utilized in this thesis, namely latent and sensible heat flux, and solar and infrared back radiation.

The density of observations varies considerably in space and time (Fig. 2.3). The data density is lowest south of the equator and east of the date line, between 80W and 140W in the eastern Pacific Ocean and below 20S. Several quadrangles off the coast of eastern Australia have as many as 3000 total observations, while half of the 240 months have no recorded observations. The effect of these variations, must be considered in evaluating the analysis. A large region along the Equator (from 160E to 125W) has only 50 (out of a total of 240) months with ten or more observations, whereas the subtropical regions have four times as many months with ten or more observations.

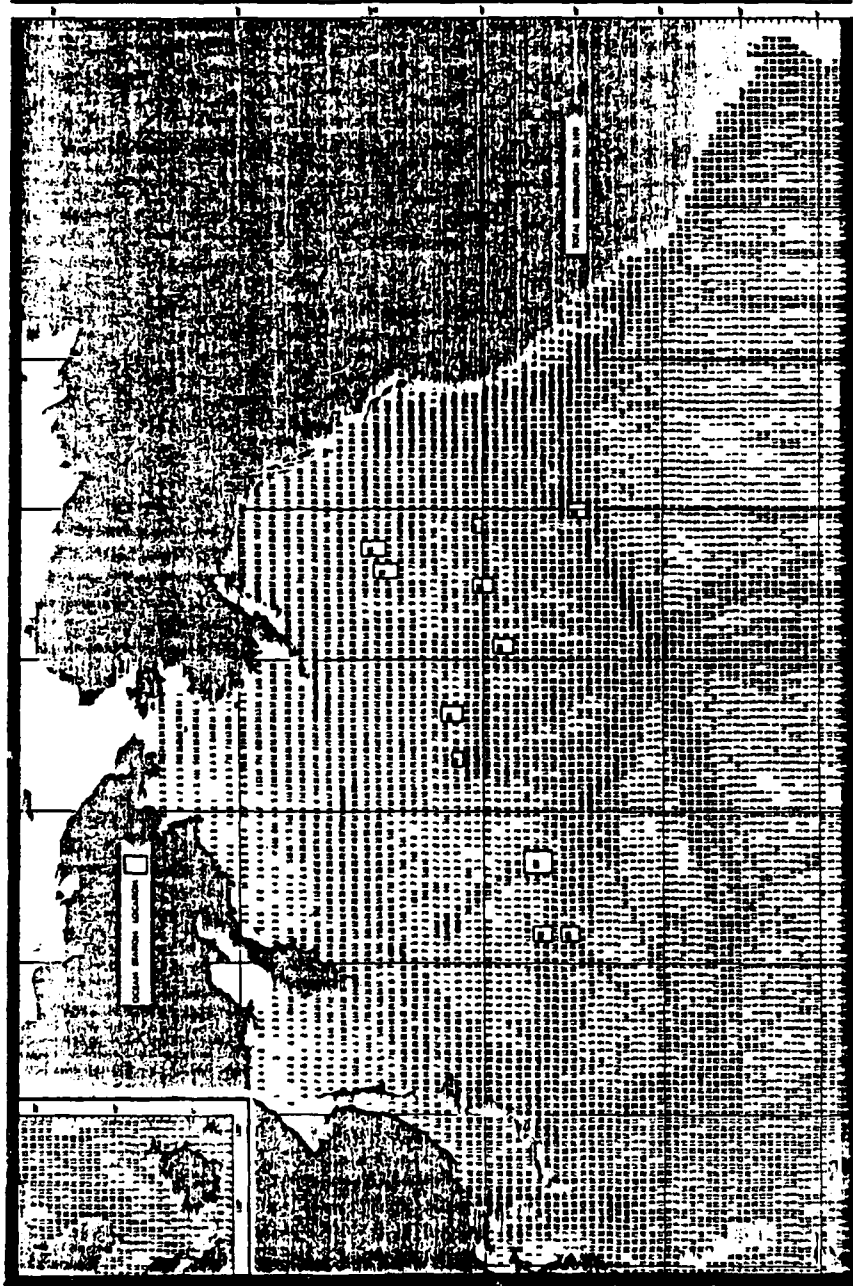


Fig. 2.1 Numbers of Temperature Profiles for the North Pacific Ocean from the Robinson Atlas (1976).

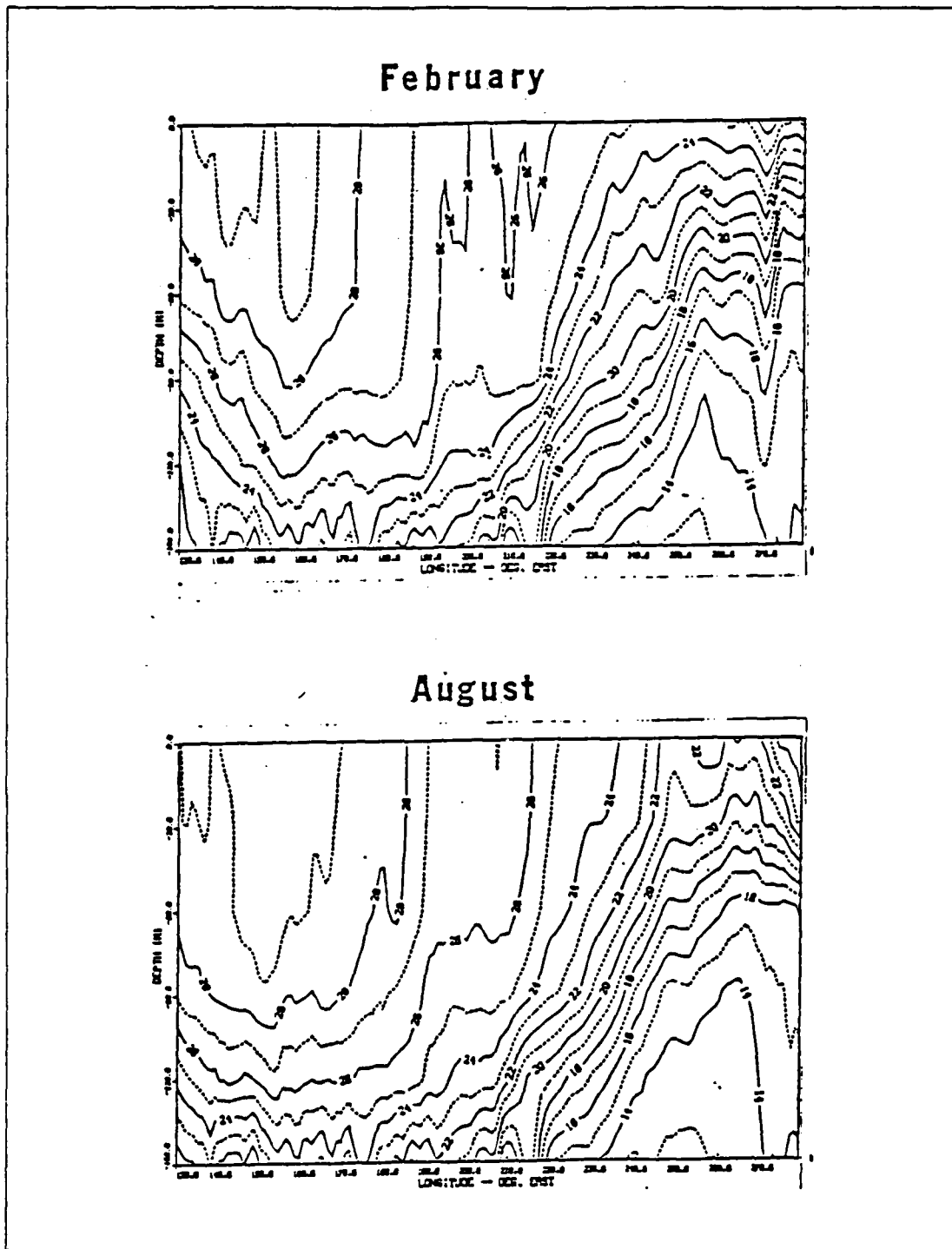


Fig. 2.2 Zonal Sections of Temperature ($^{\circ}\text{C}$)
at 1°N for (a) February and (b) August.

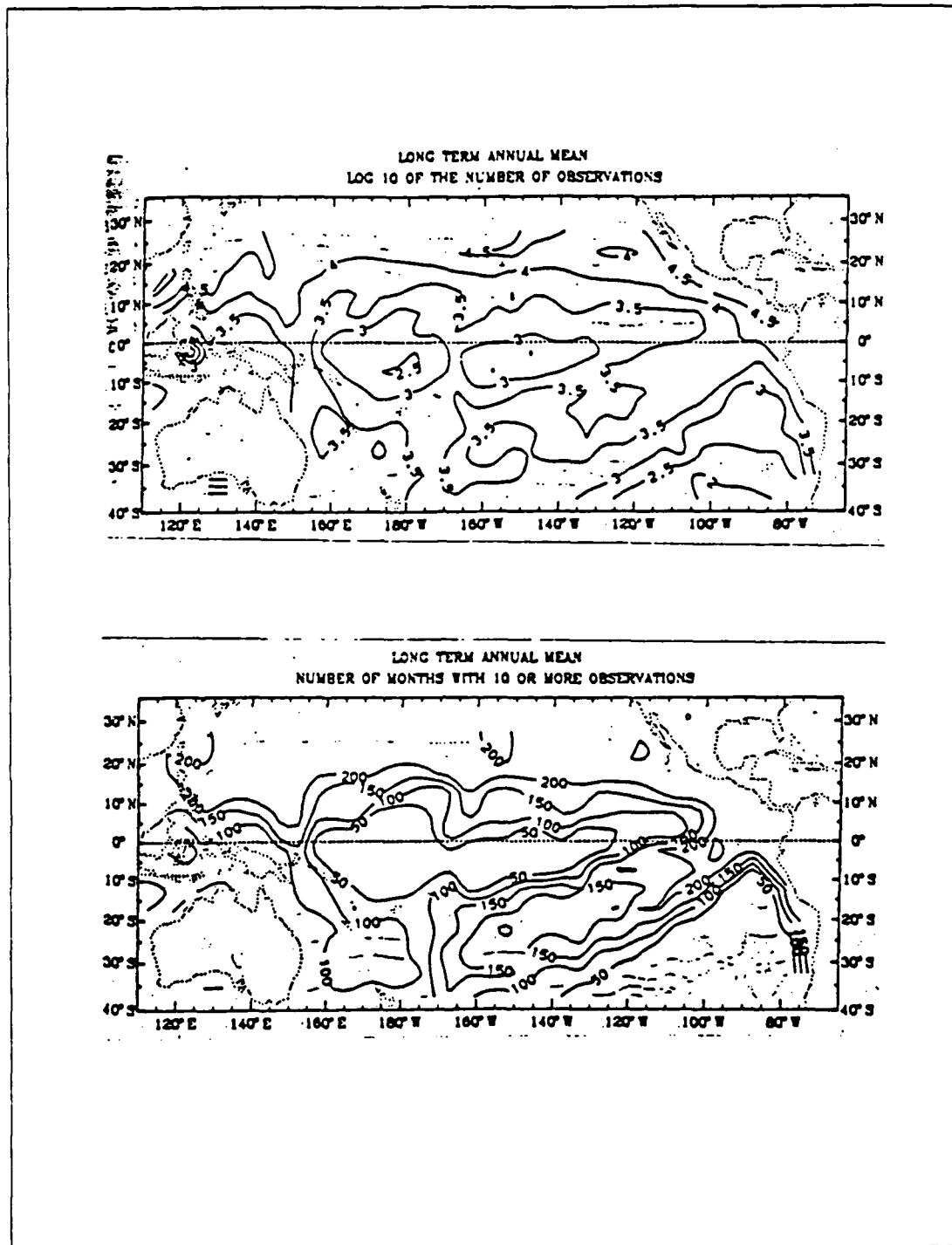


Fig. 2.3 Density of Atmospheric Data
from Weare, et. al.(1980).

B. METHODS OF DETERMINING MIXED LAYER DEPTH

In this study, the depth of the mixed layer is defined as the base of that portion of the turbulent ocean planetary boundary layer that is well mixed and homogeneous in the temperature of the sea water contained in this layer. It is important to note that everywhere there is an air-ocean interface (or ice-ocean interface), there will be a turbulent, well mixed boundary layer dynamically distinct from underlying layers.

The vertical temperature profile is typically the only available indicator of the extent of the mixed layer depth, although there are known to be conditions of deep isothermal temperature structure where mixing is controlled by the presence of a halocline. In the case of convective overturning due to salinity effects, the mixed layer depth is known to extend deeper than that which is to be indicated by the temperature profile. For this reason, Levitus (1982) utilized a density criterion to determine mixed layer depth. A temperature criterion of sea surface temperature (SST) minus 0.5°C ($\text{SST} - 0.5^{\circ}\text{C}$) was equated to a $\sigma\text{-t}$ change of 0.125. The direct comparison of a strictly temperature-derived mixed layer depth (MLD) field, and one that is derived from the density criterion is misleading. The coefficient of expansion for sea water is a strongly non-linear function of temperature. A temperature increment of 0.5°C corresponds to a broad range of temperatures and salinities extant in the world ocean. In water with a salinity of 35.0 parts per thousand, the 0.5°C temperature difference corresponds to a $\sigma\text{-t}$ change of 0.075 in the 6°C to 10°C range, and, to 0.15 in the 24°C to 26°C range. This method of mixed layer depth determination, based on a density change was attempted in the initial stages of this thesis, but was later abandoned, due to the absence of monthly salinity data in the numerical atlas. Use of monthly temperature data and yearly average salinities produced ambiguous results. However it must be noted that this method would produce physically meaningful results had salinity data been available in the same temporal and spatial resolution as the temperature data.

A statistical approach was employed in Bathen (1972) in which a Student-t test (at the 5% level) evaluated the average of successive groups of three temperatures. This was continued down the temperature profile until an average was encountered that was significantly different from the surface value. MLD was determined to be at this point. Also utilized was a method of fitting lines through successive three-step increments, and comparing the slope of these lines with the slope of a test line. Neither of these methods were used in this study because the temperature data are

based on 30 meter levels and they are too coarsely resolved in the vertical for the above techniques.

Another method, using an average of two techniques, was employed in Colburn (1975) and Wyrski (1962). The first technique derived a depth that was based on a simple difference of 0.5°C from the SST ($\text{SST} - 0.5^{\circ}\text{C}$). The second technique examined the temperature profile for the maximum temperature gradient. A depth was determined from the intersection of this maximum gradient line with a constant temperature line equal to the SST.

A simple SST - 1.0°C difference method was used in Robinson (1976) to determine the top of the seasonal thermocline. In this study, a simple linear interpolation technique was used to establish the depth at which there existed a temperature value of sea surface temperature minus 0.5°C ($\text{SST} - 0.5^{\circ}\text{C}$). A visual inspection of this method using sample temperature profiles indicates that a non-absolute measure of MLD is obtained. A non-absolute measure of MLD is one that, when the temperature profile is plotted versus depth, the MLD so determined does not fall on or within the entrainment zone (see Fig. 2.4). The mixed layer depth value falls just above the entrainment zone. This non-absolute, but accurate, measure of mixed layer depth is considered better suited for analysis of fluctuations (Levitus, 1982) and for comparison with the atmospheric forcing variables, and so is used in this study.

C. A ONE-DIMENSIONAL MODEL OF THE MIXED LAYER

In Kraus and Turner (1967) a one-dimensional model of the seasonal movements of the thermocline is proposed. The rate at which the ocean mixed layer will deepen or shallow is dynamically dependent upon the conversion of turbulent kinetic energy (TKE) to potential energy (PE). This conversion results from a balance, or imbalance, in the rate of production of TKE, due to wind stirring, and the rate of buoyant damping within the turbulent mixed layer, due to surface heating (conversion of TKE to PE). The temperature of such a dynamic mixed layer is determined by the sum of the surface heat flux and the entrainment heat flux. The entrainment heat flux, at the base of the mixed layer, with an active entrainment zone, is depicted in Fig. 2.4, which also depicts the conceptual model used in the analysis of data in this study.

The seasonal changes in MLD can be related to seasonal changes in wind stress and surface heating. The wind stress provides the turbulent energy required for mixing the ocean boundary layer. The gain or loss of heat at the top of the ocean boundary layer will either augment or dampen the turbulence caused by wind mixing. A solution

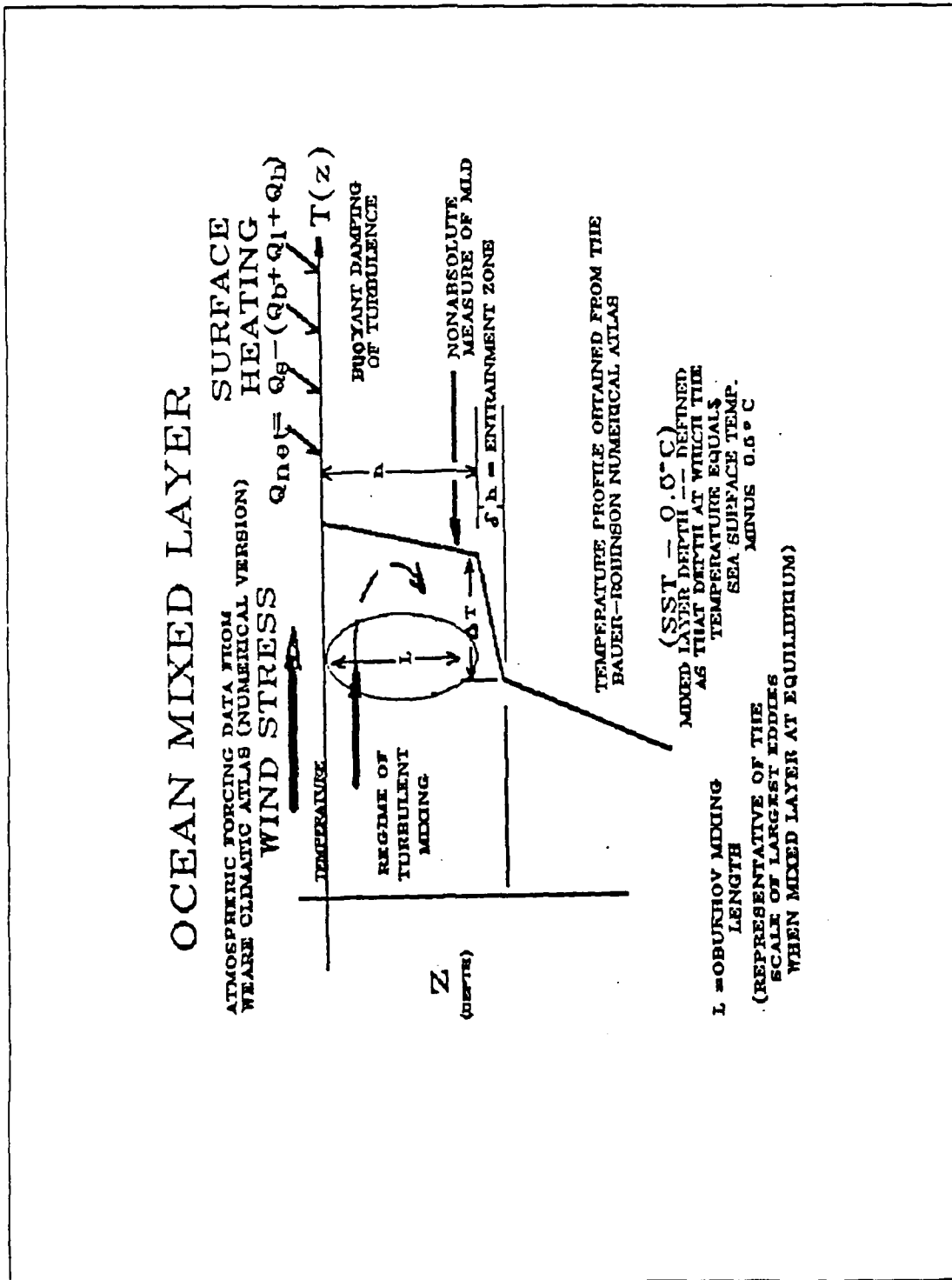


Fig. 2.4 A Conceptual Model of the Ocean Mixed Layer.

for a diagnostic depth of retreat (the depth to which MLD, h , will shallow or retreat) can be obtained which is proportional to the Obukhov Mixing Length when the mixed layer achieves steady state $\partial h / \partial t = 0$, or is no longer entraining cold water from below the mixed layer.

1. The Temperature Equation

The time rate of change of temperature within the surface layer is derived from a one-dimensional heat equation (2.1). Averaged quantities are denoted by an overbar (-), while fluctuation quantities are denoted by a prime ('). The subscripts h and 0 respectively denote quantities at MLD and at the surface.

$$\partial T / \partial t = - \partial / \partial z (\overline{W'T'})_h + \partial / \partial z (\overline{W'T'})_0 - W \partial T / \partial z + \kappa (\partial^2 T / \partial z^2) \quad (\text{eqn 2.1})$$

Starting from the right hand side (RHS) of equation 2.1, term (1) is the vertical turbulent heat flux (entrainment heat flux); term (2) is the net surface heat flux ($Q_0 / \rho C_p$); term (3) is the vertical temperature advection (resultant from internal adjustments); and term (4) is the eddy diffusion.

Scale analysis, from Garner (1983), of equation 2.1, uses similar values for variables found in the climatologies, currently under study on a seasonal time scale, and permit the omission of the eddy diffusivity (term 4). Eddy diffusivity typically ranges from approximately 0.1 to 0.5 (cm^2/sec), while the second derivative of temperature is 5 degrees C. (5000cm^2), which is on the order of $1/10^7$ (all other terms in the above are $1/10^3$). Thus, equation 2.1 is simplified to the form of equation 2.2

$$\partial T / \partial t = - \partial / \partial z (\overline{W'T'})_h + \partial / \partial z (\overline{W'T'})_0 - W (\partial T / \partial z). \quad (\text{eqn 2.2})$$

Term 1 on the RHS of equation 2.2, i.e., the entrainment heat flux at the base of the mixed layer, is equal to the magnitude of the temperature jump (ΔT) in the entrainment zone multiplied by the entrainment rate (W_e) as in equation 2.3

$$(\overline{W'T'})_h = -\Delta T W_e. \quad (\text{eqn 2.3})$$

After a vertical integration and using $(\overline{W'T'})|_0 = Q_0 / \rho C_p$, equation 2.2 simplifies to equation 2.4

$$\partial T / \partial t = Q_0 / (\rho C_p h) - (\Delta T W_e) / h. \quad (\text{eqn 2.4})$$

The density of seawater is ρ and the specific heat of seawater is C_p . Vertical advection does not appear in equation 2.4, since it does not affect the time rate of change of temperature in the mixed layer. Vertical advection can actually advect the thermocline to the surface *only in coastal waters* and thus directly affect SST. Interior adjustment (due to advective processes) can indirectly affect mixed layer temperature. Advection can reduce, via the variables W_e , and ΔT , h which in turn can increase the entrainment.

The rate of change of turbulent heat flux as a function of depth within the (well-mixed) turbulent ocean boundary layer is linear. The vertical turbulent heat flux at the base of the mixed layer is usually negative, given the predominant climatological conditions of $\partial T / \partial z > 0$ in the world's oceans. The entrainment rate becomes zero when the mixed layer is in a steady state or in retreat. It is physically impossible to unmix the water in the mixed layer upon application of the Second Law of Thermodynamics. For this reason, a Heaviside step function (Λ), which is zero when in steady state or when in retreat, is introduced into equation 2.4 so that the final equation is 2.5

$$\frac{\partial T}{\partial t} = Q_o / (\rho C_p h) - \Lambda (\Delta T W_e) / h. \quad (\text{eqn 2.5})$$

2. The Structure Equation

The structure of the turbulent mixed layer is best examined by evaluating the time rate of change of mixed layer depth (h). The time rate of change of MLD is represented dynamically by the difference between the entrainment rate and the rate of movement of the interface at the base of the mixed layer due to advective processes as expressed in equation 2.6

$$\frac{\partial h}{\partial t} = W_e - W(z = -h). \quad (\text{eqn 2.6})$$

From the shear production term of the TKE equation as developed in Kraus and Turner (1967) we know that the kinetic energy (KE) of wind stresses is converted into TKE, which in turn is used in the entrainment process to maintain or deepen the mixed layer. The entrainment rate is identically equal to the rate of work done in the production of turbulence by wind stresses as applied at the ocean surface. As shown in equation 2.7, the wind stress (τ) is computed as the product of the density of air (ρ_a), a

drag coefficient (C_d), and the wind velocity measured at ten meters above the ocean surface, and is also equal to the product of the density of air and the vertical turbulent momentum flux at the surface:

$$\tau = \rho_a C_d (u_{10})^2 = \rho_a (\overline{u'w'})|_0. \quad (\text{eqn 2.15})$$

Let the last term in equation 2.15 be representative of a velocity scale for the atmospheric boundary layer or friction velocity (u^*), then the vertical turbulent momentum flux across the air-ocean interface can be related to u^{*2} for each of the respective layers. Given that the density of seawater is 800 times greater than that of air, an important comparison of the velocity scales of the atmospheric and oceanic boundary layers is shown in equation 2.8.

$$u^{*2}(\text{ocean}) = u^{*2}(\text{atmosphere})/800 \quad (\text{eqn 2.8})$$

The velocity scale for the ocean boundary layer will be represented by u^* . This velocity scale is representative of the largest eddies in the wind driven mixed layer.

The effect of surface heating is to make the water of the mixed layer more buoyant. More work must then be expended to mix this warm water down towards the entrainment zone. Under conditions of a net surface flux into the water of the mixed layer ($Q_o > 0$), the heating term is a sink of turbulent energy, as represented in equation 2.9, where α is the coefficient of expansion for seawater, g is the gravitational acceleration, C_1 and C_2 are proportionality constants.

$$W_e \propto C_1(u^*)^3 - C_2 \alpha g Q_o / (\rho C_p) \quad (\text{eqn 2.9})$$

As shown in equation 2.10 the conversion rate of TKE to potential energy (PE), due to entrainment, (term 1) is expressible as a difference between the rate of the creation of turbulent kinetic energy by wind stirring (term 2), and the conversion of TKE into PE due to buoyant damping (term 3).

$$\alpha g h \Delta T W_e = C_1(u^*)^3 - C_2 \alpha g h [Q_o / (\rho C_p)] \quad (\text{eqn 2.10})$$

Windspeed is proportional to u^{*3} . Thus it can be shown in equation 2.10 that by doubling the wind speed the entrainment rate (W_e), and hence the deepening rate ($\partial h / \partial t$), increases by a full order of magnitude.

3. The Equilibrium Solution

In the absence of vertical advection and in the steady state (i.e. $\partial h / \partial t = 0$), an equilibrium depth of retreat (h_r) be derived. Solving equation 2.10 for W_e and substituting equation 2.10 into equation 2.6 subject to the prescribed steady state conditions (and $W(z=-h) = 0$), the depth of retreat is:

$$h_r = (C_1 C_2) \{ (u^*)^3 / [\alpha g Q_o / (\rho C_p)] \} \propto L. \quad (\text{eqn 2.11})$$

The depth of retreat is proportional to the Obukhov length scale (L). This length scale is physically representative of the maximum depth of turbulent mixing, constrained by the surface boundary conditions of heat flux and wind stress, for a mixed layer in equilibrium and not affected by vertical advection (Muller, Garwood, and Garner, 1983).

4. The Equilibrium Solution in the Presence of Vertical Advection

The term $W_o D$ in equation 2.12 is a measure of the vertical advective velocity at the base of the mixed layer. If vertical advection is present and MLD is at equilibrium (i.e. $dh/dt = 0$), then it can be shown from equation 2.10 that the vertical advective velocity must be balanced by the rate of mechanical production of turbulence (by wind stirring) minus the buoyant damping of the turbulence (by surface heating). Such a balance is shown in equation 2.12. Equation 2.13 is derived from 2.10 when the Heaviside step function is set to zero. When the differential equations 2.12 and 2.13 are solved numerically, the results indicate that mixed layer depth adjusts to an equilibrium depth equivalent to one-half the Obukhov mixing length ($L/2$) as in equation 2.14.

$$W_o h D = (C_1 u^{*3}) (\alpha g h \Delta T) - (C_2 Q_o) (\rho C_p \Delta T) \quad (\text{eqn 2.12})$$

$$\partial T / \partial t = Q_o / (\rho C_p h) - [\Delta T W_e / h] (\Lambda = 0) \quad (\text{eqn 2.13})$$

$$h = [C_1 / (1 + c_2)] [(u^*)^3 / (\alpha g Q_o / \rho C_p)] = L/2 \text{ (if } C_2 = 1) \quad (\text{eqn 2.14})$$

As shown in equation 2.14, MLD is not sensitive to the rate of vertical advection, but the numerical solution for the equilibrium time of adjustment indicates that it is sensitive to variance in the rate of upwelling of downwelling. The subject of enhanced time rate of change of MLD in the presence of downwelling and upwelling is discussed in Appendix C.

D. SUMMARY OF EQUATIONS IN THE CONCEPTUAL MODEL

A Summary of principle equations from the preceding sections is used to relate seasonal fluctuations in MLD to seasonal fluctuations in atmospheric forcing in the tropical and equatorial Pacific Ocean. This summary of equations forms the basis of the conceptual model that is used to establish and evaluate the relationship between the seasonal response of MLD to atmospheric forcing in this study. The first four equations use atmospheric forcing data and the fifth uses oceanic data. The temperature equation (Equation 2.16) is obtained from Equation 2.4. The structure equations (Equations 2.17 and 2.18) are obtained from Equations 2.10 and 2.6. The equilibrium solution for depth of retreat (Equation 2.19) is obtained from Equation 2.11. Mixed layer depth (Equation 2.20) is determined to be at the depth at which the temperature equals the SST minus 0.5°C.

$$\frac{\partial T}{\partial t} = Q - (\rho C_p h) \frac{\partial T}{\partial t} - (\Delta T W_e) h \quad (\text{eqn 2.16})$$

$$\alpha g h \Delta T W_e = C_1 (u^*)^3 - C_2 \alpha g h [Q_o / (\rho C_p)] \quad (\text{eqn 2.17})$$

$$\frac{\partial h}{\partial t} = W_e - W(z = -h) \quad (\text{eqn 2.18})$$

$$h_r = 2u^{*3} / (\alpha g Q_o / \rho C_p) \propto L \quad (\text{eqn 2.19})$$

$$\text{MLD} = (\text{Depth where temperature} = \text{SST} - 0.5^\circ\text{C}) \quad (\text{eqn 2.20})$$

III. RESULTS: SEASONALLY CHANGING CLIMATOLOGICAL ASPECTS OF MIXED LAYER DEPTH

A. LARGE AREA CONTOURS OF MIXED LAYER DEPTH

Here we examine a region of the Pacific Ocean that lies between 40S and 30N, and 110E and 75W. It is within this region that the two principle climatologies under study overlap. The seasonal variations of MLD will be examined within this region, since recent efforts of numerical modeling have begun to focus on this region, and useful information about climatological seasonal variations is needed. Mixed layer depths for each one degree quadrangle were computed using the SST minus 0.5°C criterion method which was described in Chapter II. For those quadrangles covered by land, and consequently with no data, filler values were inserted so as not to distort adjacent contours. Each of the monthly fields were then contoured on a Mercator projection, producing minimal distortions and inaccuracies.

An average annual field of MLD was computed from the average of the monthly temperature profiles in each quadrangle. Fig. 3.1 shows the yearly average mixed layer depth. The monthly variations of mixed layer depth from the annual mean are shown in Appendix B.

1. The Slope of the Equatorial Thermocline

The westward deepening of the equatorial thermocline is an observed phenomenon that is generally well understood. A westward deepening of the region of tightly packed isotherms is evident in the latitudinal cross-section at 1N in Fig. 2.2. Moreover, a seasonal change is evident in the slope of this region. In the February plate (Fig. 2.2a) the 25°C isotherm intersects the surface at 120W and is at a depth of 80 meters at 130E, while in the August plate (Fig. 2.2b) it intersects the surface at 145W and it is at a depth of 90 meters at 130E.

As described in Pickard and Emery (1982), the wind over the equatorial Pacific Ocean is predominantly westward. As a result, the South Equatorial Current flows towards the west. As the westward flowing currents encounter the land barriers on the western side, a surface slope develops that is upward toward the west, and a pressure gradient develops toward the east. A thicker surface layer is developed, and the thermocline has a slope opposite to the surface slope. This upward sloping (toward the east) thermocline has an important effect on the mixed layer, in both the western and Eastern Pacific Ocean, according to Gill (1982).

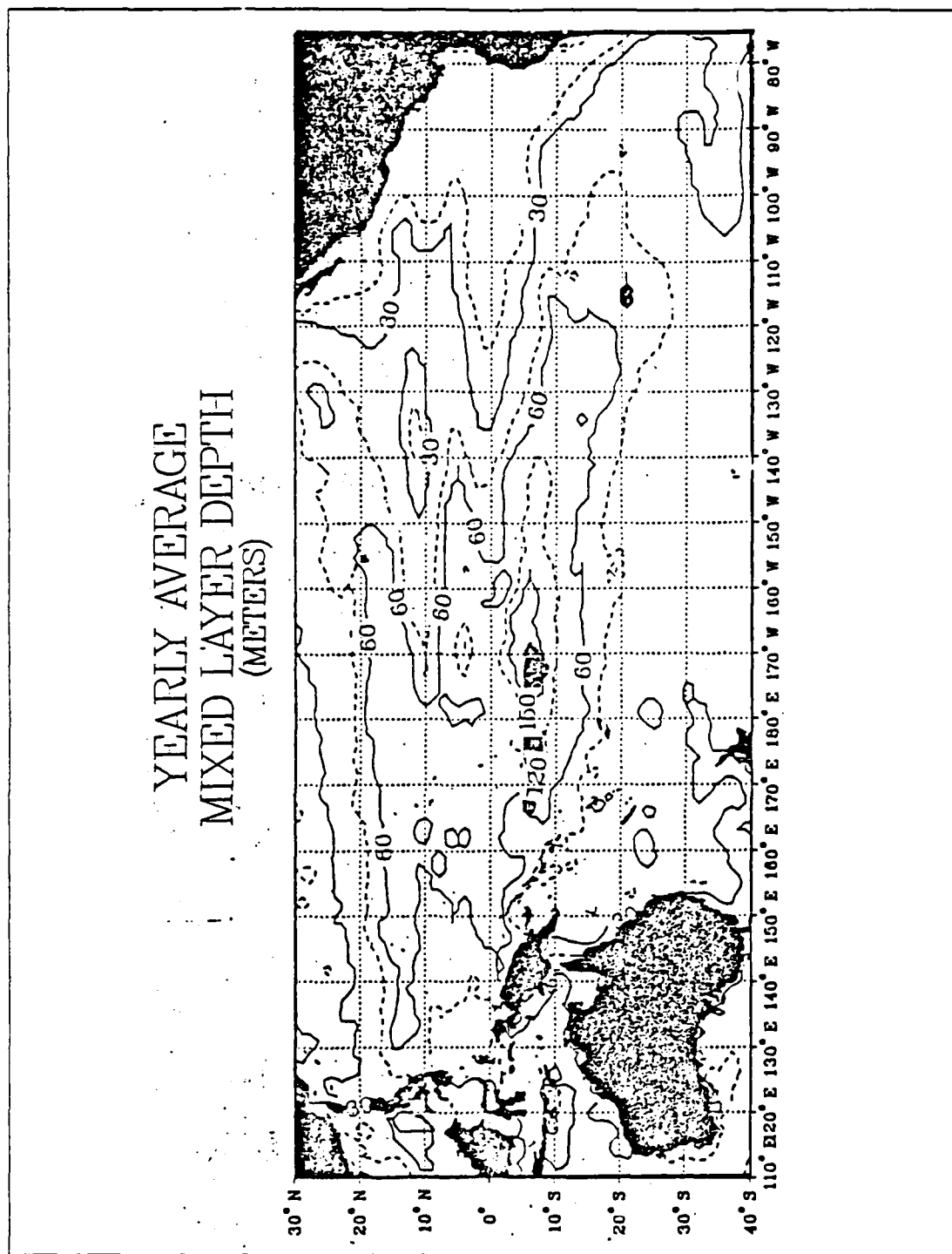


Fig. 3.1 Yearly Average Mixed Layer Depth
Contour Interval is 15 meters.

This effect is evident in the reduction of the time rate of change of mixed layer temperature. In equation 2.4, MLD (h) appears in the denominator of the surface heat flux and entrainment heat terms. An increase in MLD reduces both terms in equation 2.4. In the Eastern Pacific Ocean, cold water exists close to the surface due to upwelling (see below). Again examining equation 2.4, it is evident that a shallower MLD (h) will increase the time rate of change of the temperature of the mixed layer. The role of a shallower MLD (h) is also important in the structure equation (equation 2.10), where h also appears in the denominator of both terms on the RHS when the equation is rearranged so that only the entrainment rate (W_e) appears on the LHS. A smaller h will result in an increased entrainment rate. The effect of an increased entrainment rate is evident in equation 2.6 and an increase in the time rate of change of MLD will result. The water of such a shallower layer is thusly more easily mixed, and cooling of the surface waters during periods of active entrainment. During inactive periods, the surface layer can become a thin, relatively warm skin of water, in response to the high levels of surface heating. The surface layers above the thermocline in the western Pacific are warm and deep. Changes in entrainment, or heating rates, do not affect the surface temperature a great deal.

2. Seasonal Changes of Mixed Layer Depth Contours in the Eastern Pacific Ocean

The most prominent feature of the yearly average field (Fig. 3.1) is the tongue of shallow mixed layer depths protruding westward, along the equator, from the Eastern Pacific Ocean. Further inspection of the monthly fields (see Appendix A) reveals that this feature moves meridionally and zonally throughout the year. The 30 meter contour recedes to its minimum westward extent in December, and extends to its maximum extent in April. The minimum and maximum longitudinal extent of the 30 meter contour is shown in Fig. 3.2, and the full annual cycle is shown in Fig. 3.3. The annual cycle of latitudinal movement is shown in Fig. 3.4.

The general appearance of this 30 meter mixed layer depth contour closely resembles the patterns of SST which feature a tongue of cold water extending east-west along the equator. This cold tongue is associated with strong upwelling occurring in the water column. In Wyrski (1981), the tongue of surface cold water was investigated and determined to be maintained by the process of advection of cold water from the east, and by upwelling of cold water from below. Wyrski (1981) further established that the cause of this tongue was due to the upwelling process.

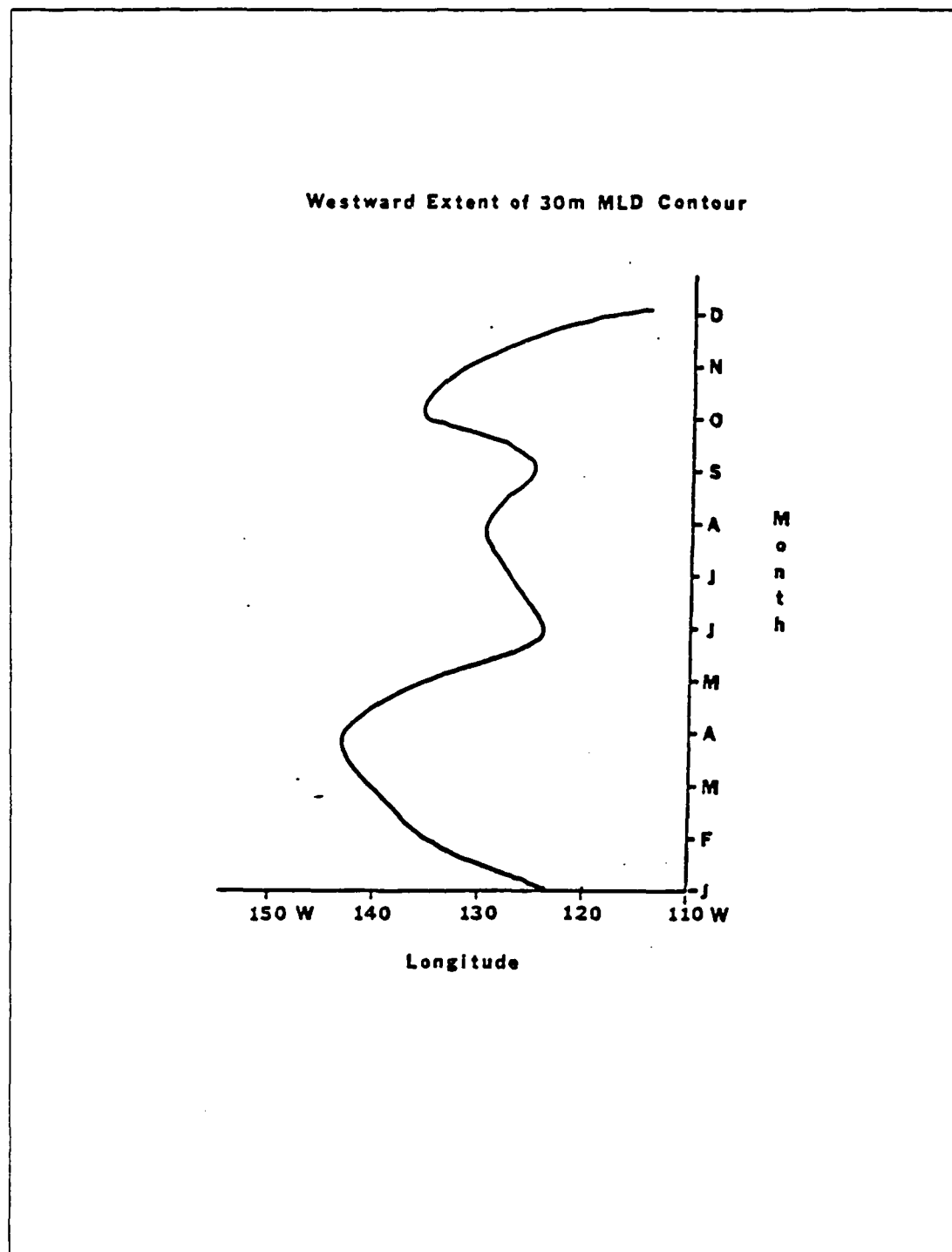


Fig. 3.2 Maximum and Minimum Westward Extent of the 30m MLD Contour.

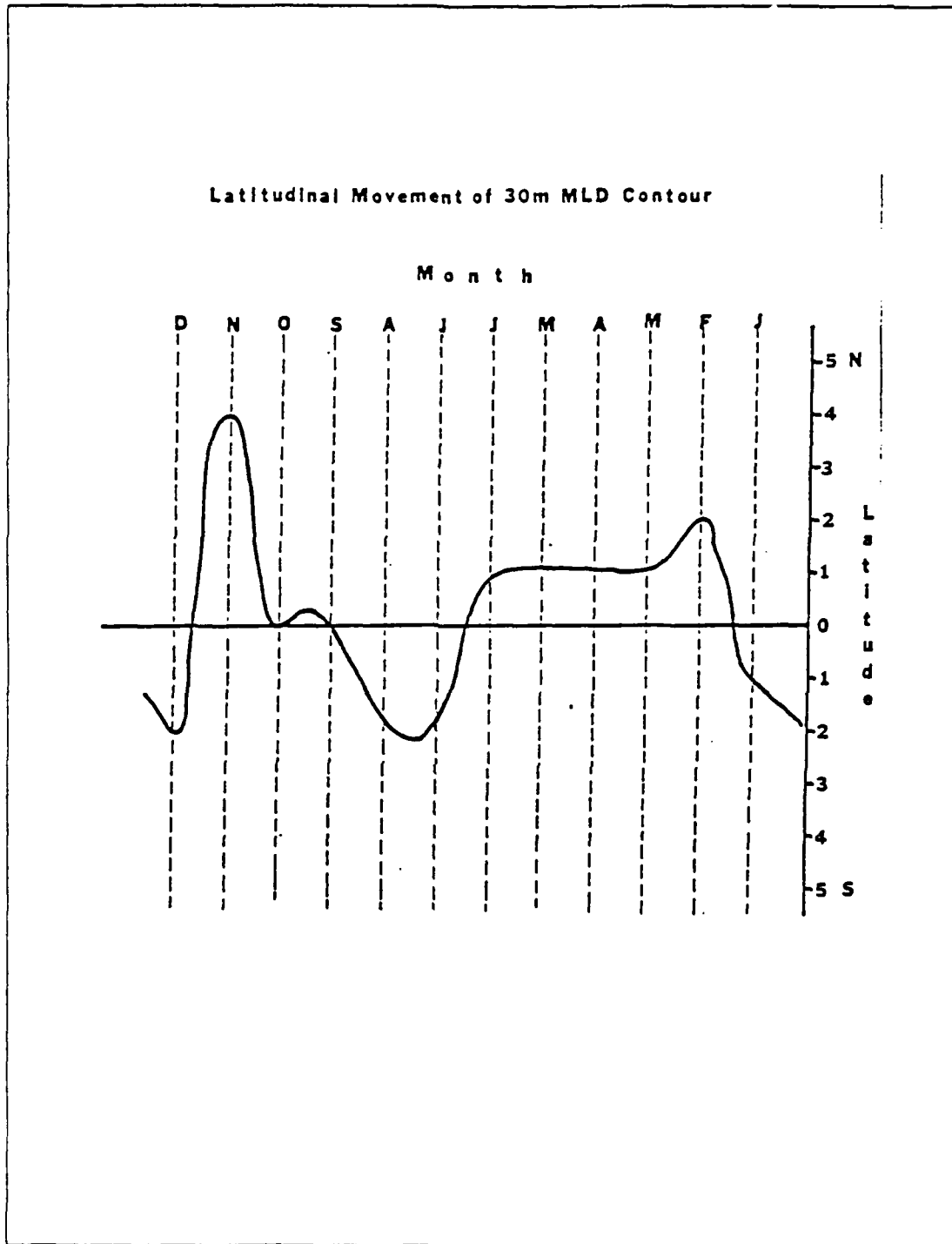


Fig. 3.3 Annual Cycle of North-South Movement of 30m MLD Contour.

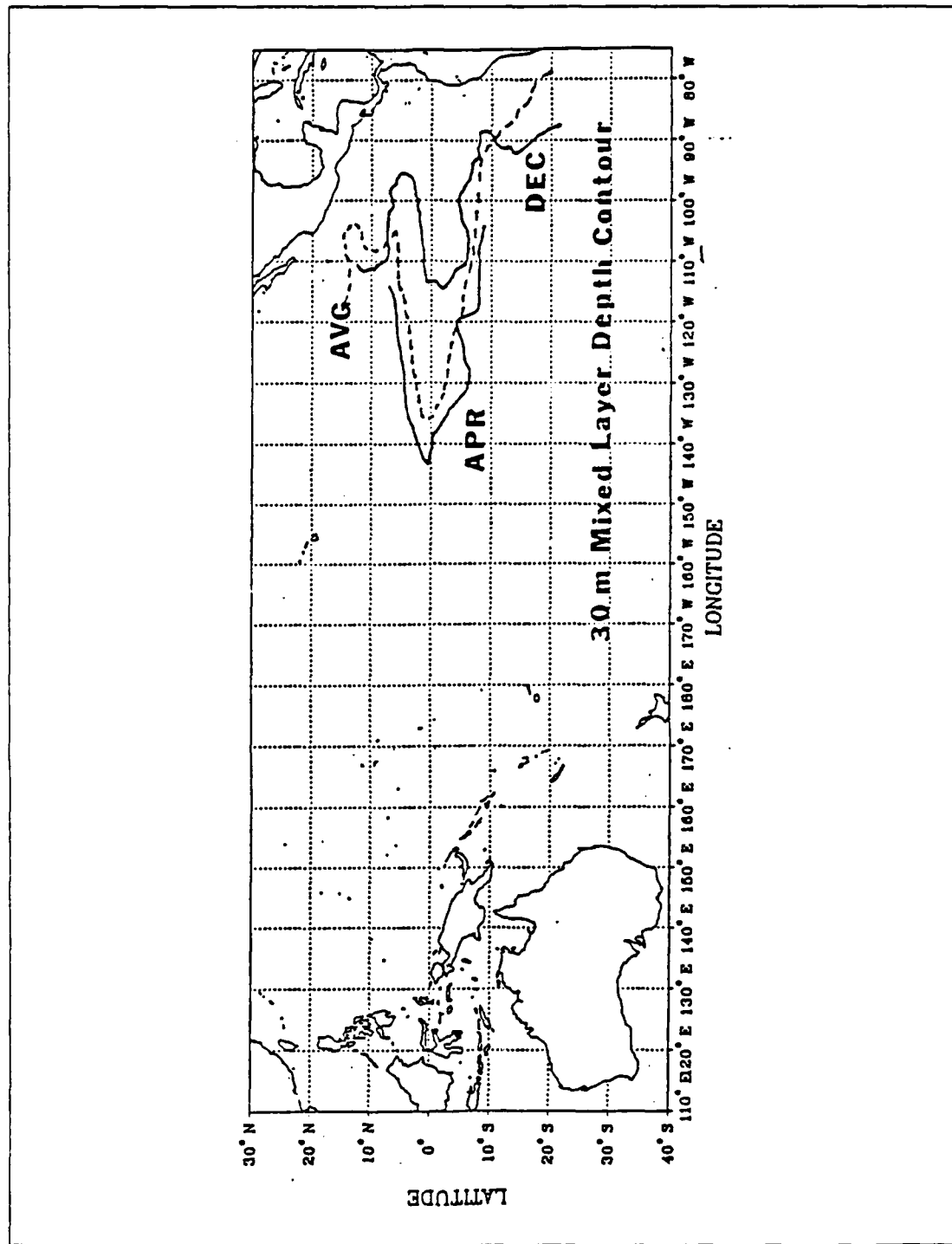


Fig. 3.4 Annual Cycle of Movement of 30m MLD Contour.

The seasonal variation of upwelling rates are related to the annual fluctuations in the trade winds. The upwelling is stronger on average from September to November. The upwelled water is found to "preferably go to the winter hemisphere, while the supply comes from both hemispheres" (Wyrтки, 1981). This seasonal cycle in upwelling, due to Ekman divergence, corresponds to the minimum and maximum in the westward extent of the 30 meter mixed layer depth contour, as illustrated in Figs. 3.2 and 3.3. In Fig. 3.4, the 30 meter contour appears to be shifting toward the winter hemisphere.

Although these results are not conclusive, they seem to suggest that on seasonal time scales in the equatorial region of the Eastern Pacific Ocean, the dominant term in equation 2.18, which most affects changes in mixed layer depth with respect to time, would appear to be the upwelling rate rather than the entrainment rate. A measure of vertical advection $W(z=-h)$ is presented later in this chapter in the Difference of Net Surface Heating and Heat in the Water Column data fields. Comparison of the magnitude of these data fields indicate that advective processes are most dominant in the Eastern Pacific Ocean.

B. SMALL AREA ANALYSIS OF ATMOSPHERIC FORCING AND MIXED Layer Depth

The large area contours of mixed layer depth do not prove useful for detailed analysis of atmospheric forcing and mixed layer response, since many of the contours are poorly resolved. For this reason, the area of study has been cross-sectioned by the Equator and three principal meridians at 155E, 155W, and 105W, as shown in Fig. 3.5. In this way it becomes easier to focus on the seasonal variations of MLD and how these variations differ by latitude and by meridional region within the area of study.

1. Atmospheric Forcing

The net heating of the sea surface (Q_o) is the algebraic sum of the primary sources of heating, to solar radiation (Q_s), minus the losses of heat due to long wave back radiation (Q_b), and latent (Q_l) and sensible (Q_h) heating of the atmosphere by the sea, as described in equation 3.1

$$Q_o = Q_s - (Q_b + Q_l + Q_h). \quad (\text{eqn 3.1})$$

Large area contours of the atmospheric forcing variables for the area of study are included in Weare (1980). Only the annual mean is included here (Fig. 3.6) which

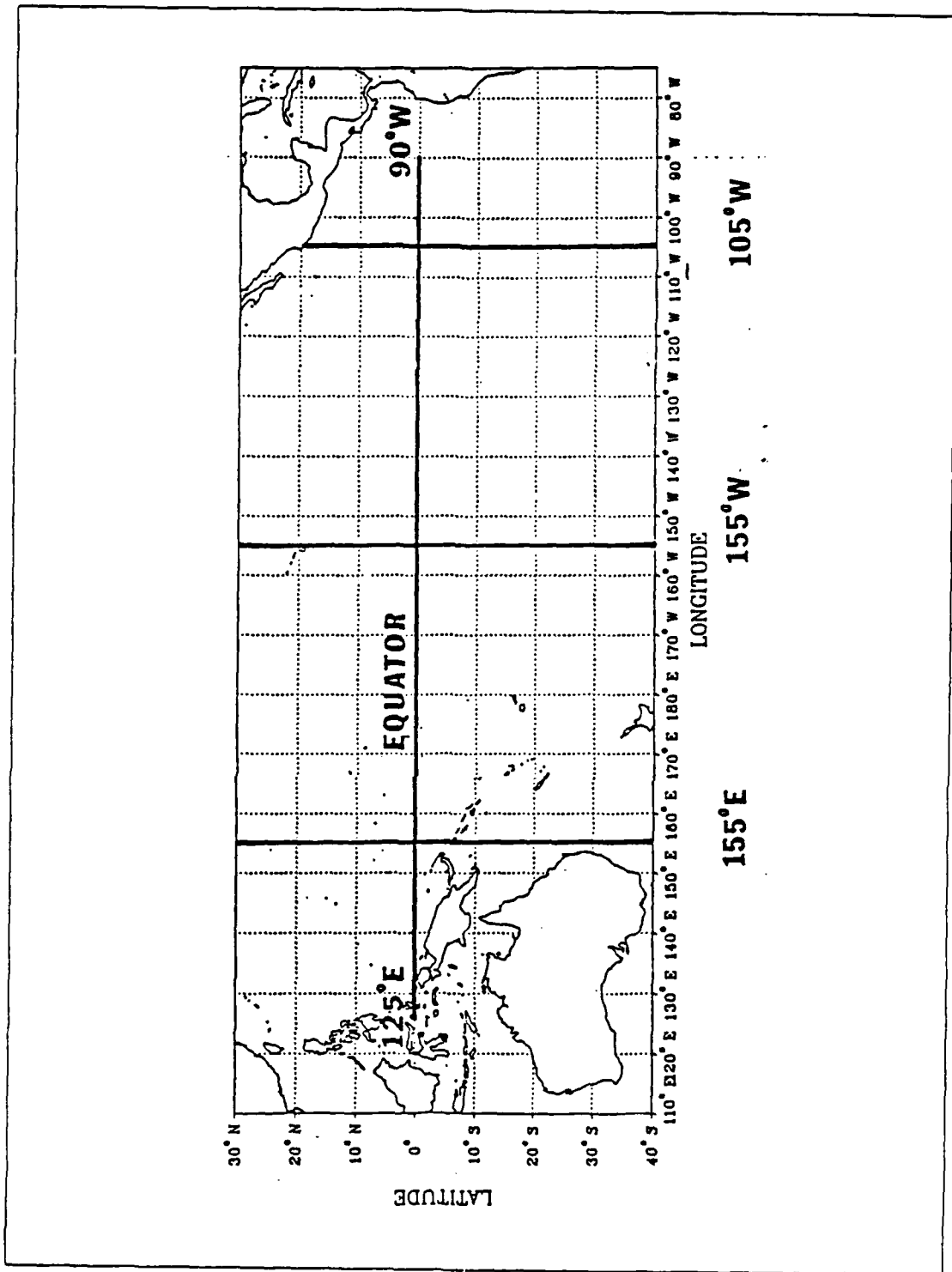


Fig. 3.5 Meridians Cross-sectioning the Area of Study.

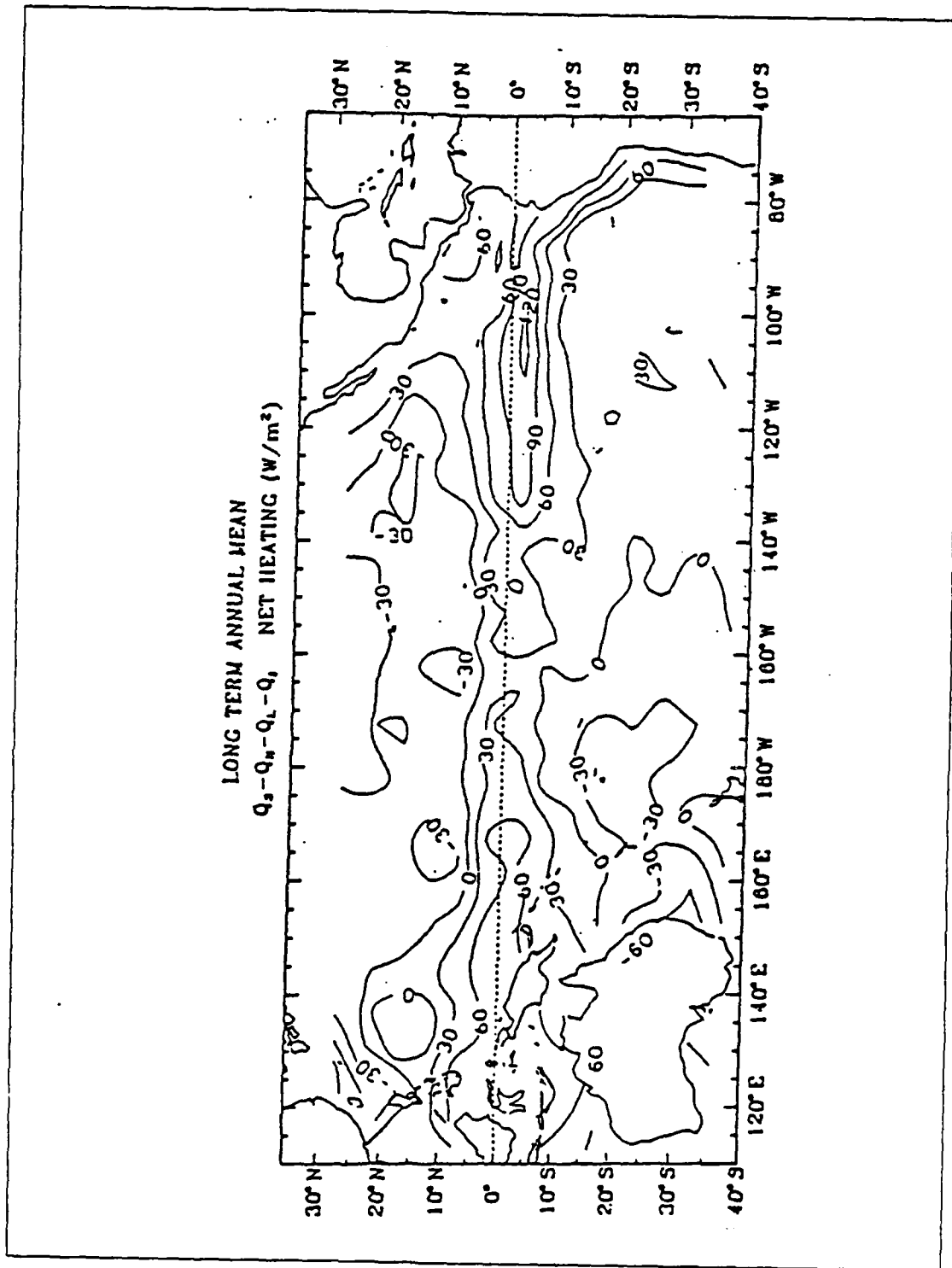


Fig. 3.6 Net Surface Heating for the Area of Study.

shows a maximum region of heating in the Eastern Pacific Ocean protruding westward along the Equator to 135W and a much lower maximum of 60 W/m^2 along the Equator in the Western Pacific Ocean. The variance of the mean values (of net oceanic heating) can vary as much as ± 30 watts per square meter, with a 95% confidence interval (Weare, 1981). Therefore, any qualitative consideration of the results in this section must be evaluated in light of these stated variances.

One of the atmospheric circulation patterns dominant in the equatorial and tropical Pacific Ocean is that of a Walker circulation. The Walker circulation pattern is that part of the meridionally averaged flow which is primarily due to the atmospheric heating symmetric about the Equator. This circulation, discussed in Gill (1982), originates in a region of rising motion over the longitudes of greatest atmospheric heating (in the western Pacific), and is perpetuated by eastward latitudinal flow aloft to a region of sinking motion over the eastern longitudes. Cyclonic motion in the air column is centered on the western flank of the heating zone. A system of easterly winds at the surface connects the sinking and rising regions. The zonally averaged flow, in the area of study, is typified by Hadley cell circulations, with rising motion occurring over and on each side of the Equator. In the northern cell, the upper air flow turns to the north, where the flow will eventually sink to the surface and flow south, completing the circulation. The converse is true south of the Equator, where the upper air part of the circulation turns southward. The combined averaged flow at the surface, for the most part, produces the Easterly Trade Winds. In the southern hemisphere a regime of southeasterly flow converges on a region of calm winds known as the Doldrums. The Doldrums occur between 4N and 10N (Pickard and Emery, 1985). In turn, the northeasterly trade regime converges upon the doldrums in the northern hemisphere. Divergent flow within the wind-driven, westward flowing South Equatorial Current along the Equator is the primary cause of the equatorial upwelling referred to in the last section.

It is within the context of these atmospheric circulation patterns that fields of surface heating and wind speed must be discussed. The surface heating field, in Fig. 3.7, presents seasonally varying regions, within the area of study, that are very different from each other.

In the Western Pacific Ocean the average annual ocean heating is less than in the Eastern Pacific, as seen in Fig. 3.6 A seasonal pattern is evident, in Fig. 3.7, at 155E with a strongly pronounced region of upward heat flux (Q_0 is negative), located

in the southern latitudes below 5S, during the southern hemispheric winter months of March through September. Directly to the north is a weaker pattern of downward heat flux (with a maximum of $+120 \text{ Watts.m}^2$) during the northern hemispheric summer months. In the central Pacific region, the summer heating and winter cooling of the sea surface is not as strong as it is to the west. In the Eastern Pacific Ocean, strong winter cooling occurs in the southern tropics and sub-tropics. Along the Equator, a narrow band of strong heating is prevalent through nine months of the year. In the northern hemisphere, heating decreases and a minimum occurs during the summer months. To explain this summer minimum, it is necessary to recall that large scale subsidence exists in the air column above the eastern Pacific Ocean as part of the Walker Circulation. The latent heating losses from the sea surface to the atmosphere are at a maximum when cloud cover is also at its maximum in the Eastern Pacific ocean. This is caused by low level cloud cover which becomes thickest during the summer months and is associated with a subsidence produced inversion. However, throughout most of the year the largely cloud free air column permits a greater amount of solar radiation to become incident on the sea surface than in the Western Pacific Ocean. In the plot of equatorial net heating a minimum heating in the eastern Pacific Ocean during June and July is also evident. Surface heating is greater in the eastern ocean than in the western ocean. A heating cycle that is not as highly variant is observed in the central longitudes.

The contours of wind speed at 155E (Fig. 3.9) all exhibit a seasonal pattern. Winds increase at about the time of the vernal equinox and decrease upon the approach of the autumnal equinox. The seasonal pattern decreases at lower latitudes. In each of the meridional fields of wind speed a curved locus connecting wind minima can be drawn through the low tropics and equatorial region. This locus of wind minima is interpreted as a line or band of minimum convergence between the southeasterly and northeasterly trade winds. A diagrammatic and general pattern of seasonal influence along with a curved line of wind minima are shown in Fig. 3.8 In the western Pacific Ocean, Fig. 3.9, the curved line of wind minima bulges from the winter into the summer hemisphere. This was the effect noted by Wyrтки and Meyers (1976), such that the trade wind regime of the winter hemisphere is the larger and stronger of the two regimes. The wind minima line is not as symmetrically shaped in the central Pacific Ocean as is that occurring in the west. The wind minima line does, however, conform to an irregular seasonal influence pattern. In the Eastern Pacific

Ocean, the magnitudes of the wind minima are lower and it is apparent that the southeasterly trade wind pattern extends far into the northern hemisphere. The southeast trades do, in fact, extend far into the northern hemisphere for most of the year as indicated in the wind vector diagrams in Weare (1980) and the Handbook of Oceanographic Tables (Bialek, 1966). The equatorial section of wind speed is lower than in either the Central or Eastern Pacific Ocean. The Central Pacific Ocean has the strongest wind speeds along the equator, and the Eastern Pacific Ocean wind speeds are greater than those in the Western Pacific Ocean.

2. The Oceanic Response

The fields of MLD (Fig. 3.10) exhibit pronounced patterns of seasonal influence. In the Eastern Pacific Ocean and north of 10S, the pattern is not so pronounced. One probable explanation is that equatorial and tropical upwelling is dominant in determining changes of the mixed layer in this part of the Pacific Ocean. Examining equation 2.6, the seasonally changing wind speed and surface heating are part of the entrainment rate term which is balanced by the rate of vertical advection. If their respective maxima are out of phase, then a mollified pattern of MLD is possible. This is examined in detail in Appendix D.

The fields of time rate of change of MLD show a response to atmospheric forcing that is predicted by the one-dimensional model used in this study. In the Western Pacific Ocean in Fig. 3.11, the $\partial h/\partial t$ contour lines enclose the regions of shallowing MLD. When this pattern is compared with corresponding wind speed and surface heating fields, the relationship of atmospheric forcing to the depth of retreat (see equation 2.11) becomes apparent. Namely, a small decrease in wind speed (raised to the third power), coupled with a linear increase in heating, does produce the expected shallowing or retreat of the mixed layer. The converse is true for the region of deepening. Deepening also occurs at a greater rate in the tropics at the onset of the winter storm season (between March and May). This rate is greater than it is in any other time of the year. This is consistent with the mid-latitude results of Elsberry and Camp (1978). The $\partial h/\partial t = 0$ contour enclosing the region of southern hemispheric shallowing extends far into the northern hemisphere in Fig. 3.11 This corresponds to a sharp decrease in wind speed associated with the southeast trade winds that extend far to the north in this region.

155 E
Q(NET)
(WATTS/METER²)

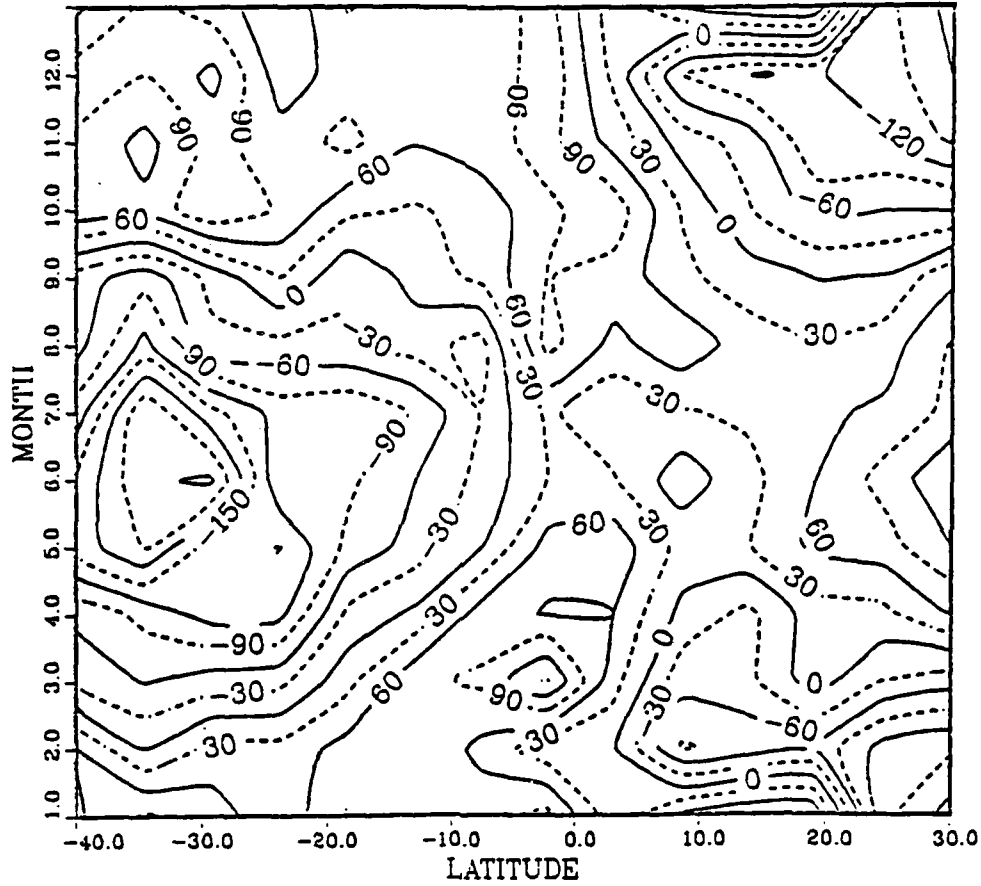


Fig. 3.7 Net Surface Heating at 155 °E
Contour Interval is 30 W/m.²

155 E
WIND SPEED
(METERS/SECOND)

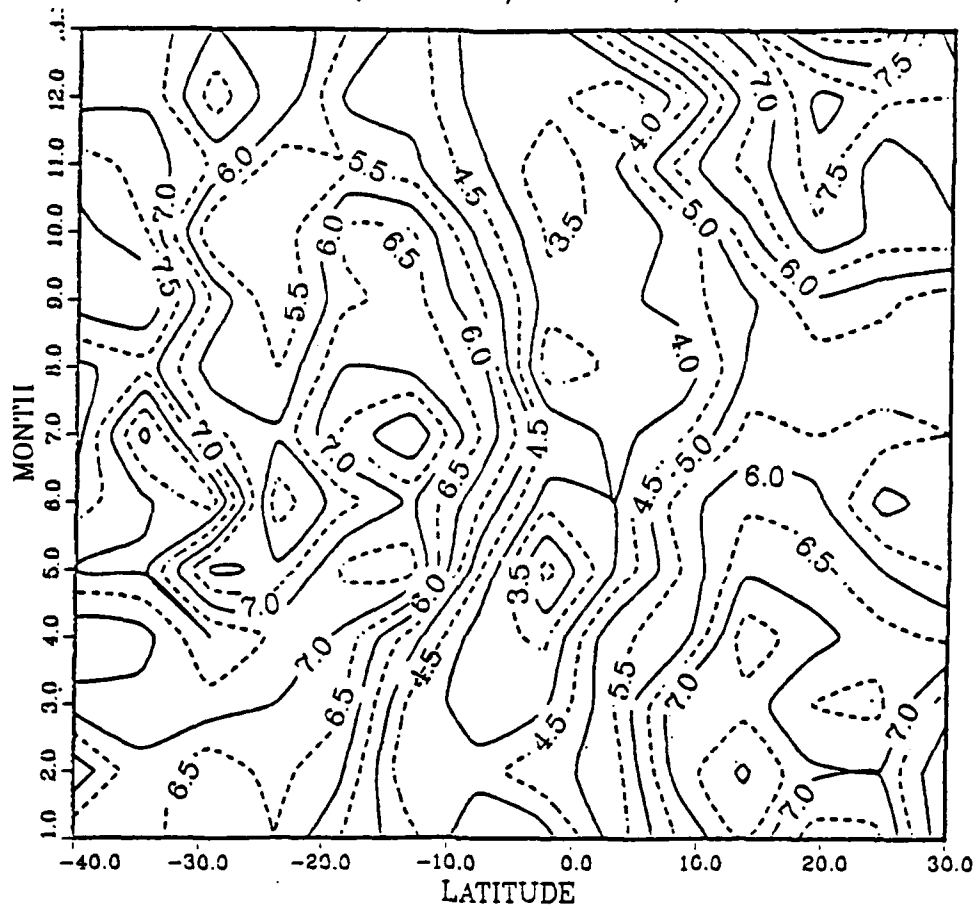


Fig. 3.8 Wind Speed at 155 °E
Contour Interval is 0.5 m/s.

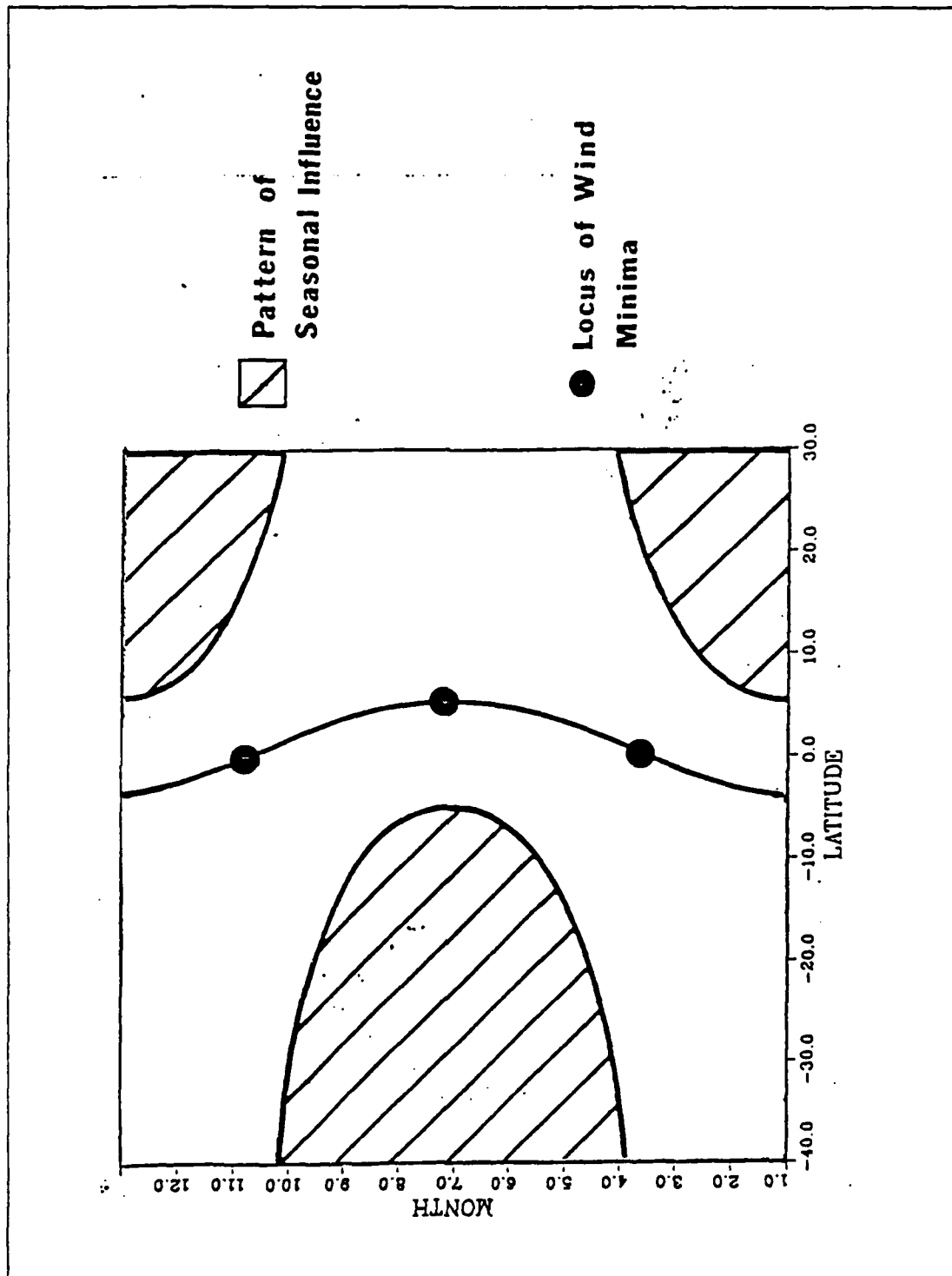


Fig. 9 Pattern of Seasonal Influence.

155 E
MIXED LAYER DEPTH
(METERS)

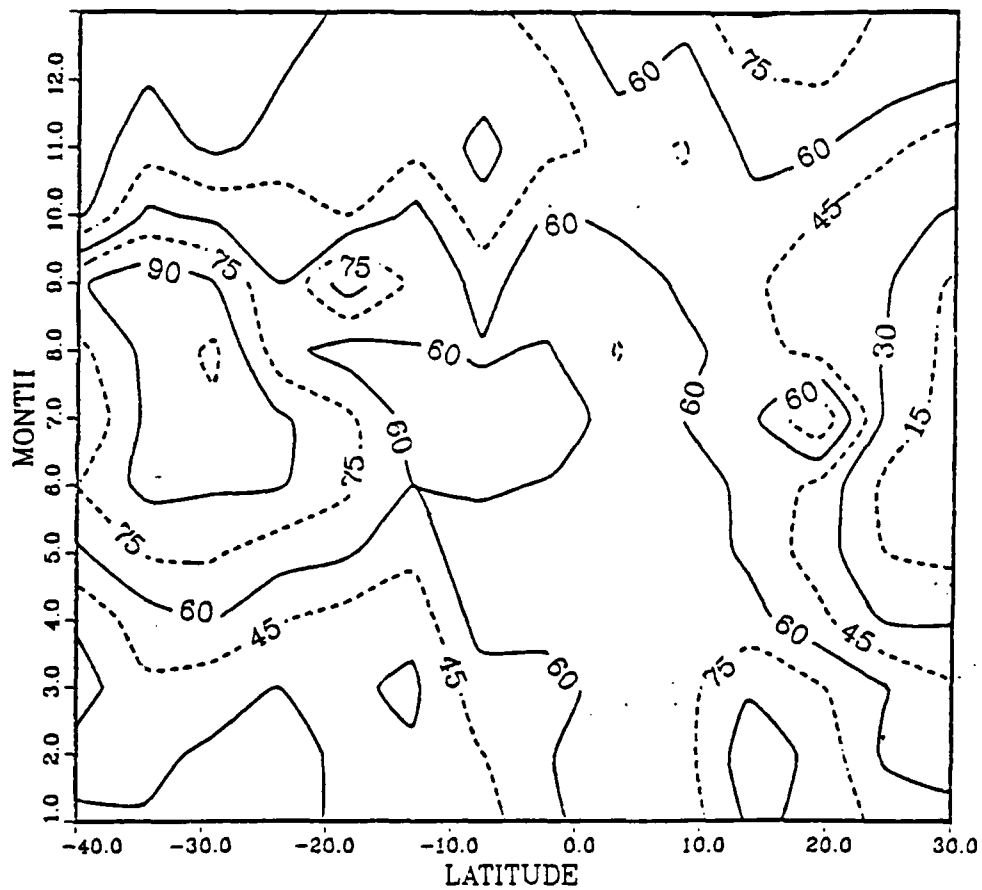


Fig. 3.10 Mixed Layer Depth at 155 °E
Contour Interval is 15 m.

155 E
DH/DT
(METERS/MONTH)

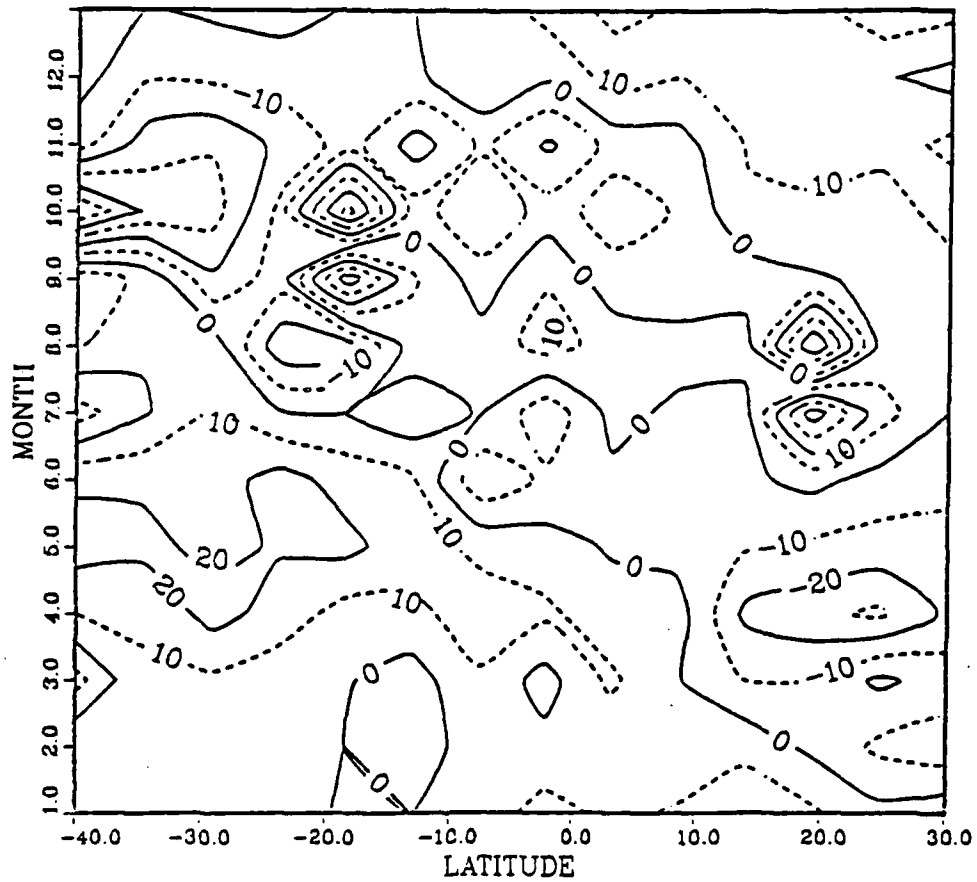


Fig. 3.11 Time Rate of Change of Mixed Layer Depth
at 155°E
Contour Interval is 10m./month.

C. THE FLUCTUATION FIELDS

1. The Derivation of Fluctuating Quantities

As expected, the atmospheric forcing fields and the fields of oceanic response show that the seasonal pattern becomes more pronounced as latitude increases north and south of the equator. The contoured fields of fluctuation from average quantities also illustrate this pattern. Both the atmospheric forcing fields and the oceanic response fields for any particular month at a particular location are the sum of a mean value for that location and a perturbation quantity for that location for that month. This relation can be expressed:

$$h(x,y,t) \equiv \bar{h}(x,y) + h'(x,y,t) . \quad (\text{eqn 3.2})$$

The fluctuation from average quantities was computed by subtracting the annual average of the variable in question from the monthly value:

$$h' = h - \bar{h} . \quad (\text{eqn 3.3})$$

The fluctuation fields of wind speed, net surface heating, and mixed layer depth so determined are shown in Figs. 3.12, 3.13, 3.14. The oceanic response of the monthly fluctuation in MLD to the monthly fluctuation in atmospheric forcing of wind speed and net surface heating is easily compared on these diagrams. The expected correlation between these variables based on the conceptual model developed in the last chapter is readily apparent in the higher tropical latitudes (greater than 10°N and 10°S), but the correlation degrades considerably along the Equator. For example, figure 3.14 shows a deeper than average MLD in the northern latitudes during the winter months of January and February. As would be expected from the conceptual model the fluctuation in wind speed in Fig. 3.12 shows a large positive fluctuation. The fluctuation in surface heating is a large negative one as shown in Fig. 3.13. This pattern of correlation varies with the seasons in the respective hemispheres and with position. Stronger correlations exist along the 155°E and 155°W meridians and weaker correlations along 105°W. This is a possible consequence of the strong influence of vertical advection in the eastern tropical Pacific Ocean. The special utility of this analysis technique is revealed upon examination of the equatorial cross-sections of each variable. A very weak seasonal pattern that varies in position and time becomes

apparent across the equatorial region from east to west and from January through December. This is the seasonal response of the equatorial MLD to seasonally varying atmospheric forcing variables.

A distinct region of wind speeds that are below average is diagonally centered in Fig. 3.15 a. A similarly distinct heating pattern, although with a higher degree of variance, emerges in the net surface heating field in Fig. 3.15 b. The oceanic response, in a region of below average winds and strongly positive (downward) surface heat flux, will be to produce a region of shallower MLD. A region of distinctly shallower mixed layer depths is observed along the diagonal of the contour of the fluctuation field (Fig. 3.16 a). This pattern is somewhat broken. This disruption in the pattern is probably the result of vertical advection which may be very strong along the equator. In Fig. 3.16 (b), a region of negative time rate of change of MLD (shallowing) occurs earlier in the year along the center of the diagonal region of interest and a region of positive time rate of change of MLD (deepening) occurs later in the year. Such a pattern of shallowing and deepening supports the result found in the preceding figures.

2. Statistical Analysis

The statistical analysis using correlation coefficients between the atmospheric forcing by wind and surface heating and the oceanic response of the mixed layer is examined along the meridians at 155E, 155W, 105W in Figs. 3.17, 3.18, 3.19 respectively. A statistical model is proposed that is based on equation 2.17 of Chapter II, wherein fluctuations in MLD are positively correlated with wind speed and negatively correlated with surface heating. A general pattern of negative correlation with surface heating and positive correlation with wind speed is evident in the figures. The strongest correlations occur above 10N and below 10S.. The degree of correlation of MLD with surface heating and wind speed is strongest along 155E in Fig. 3.17. Each of the respective correlation patterns becomes weakest between 10S and 10N. These results are insufficient to indicate whether the statistical model itself is inadequate or the spatial resolution and seasonal time scale are incorrect for the equatorial region. The data presented in Figs. 3.15 and 3.16 show that the conceptual model seems to adequately describe MLD response to atmospheric forcing, but that the MLD response is very weak on a seasonal time scale.

155 E
FLUCTUATION IN WIND SPEED
(METERS/SECOND)

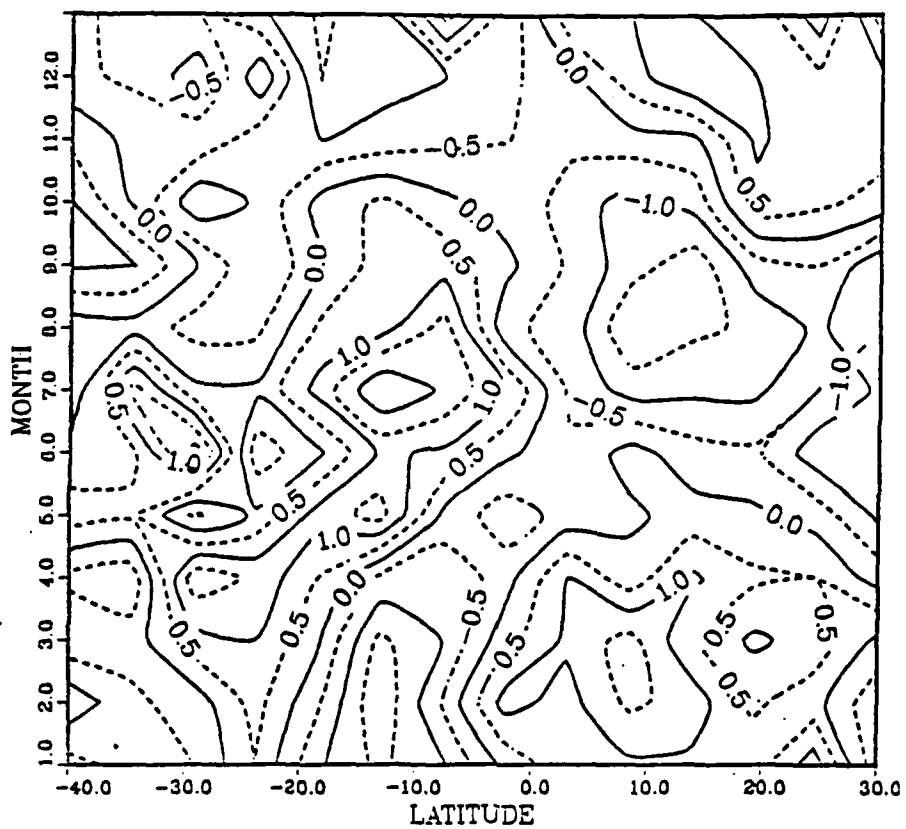


Fig. 3.12 Fluctuation in Wind Speed at 155 °E
Contour Interval is 0.5m's.

155 E
FLUCTUATION IN Q(NET)
(WATTS/METER²)

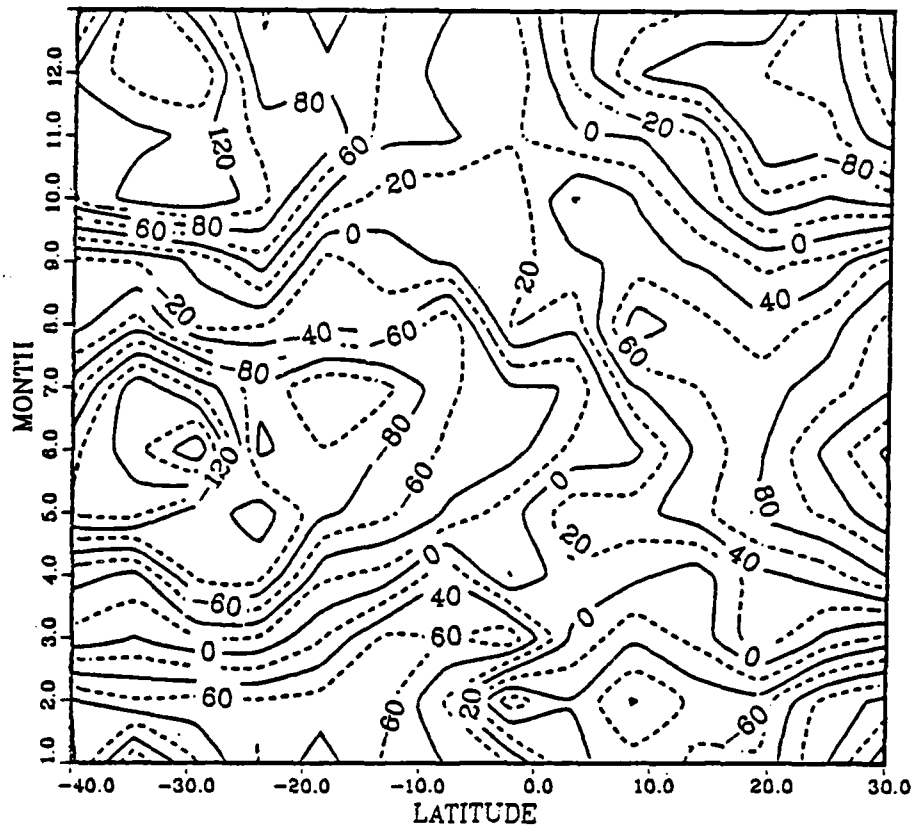


Fig. 3.13 Fluctuation in Net Surface Heating
at 155 °E
Contour Interval is 20 W/m.²

155 E
FLUCTUATION IN MLD
(METERS)

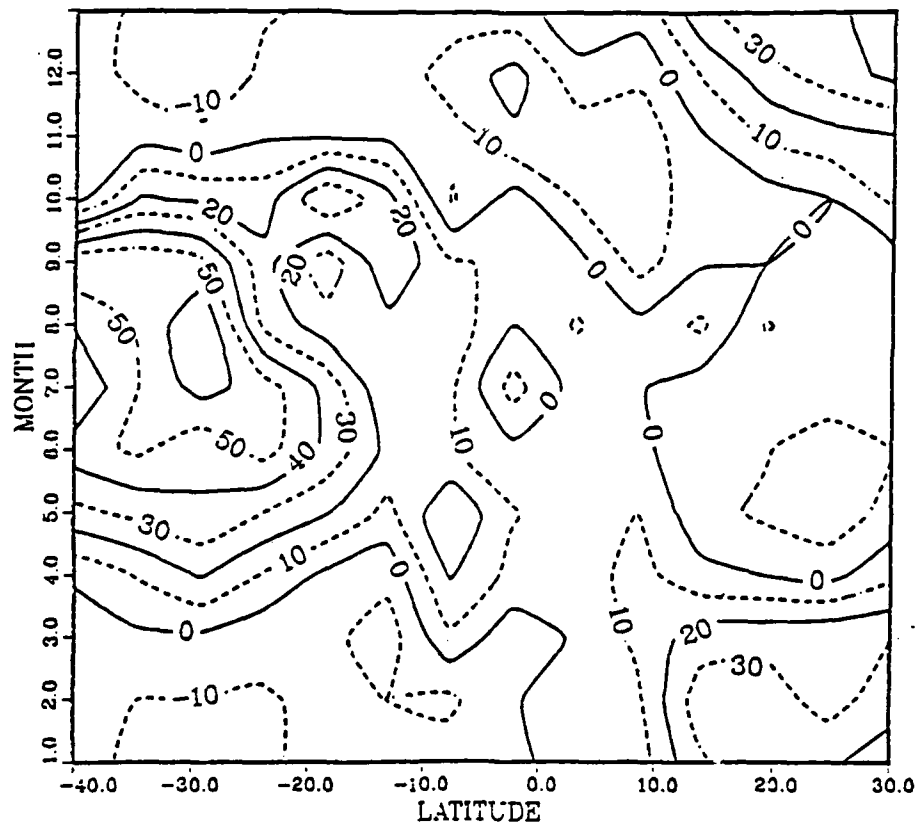


Fig. 3.14 Fluctuation in Mixed Layer Depth
at 155 °E
Contour Interval is 10m.

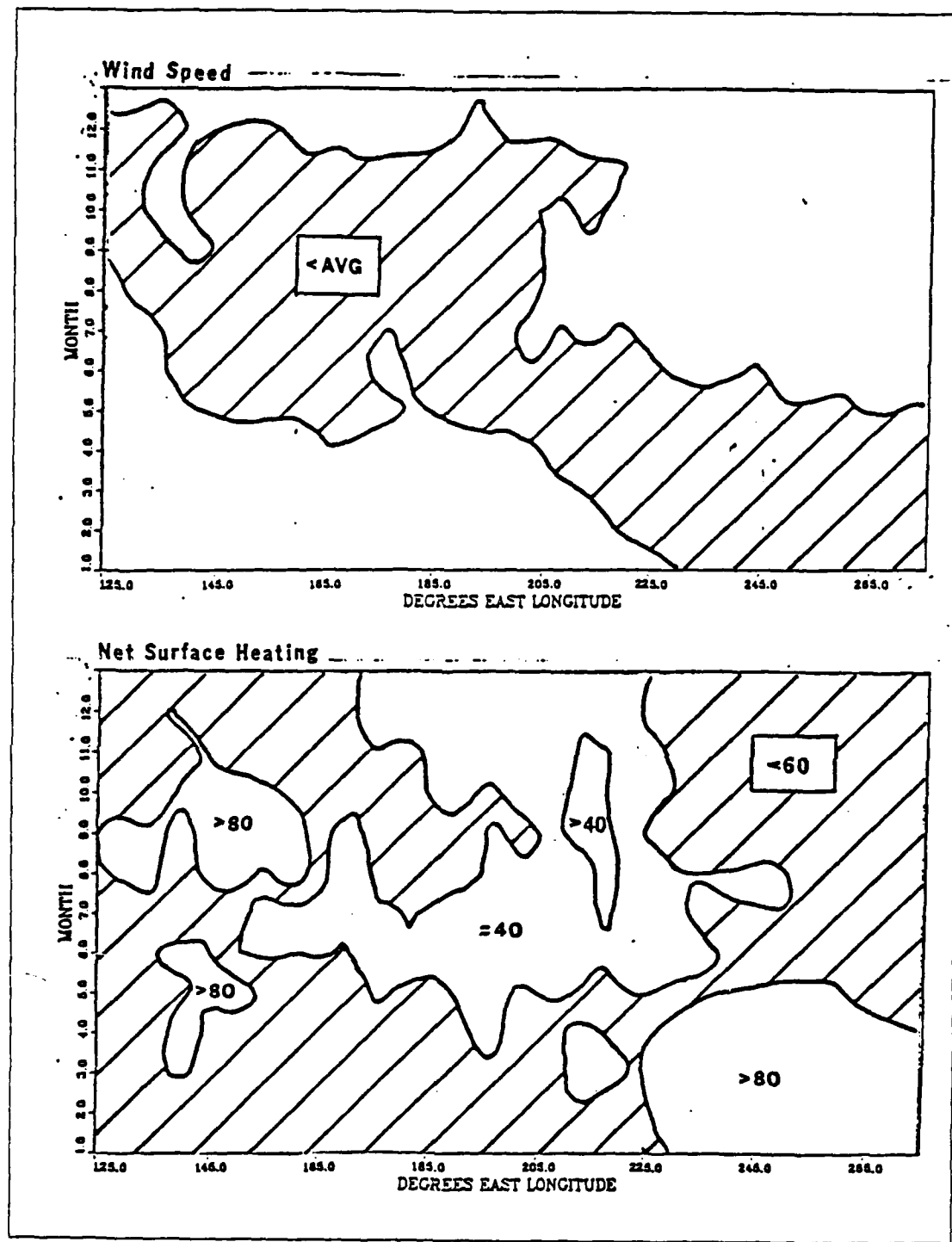


Fig. 3.15 A Seasonal Pattern of (a) Wind Speed and (b) Net Surface Heating in the Equatorial Pacific Ocean.

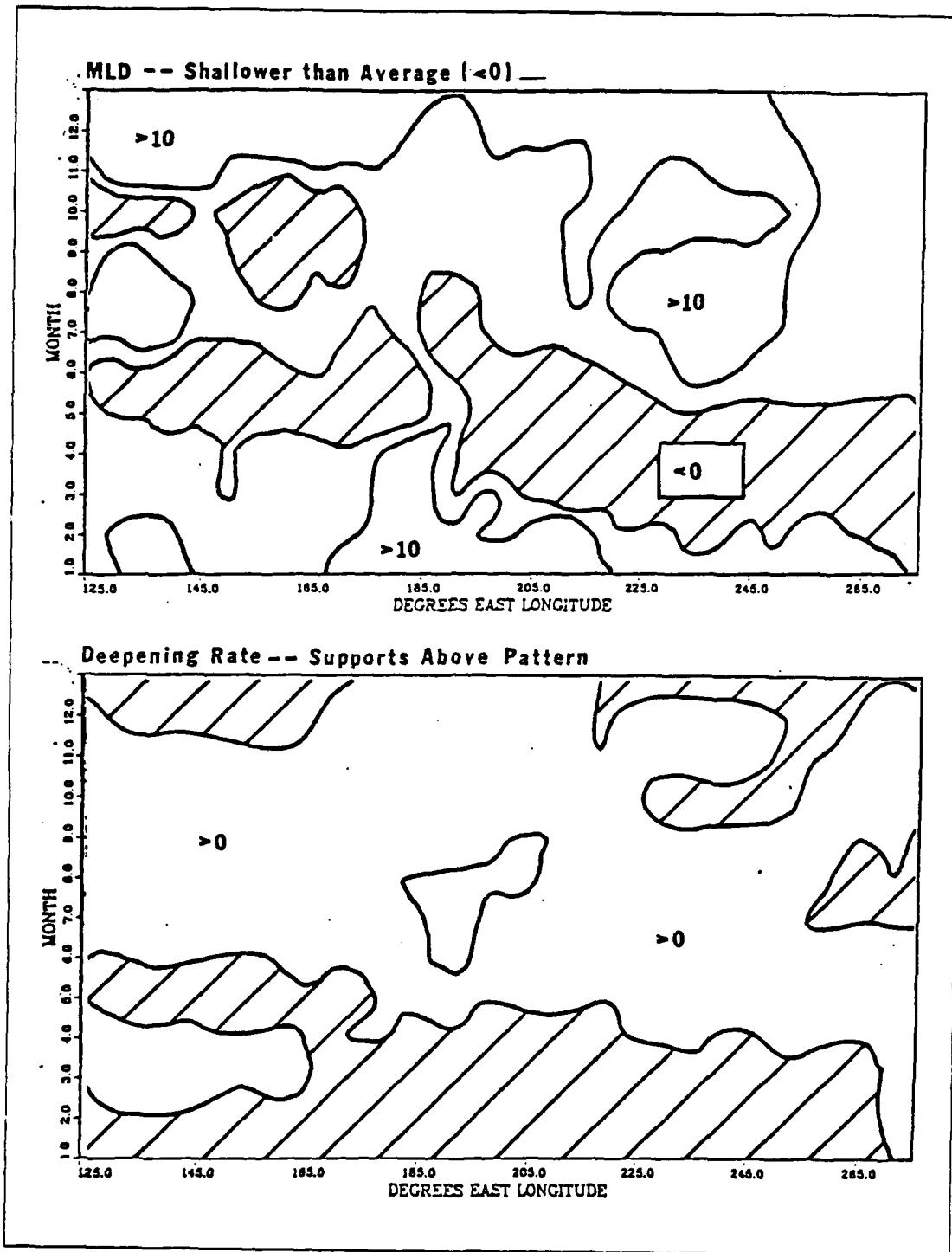


Fig. 3.16 A Seasonal Pattern of (a) Mixed Layer Depth and the (b) Time Rate of Mixed Layer Depth.

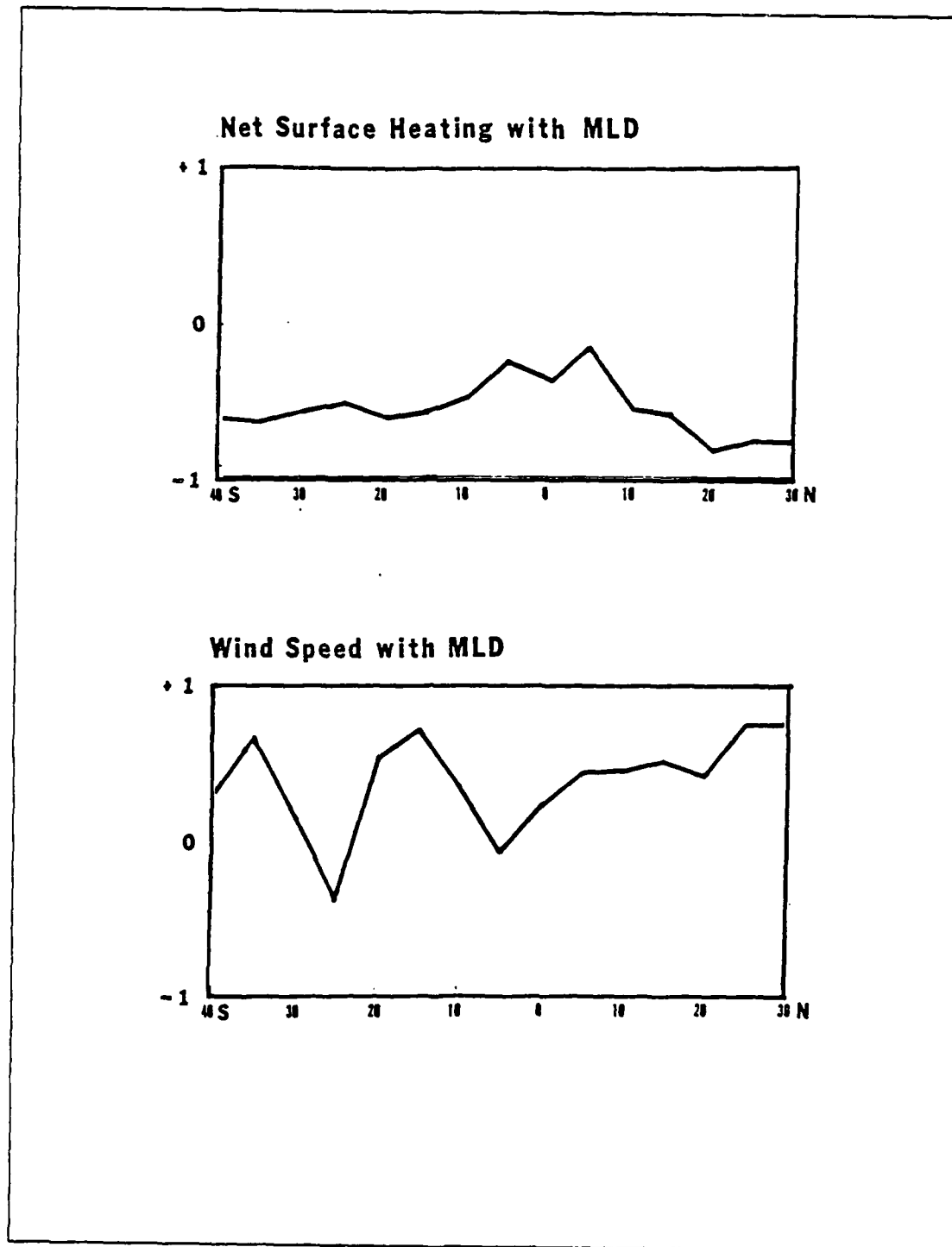


Fig. 3.17 Correlation Coefficients vs. Latitude along 155°E
 (a) Net Surface Heating and (b) Wind Speed with MLD.

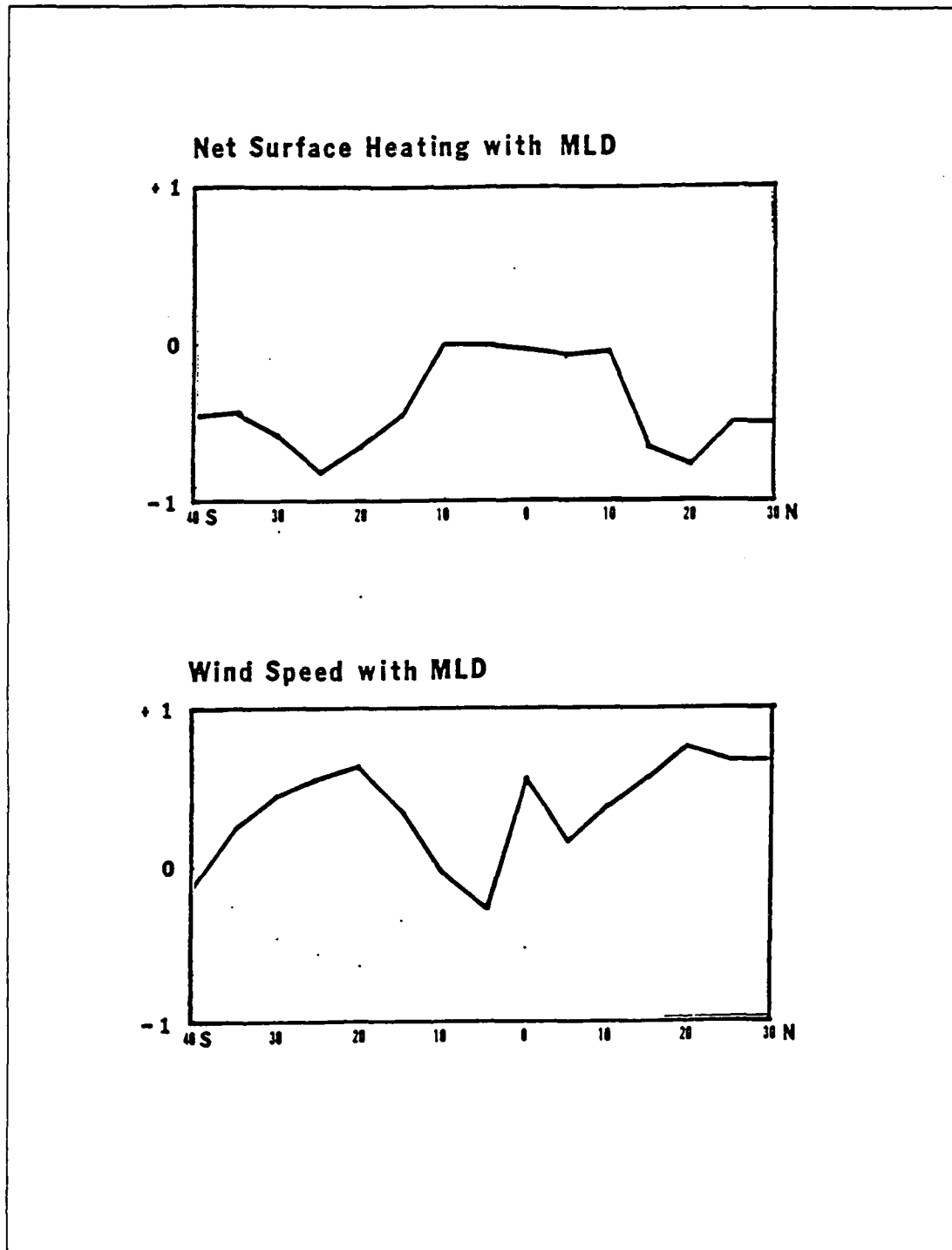


Fig. 3.18 Correlation Coefficients vs. Latitude along 155°W
 (a) Net Surface Heating and (b) Wind Speed with MLD.

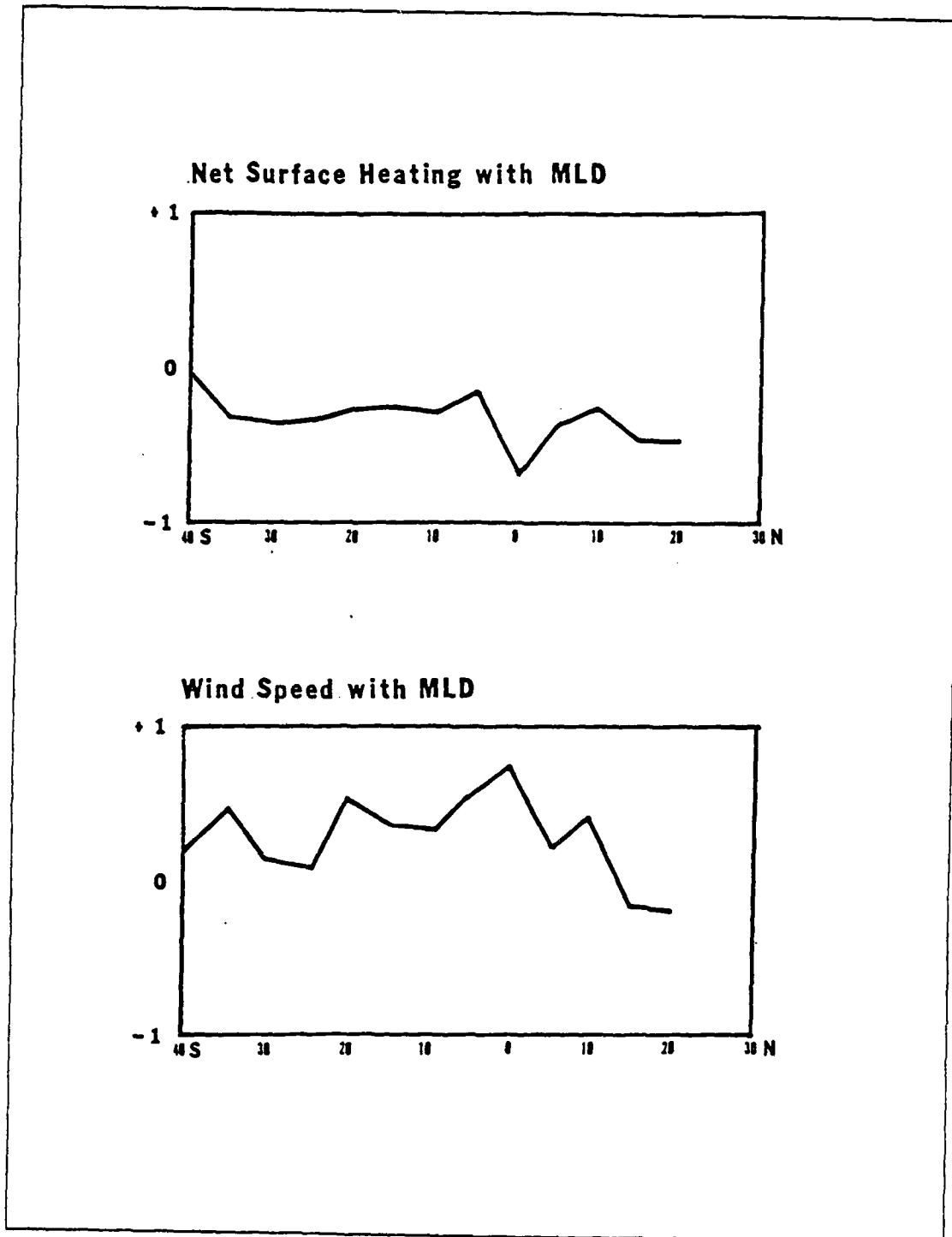


Fig. 3.19 Correlation Coefficients vs. Latitude along 105°W
 (a) Net Surface Heating and (b) Wind Speed with MLD.

D. THE VERTICAL INTEGRAL OF TEMPERATURE WITHIN THE SURFACE LAYER

The three dimensional temperature equation (eqn. 3.4) consists of the following terms on the RHS: the advection term (1), vertical diffusivity term (2), and horizontal diffusivity (3). In this analysis only the one dimensional case is considered, terms 1 and 3 are dropped.

$$\partial T / \partial t = -V \cdot \nabla T - \partial(\overline{T'W'}) / \partial z + A_h \nabla^2 T \quad (\text{eqn 3.4})$$

In equation 3.5 the vertical integral is taken over the surface layer and the temperature flux at the base of the surface layer is neglected.

$$\int \partial T / \partial t \partial z = -\overline{T'W'}_0 = Q_o / \rho C_p \quad (\text{eqn 3.5})$$

The temperature profiles in the areas under study have been numerically integrated to produce fields of the time rate of change of the heat content of the surface layer. These fields are shown in Fig. 3.20.

An indication of vertical advection, assuming horizontal advection and diffusivity are negligible, is obtained when the time rate of change of heat content in the surface layer is compared to the net heating at the ocean surface. The net surface heating is subtracted from the heat in the water column as shown in Fig. 3.21. If the difference is less than zero, then upwelling is assumed to account for the disparity in heat content and heat supply. Contoured diagrams similar to Fig. 3.21 were produced for 155W and 105W, but are not shown. A comparison of the three diagrams indicates that upwelling is stronger in the Eastern Pacific Ocean along 105W than it is along either the 155W or 155E meridian.

E. THE OBUKHOV MIXING LENGTH

The diagnostic depths of mixed layer retreat were computed using the atmospheric forcing data and equation 2.19. The depth of retreat is only a physically meaningful quantity when there is no active entrainment, and the surface heat flux is positive. When the net downward surface heat flux becomes very small or negative the mixing length becomes very large or negative, hence it retains no physical meaning. A standard value greater than 150 meters was inserted in the data matrices in place of

155 E
D/DT Q(WATER COLUMN)
(WATTS/METER²)

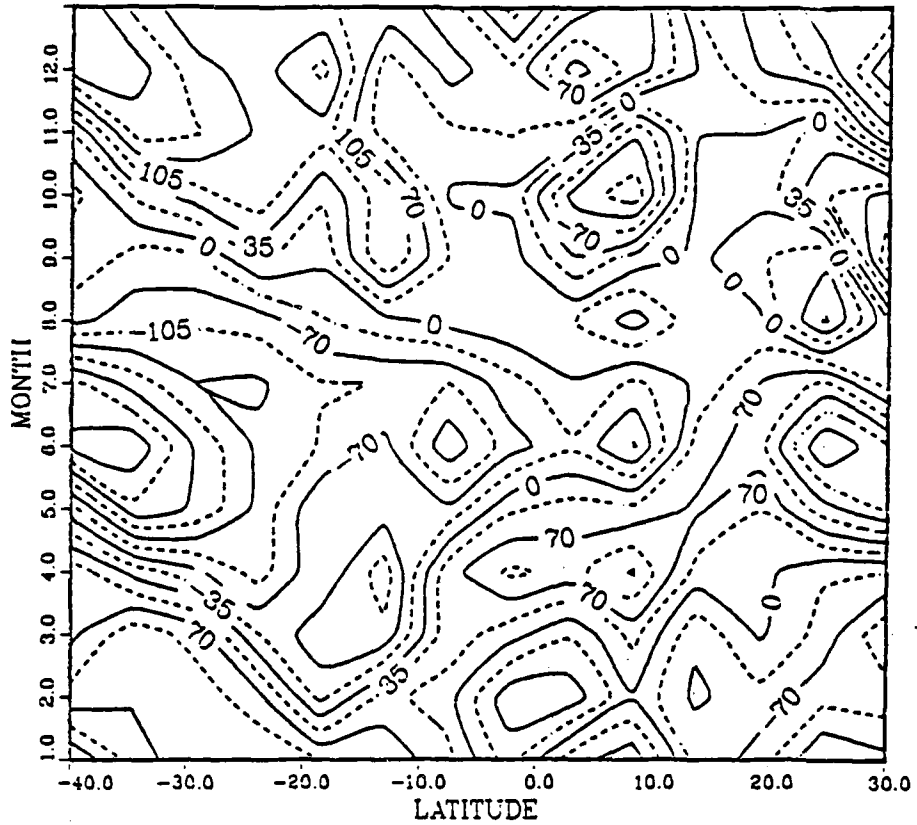


Fig. 3.20 Time Rate of Change of Heat in the Water Column
at 155 °E
Contour Interval is 35W/m²

155 E
 $Q(\text{WATER COLUMN}) - Q(\text{NET})$
(WATTS/METER²)

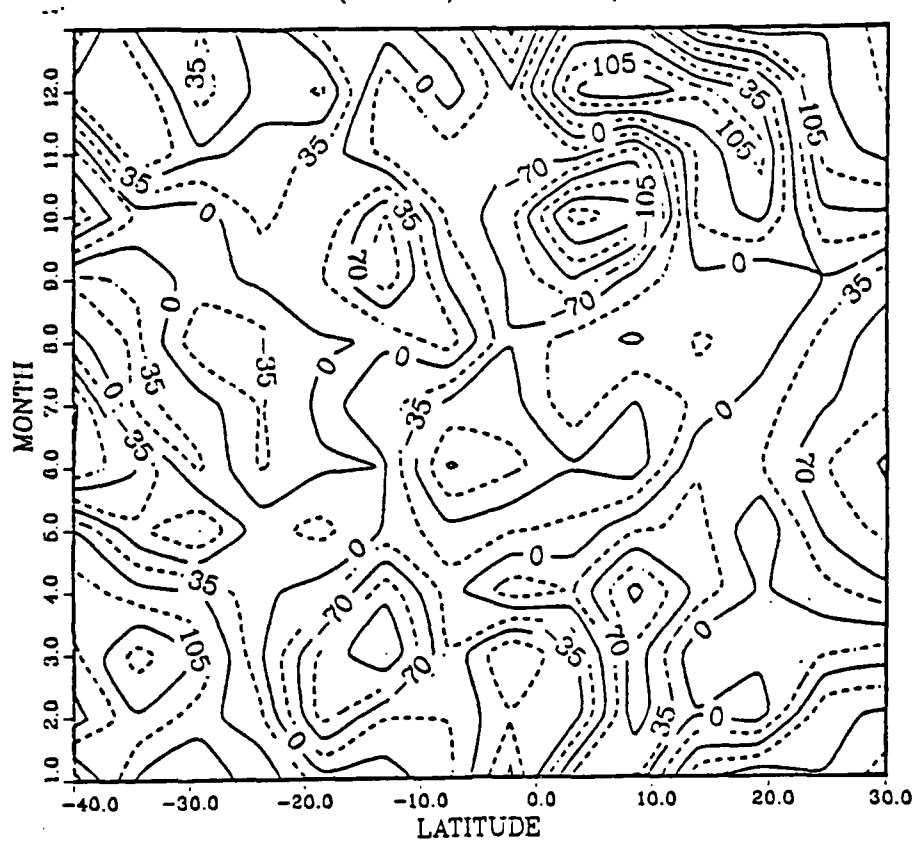


Fig. 3.21 Difference of Net Surface Heating and Heat in the Water Column at 155°E
Contour Interval is 35 W/m.²

those lengths having no physical meaning. This was done prior to contouring so that those regions at equilibrium would be unaffected by contouring problems.

The Obukhov mixing length fields are presented in Fig. 3.22, and a modified mixing scale (Garwood, et. al., 1985 a and b) and discussion are presented in Appendix D. The Obukhov mixing length fields show reasonable equilibrium depths in the tropical and subtropical parts, both north and south of the equator during the respective Summer times. All show equatorial depths that are either far too shallow or are not at equilibrium.

When the MLD is divided by the Obukhov length (producing an H/L ratio) for a given month and location, the fact that the subtropical summer regions reach a brief state of equilibrium is demonstrated more clearly. This ratio is presented in Figs. 3.23 through 3.26. Higher ratios are found along the equator. There is a large section in the eastern Pacific Ocean that does reach equilibrium (with ratios close to one), whereas in the western Pacific Ocean, the ratios are much higher. The results of this section are inconclusive in determining the role of advection in the seasonal adjustment of the mixed layer depth in the equatorial and tropical Pacific Ocean. Although inconclusive on the above stated point of inquiry, the Obukhov mixing length results do illustrate a successful attempt to relate two separate climatologies (one oceanic and the other atmospheric) with a conceptual model based on the physics of the mixed layer to produce a single additional piece of oceanographic information (MLD).

The H/L ratio presents the same information contained in the statistical approach using the correlation coefficients. The Obukhov length formulated in equation 2.11 is computed using the atmospheric forcing variables of wind speed and surface heating from Weare Marine Climatic Atlas (numerical version). The contours of Obukhov mixing length shown in Fig 3.22, within those regions at or approaching steady state from Fig. 3.11, nearly parallel those of MLD (h) in Fig. 3.10. The MLD was derived from the Bauer-Robinson Numerical Atlas. This modeling approach does not uniformly work well along the Equator from 10S to 10N. This region has H/L ratios of 5 or more as shown in Figs. 3.23 through 3.26.

155 E
OBUKHOV MIXING LENGTH)
(METERS)

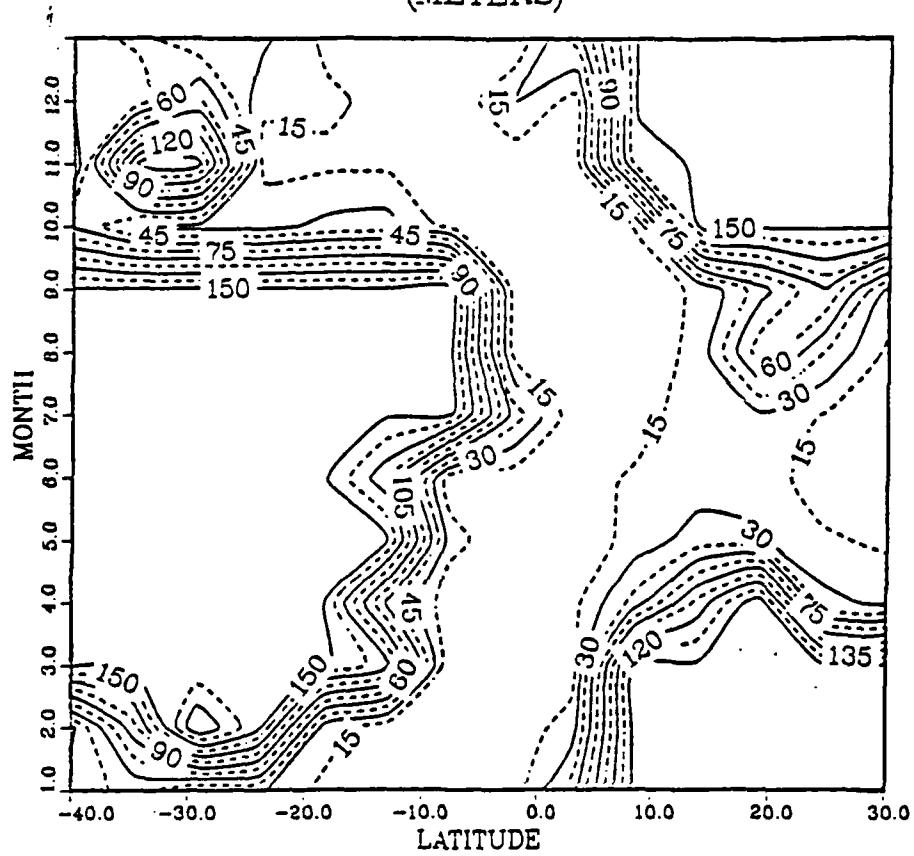


Fig. 3.22 Obukhov Mixing Length at 155 °E
Contour Interval is 15m.

155 E
H / OBUKHOV MIXING LENGTH
(RATIO)

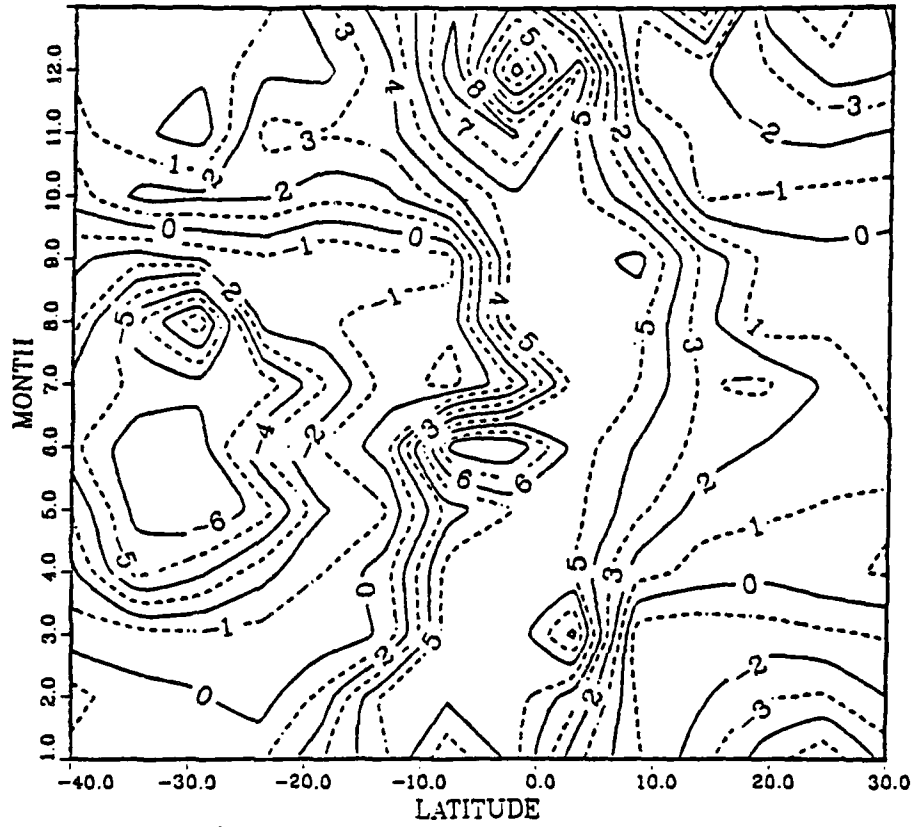


Fig. 3.23 Ratio of Mixed Layer Depth and Obukhov Mixing Length at 155 °E.

155 W
H / OBUKHOV MIXING LENGTH
(RATIO)

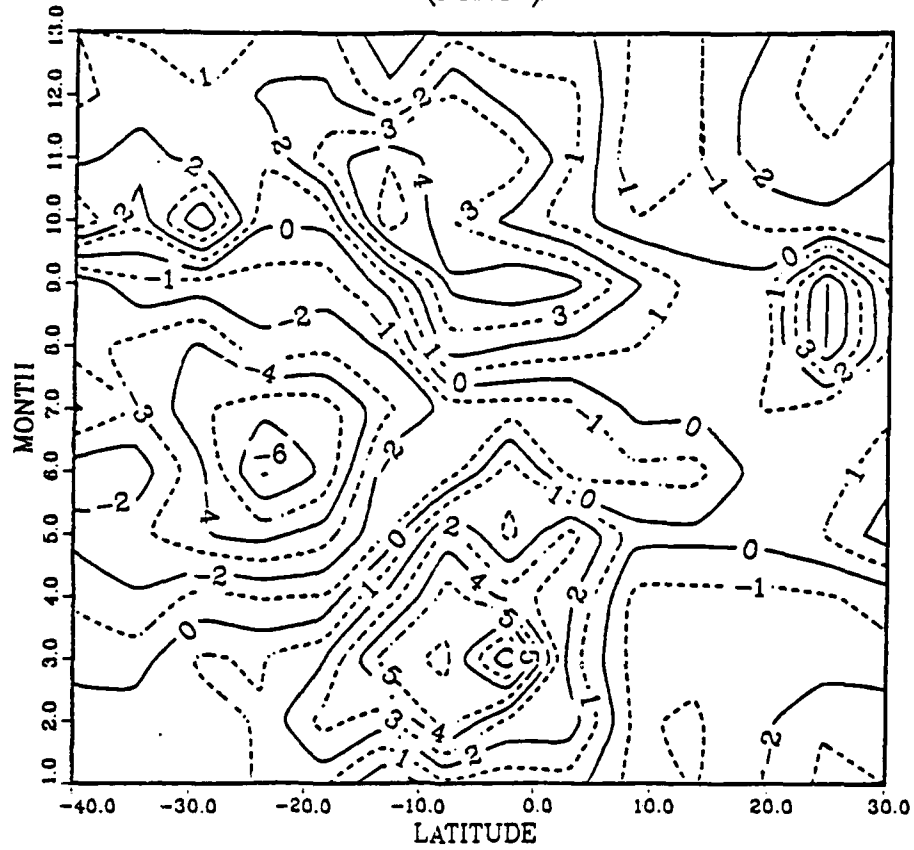


Fig. 3.24 Ratio of Mixed Layer Depth and Obukhov Mixing Length at 155 °W.

105 W
H / OBUKHOV MIXING LENGTH
(RATIO)

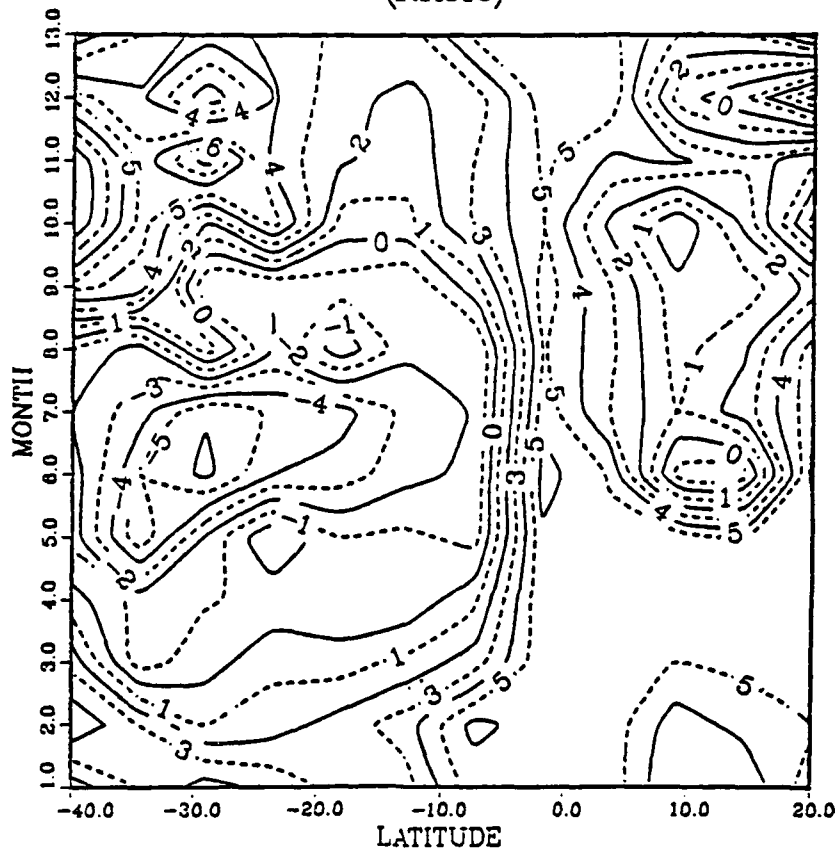


Fig. 3.25 Ratio of Mixed Layer Depth and
Obukhov Mixing Length at 105°W.

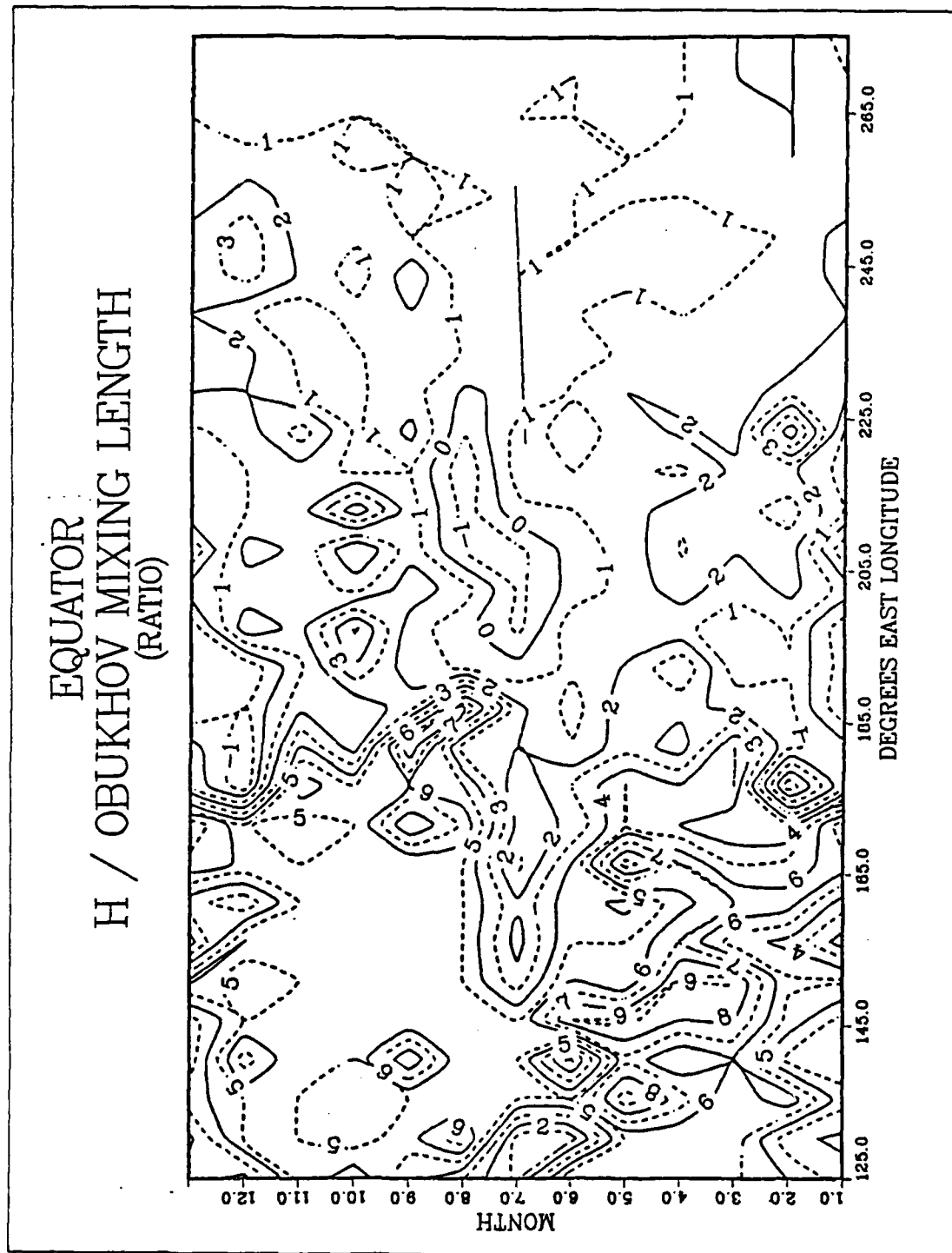


Fig. 3.26 Ratio of Mixed Layer Depth and Obukhov Mixing Length at the Equator.

IV. CONCLUSIONS

The difference in the resolution between the two climatologies must be considered when evaluating seasonal patterns in the area of study. The atmospheric forcing data, resolved on a five degree grid, is much coarser than the one degree grid on which the oceanic grid is resolved. The one degree grid of the oceanic data misses many of the most interesting seasonal variations along the Equator which occur on the scale of ± 25 km. A series of hand plotted temperature profiles were executed in the beginning of study to evaluate each of the numerical methods of determining mixed layer depth. The location of the temperature profiles varied from the subtropics and tropics to the equatorial regions in the east, central, and west of the area of study. It was stated by Levitus (1984) that, of the several methods of determining MLD from climatological data, no one method seemed superior to any other. It must be noted that the more interesting approach would have been to use temperature and salinity data together in a density defined MLD criterion. However, the lack of monthly salinity data (only annual values for each of the standard depths were available) precluded the use of this method.

A *careful* examination of the data obtained from the two climatologies does show close similarities in seasonal patterns. Although a measure of the relative strength of vertical advection is presented, it is difficult to establish that disparities in the patterns of forcing and oceanic response are caused by this advection. The use of statistical correlation coefficients verified the applicability of the conceptual model developed in Chapter Two in the tropics and subtropics at latitudes greater than 10S and 10N.

Three additional patterns were studied. The relationship between seasonal changes of the MLD and the seasonal changes in upwelling along the equator was established. A seasonal response of the mixed layer to seasonal changes in atmospheric forcing along the equator was also presented. The theory that enhancement of mixed layer deepening or shallowing can occur from interior vertical motion seems to be validated in those regions of the eastern and central Pacific Ocean where advection is strongest.

Clearly a need for more comprehensive and reliable climatological (large scale) data is demonstrated by this study. Because of the large variations in the quality of the

data within and between the two data sets, more advanced and complete statistical methods were not attempted. Instead graphical patterns were examined to establish seasonal relationships. Future large scale studies, such as the one attempted here, will require much more detailed and accurate observational data sets so that the patterns that have been shown to be graphically evident can receive meaningful statistical validation. This suggests an avenue for future investigation. The use of the Obukhov mixing length and MLD to Obukhov mixing length ratios (in a modeling approach) is equally well suited for this purpose and has been, to a large extent, successful in this study. The use of an expanded area analysis (vice the use of meridians) is necessary to fully examine and test the application of mixed layer physics in the calculation of climatological mixed layer depths (on a seasonal time scale) for large parts of the world ocean. To accomplish this in the equatorial regions, a much more finely resolved (in both space and time) oceanic data set is required on a grid at least one order of magnitude more dense than the one used in this study. The results of this study suggest that the seasonal time scale is not the most appropriate framework within which to examine mixed layer response to atmospheric forcing very near the Equator.

This study is unique since it initially involved a broad investigation of oceanic and atmospheric climatological data sources. The study then successfully synthesized the two distinct data sources, using mixed layer physics and tested these results using a conceptual model of the ocean mixed layer, into a second generation source of climatological data. The original motivation for this study was to make this synthesized information available to the numerical modeler. Unfortunately, the utility of this synthesized climatological information is limited due to the coarse resolution of the original climatologies. This suggests that the horizons of oceanographic modeling are expanding and outpacing our ability to reliably modify and verify models against accurate and detailed observational data. Studies like this one illustrate the need for a comprehensive world ocean data set that is absolute in coverage and fine in resolution (in both time and space). Sampling requirements for future large scale observational expeditions should include salinity measurements taken at the same time and space intervals as the more easily obtained temperature and pressure measurements. Endeavors such as the World Ocean Circulation Experiment (WOCE) are crucially important to the future of physical oceanography.

APPENDIX A

MERIDIONAL SECTIONS OF TEMPERATURE

The following meridional sections of temperature (Figs. A.1 - A.7) were extracted from the Bauer-Robinson Numerical Atlas during the initial stages of this study. The individual data arrays were useful in testing the several methods of determining MLD discussed in Chapter II. These figures are included in this appendix because they further illustrate the westward sloping equatorial thermocline and provide additional descriptive detail to the area of study.

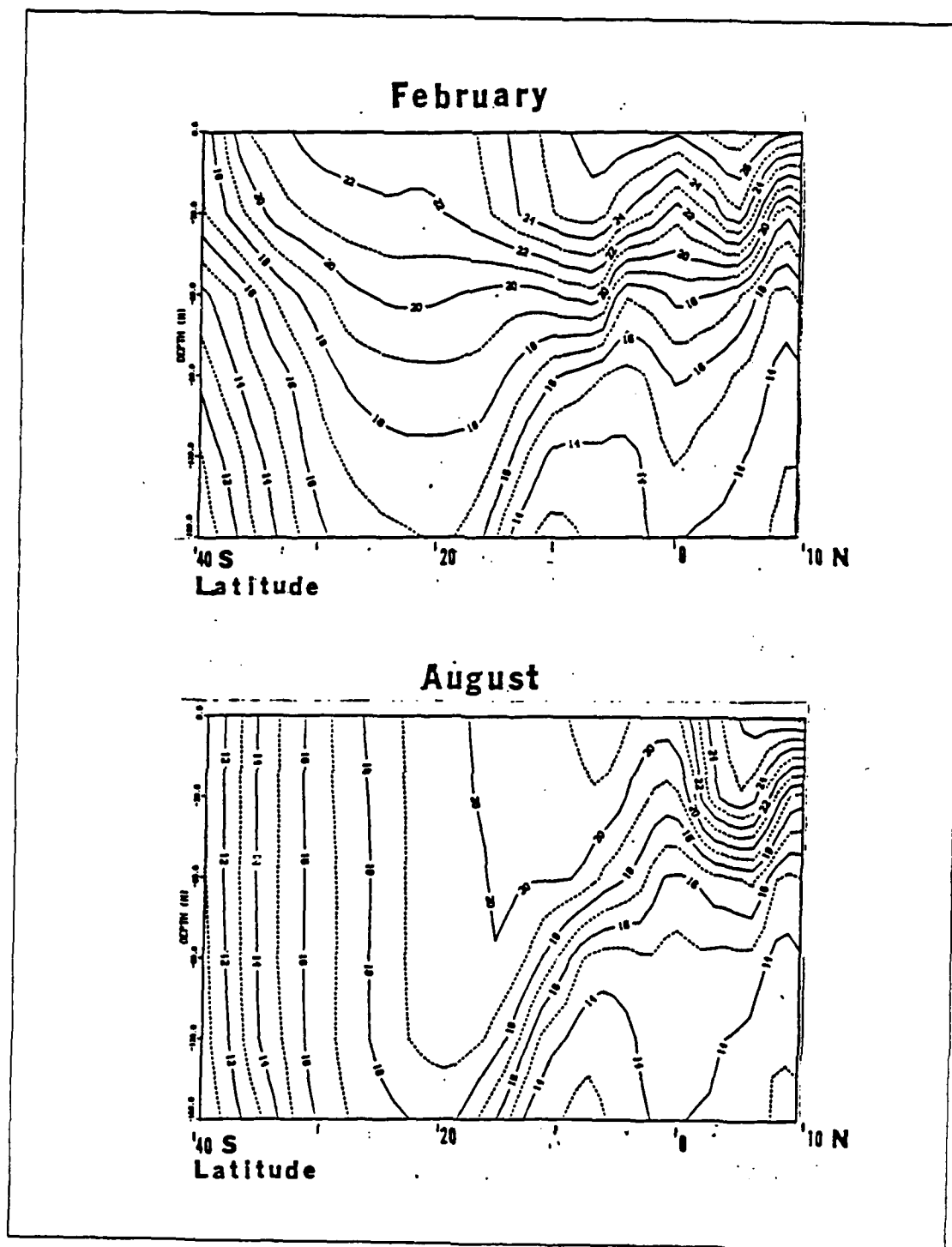


Fig. A.1 Meridional Sections of Temperature ($^{\circ}\text{C}$)
at 90°W for (a) February and (b) August.

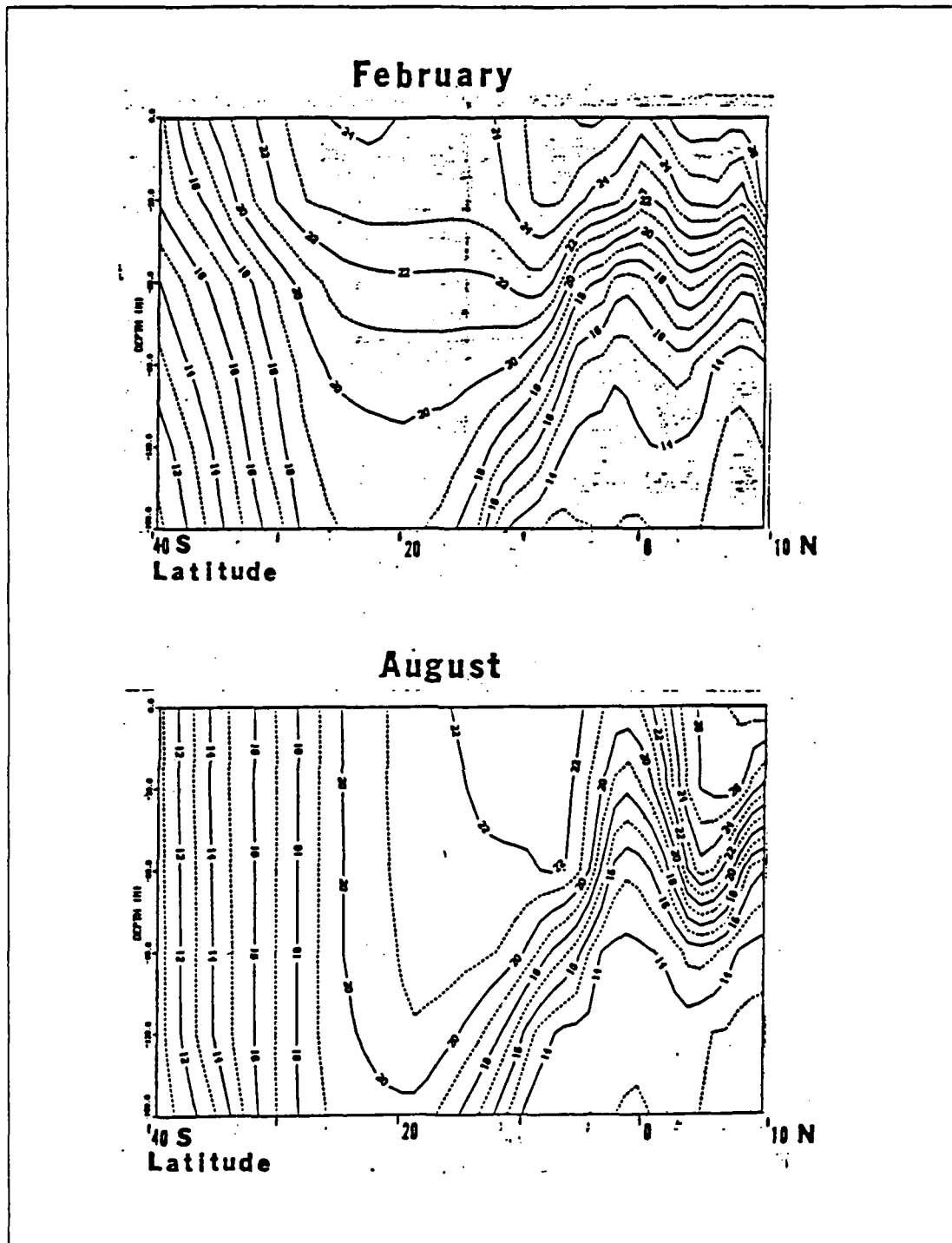


Fig. A.2 Meridional Sections of Temperature ($^{\circ}\text{C}$) at 100°W for (a) February and (b) August.

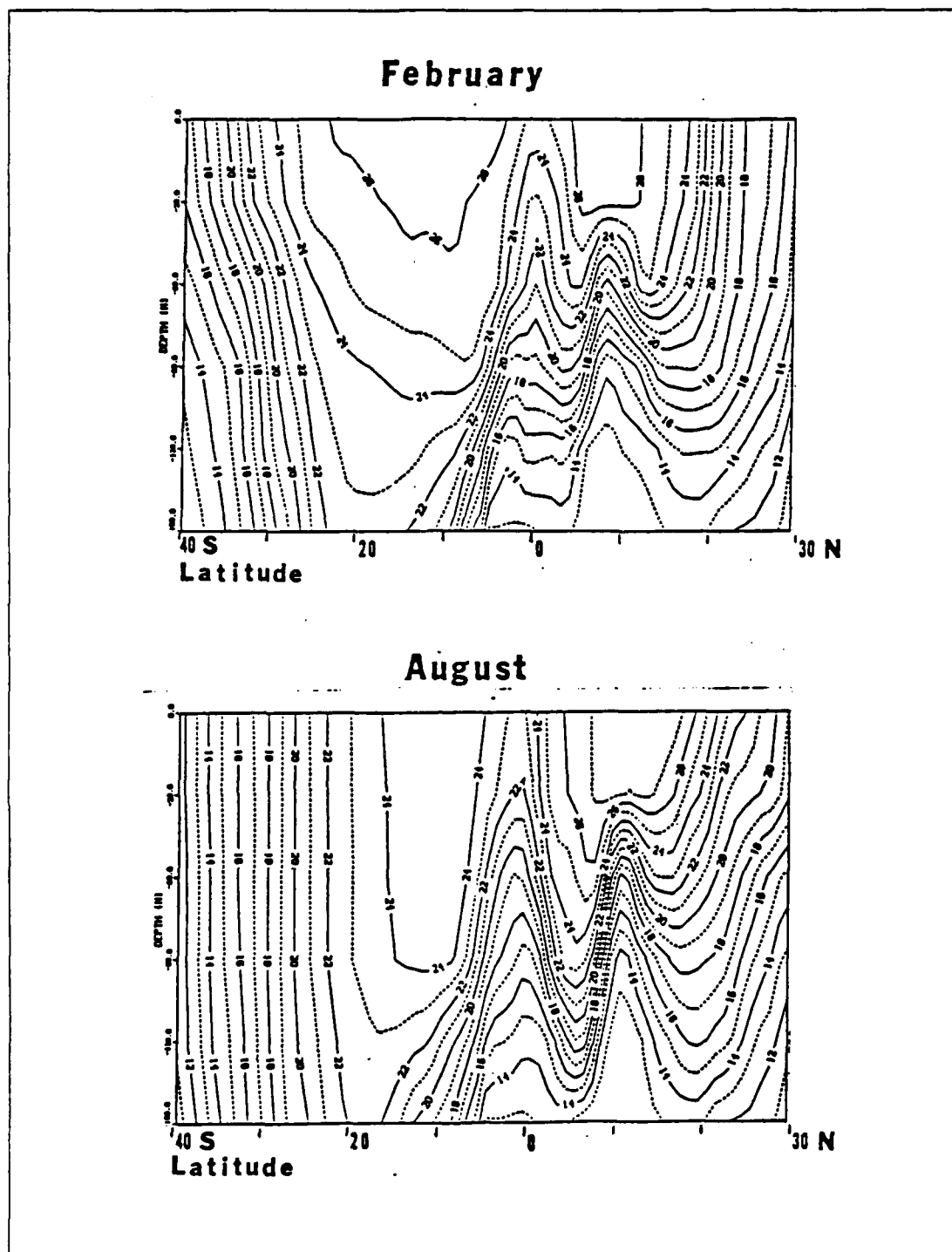


Fig. A.3 Meridional Sections of Temperature ($^{\circ}\text{C}$) at 120°W for (a) February and (b) August.

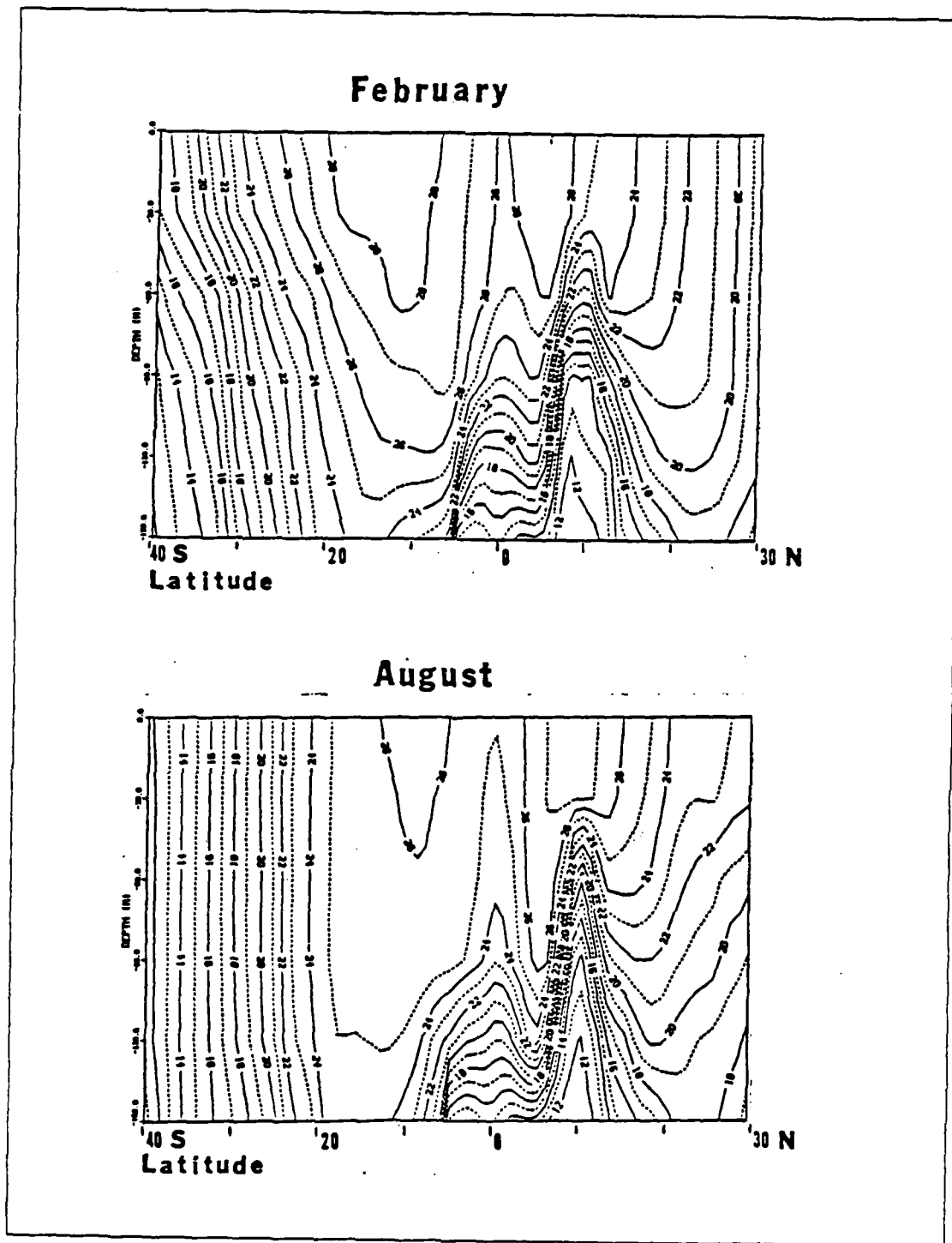


Fig. A.4 Meridional Sections of Temperature ($^{\circ}\text{C}$)
at 140°W for (a) February and (b) August.

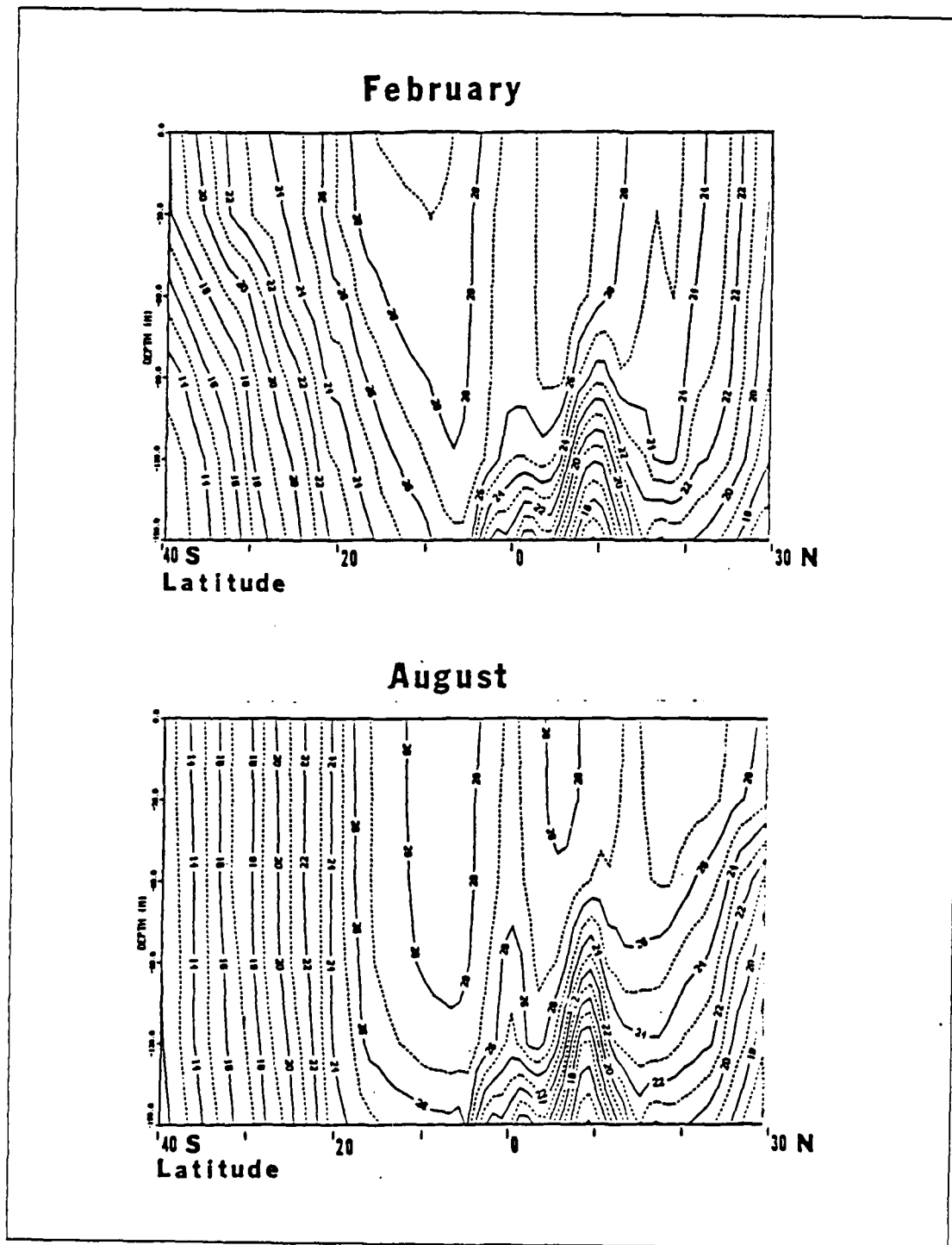


Fig. A.5 Meridional Sections of Temperature ($^{\circ}\text{C}$) at 170°W for (a) February and (b) August.

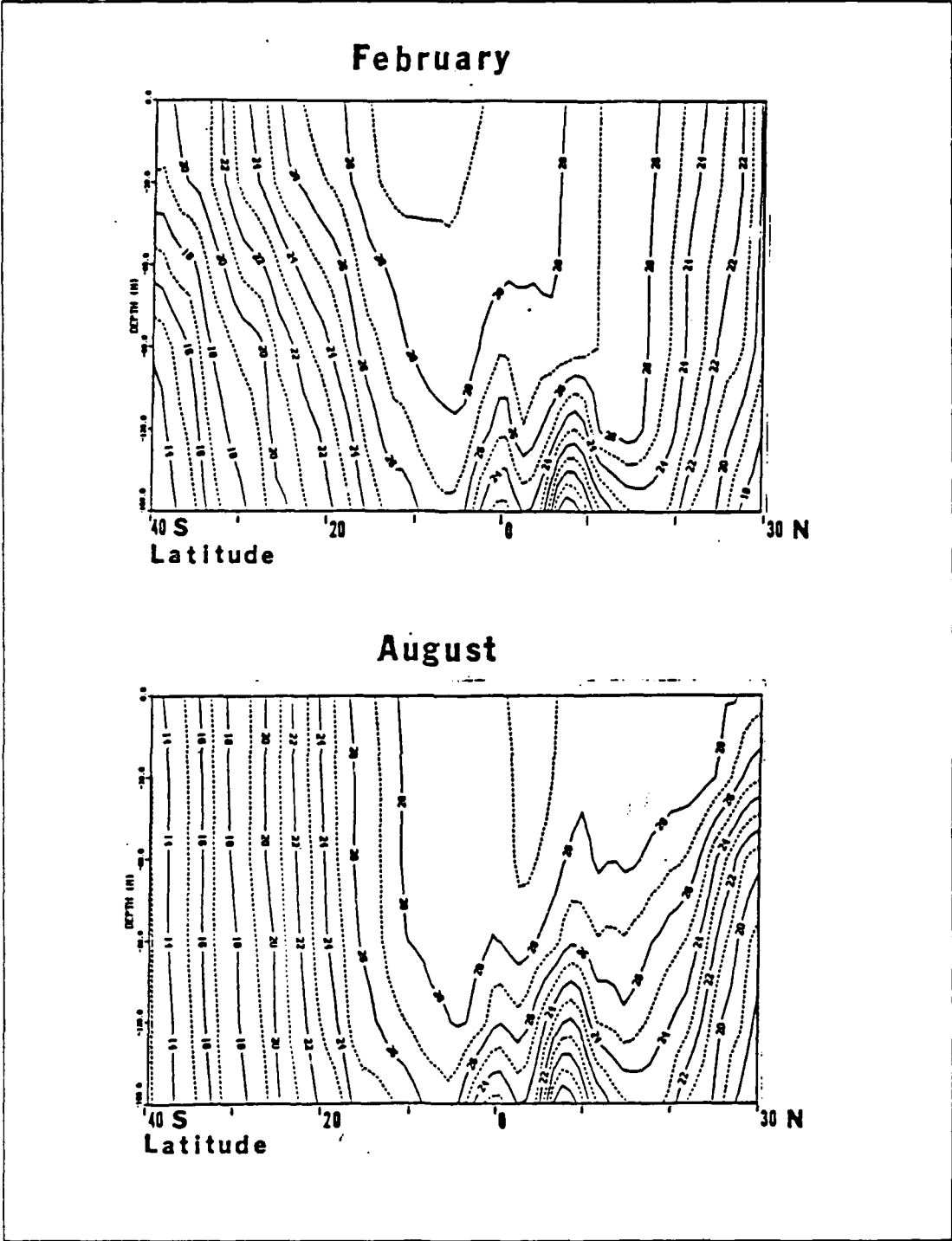


Fig. A.6 Meridional Sections of Temperature ($^{\circ}\text{C}$) at 170°E for (a) February and (b) August.

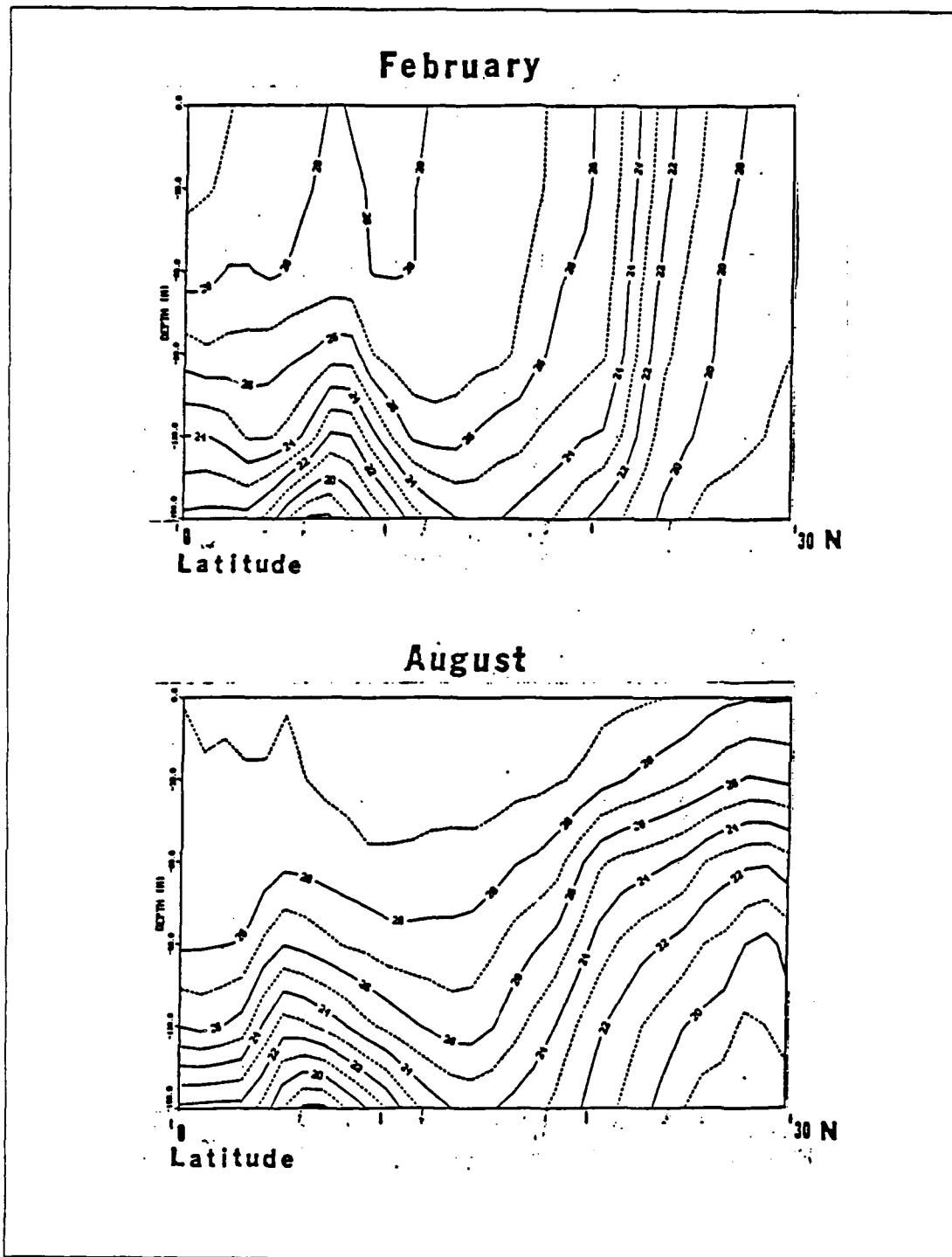


Fig. A.7 Meridional Sections of Temperature ($^{\circ}\text{C}$) at 140°E for (a) February and (b) August.

APPENDIX B

MONTHLY MLD CONTOURS

The monthly contours of MLD that follow were numerically extracted and processed within the micro-computer environment of the IBM-PC AT[™]. The resolution of the MLD contours is one degree of latitude by one degree of longitude and each field contains 12,496 data points.

JANUARY
MIXED LAYER DEPTH
(METERS)

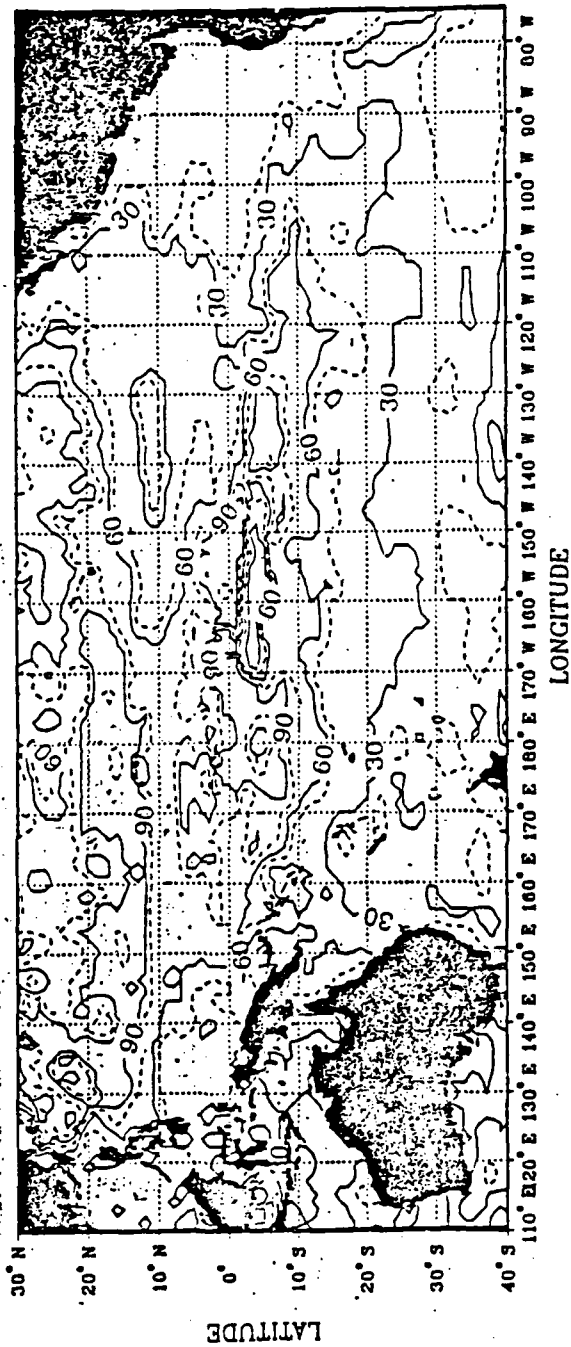


Fig. B.1 January Mixed Layer Depth.

FEBRUARY
MIXED LAYER DEPTH
(METERS)

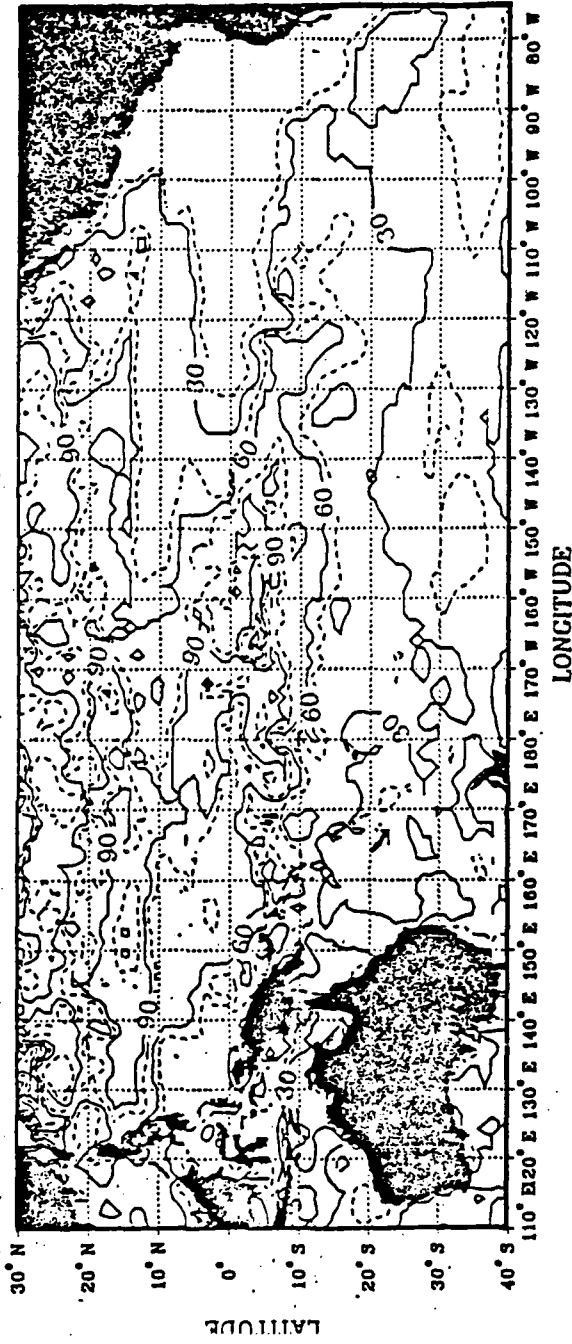


Fig. B.2 February Mixed Layer Depth.

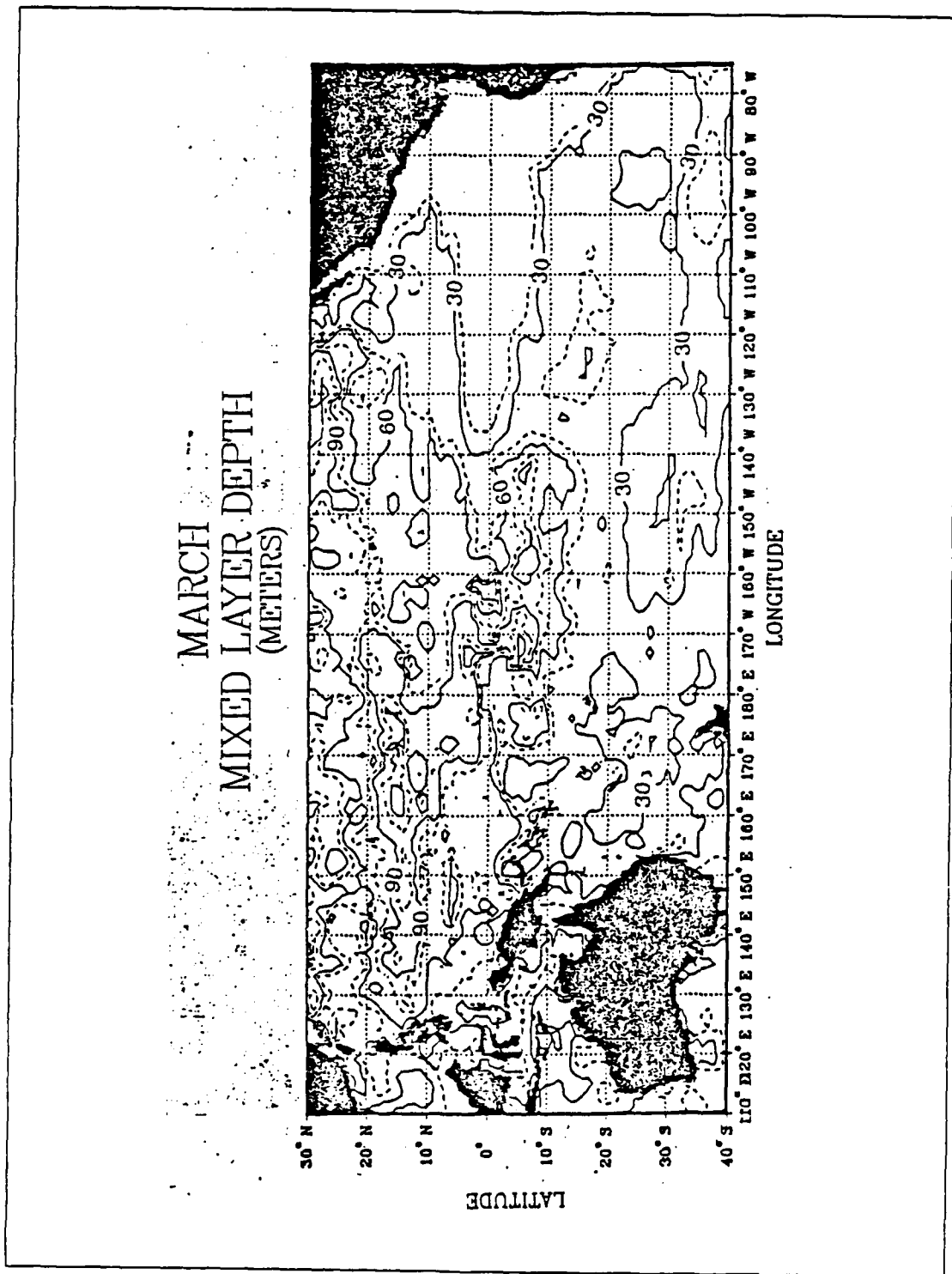


Fig. B.3 March Mixed Layer Depth.

APRIL
MIXED LAYER DEPTH
(METERS)

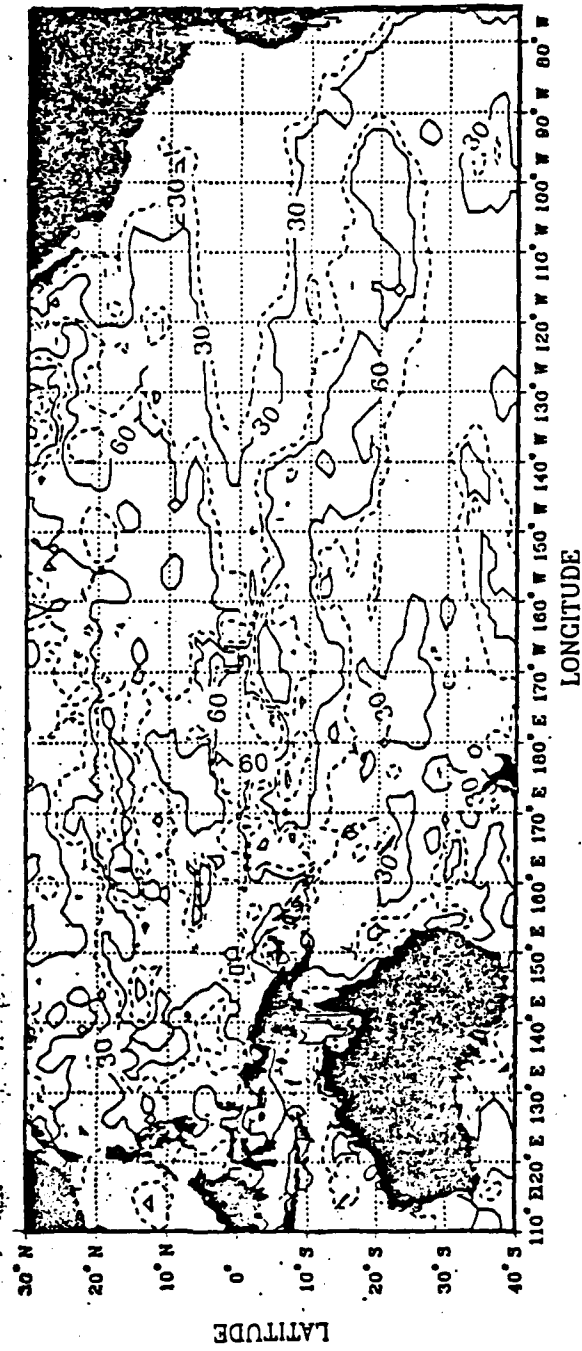


Fig. B.4 April Mixed Layer Depth.

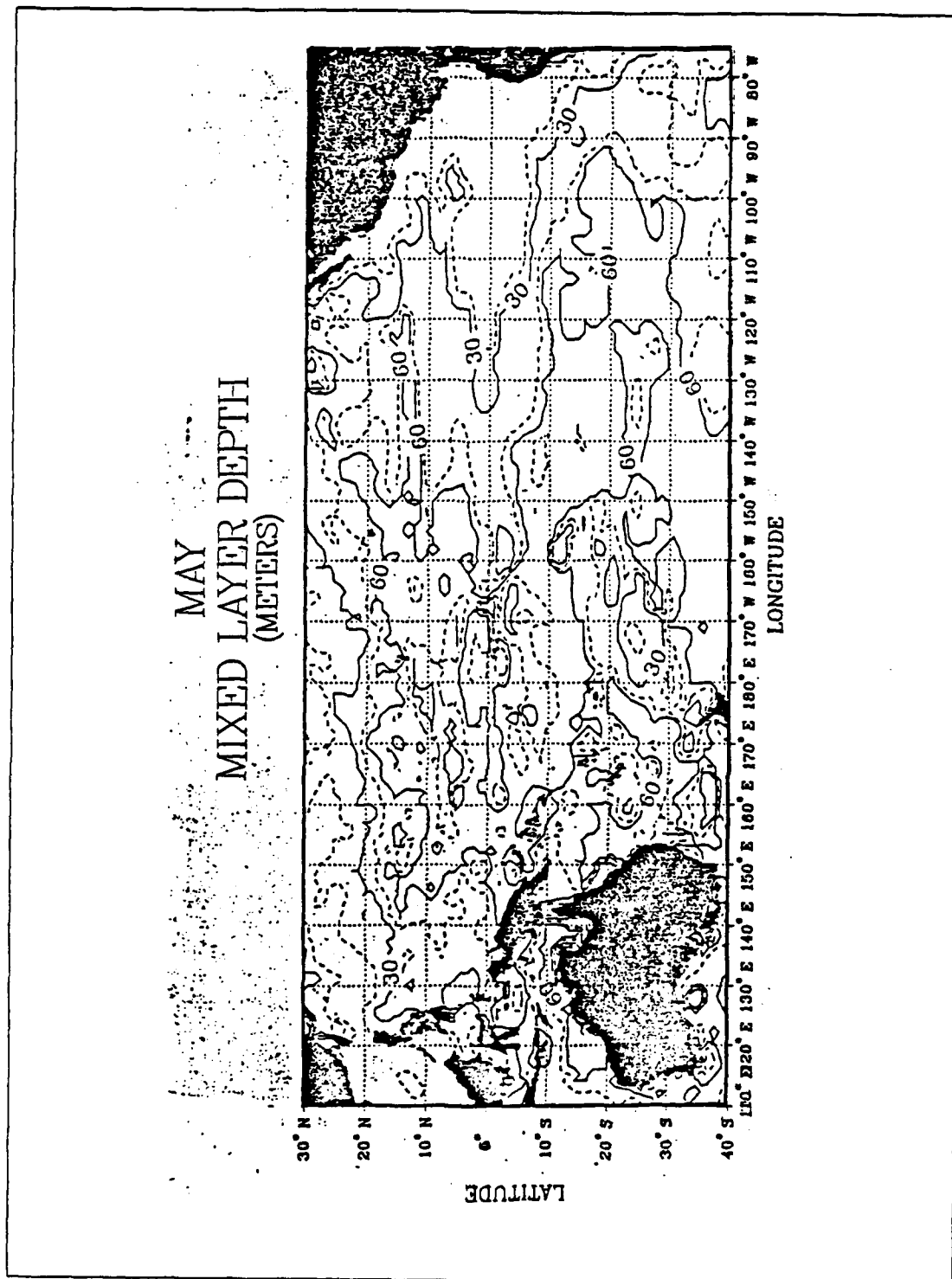


Fig. B.5 May Mixed Layer Depth.

JUNE
MIXED LAYER DEPTH
(METERS)

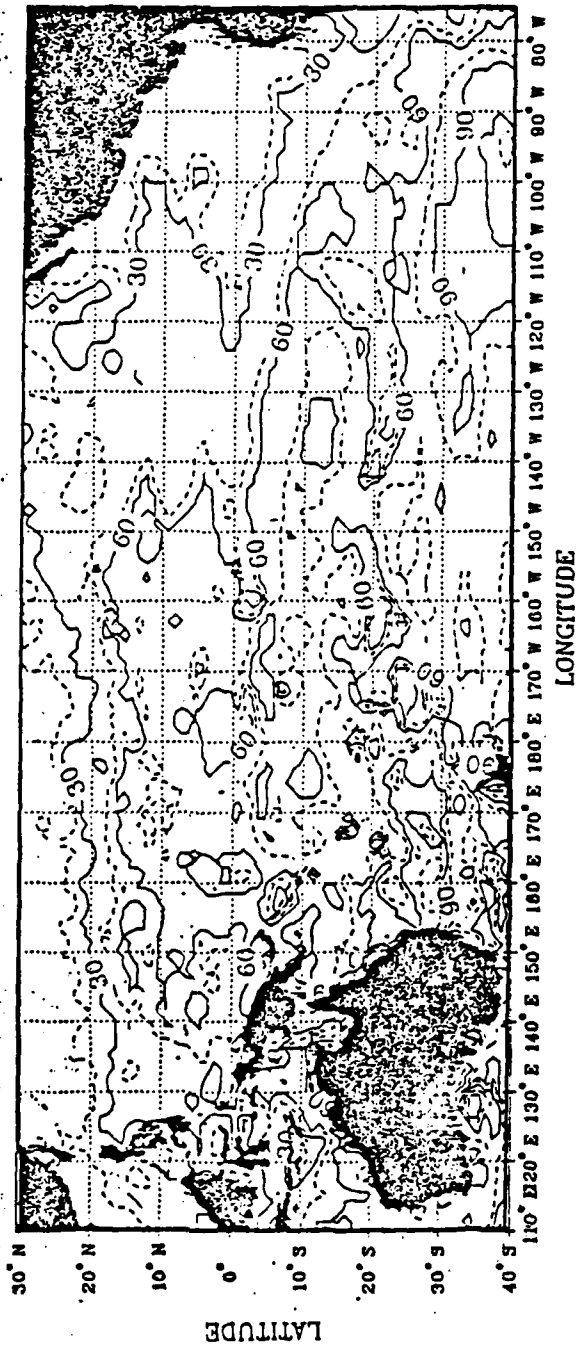


Fig. B.6 June Mixed Layer Depth.

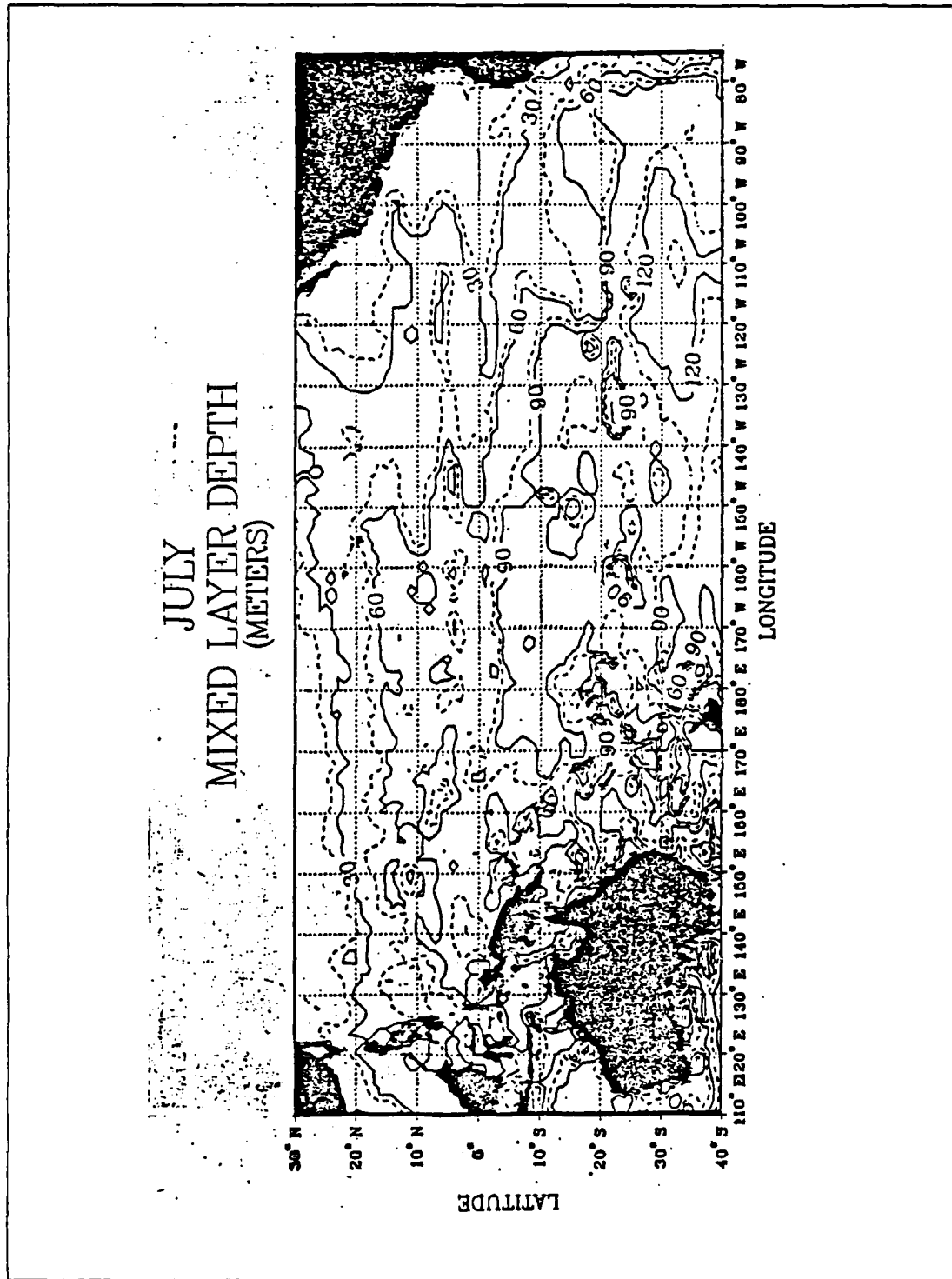


Fig. B.7 July Mixed Layer Depth.

AUGUST
MIXED LAYER DEPTH
(METERS)

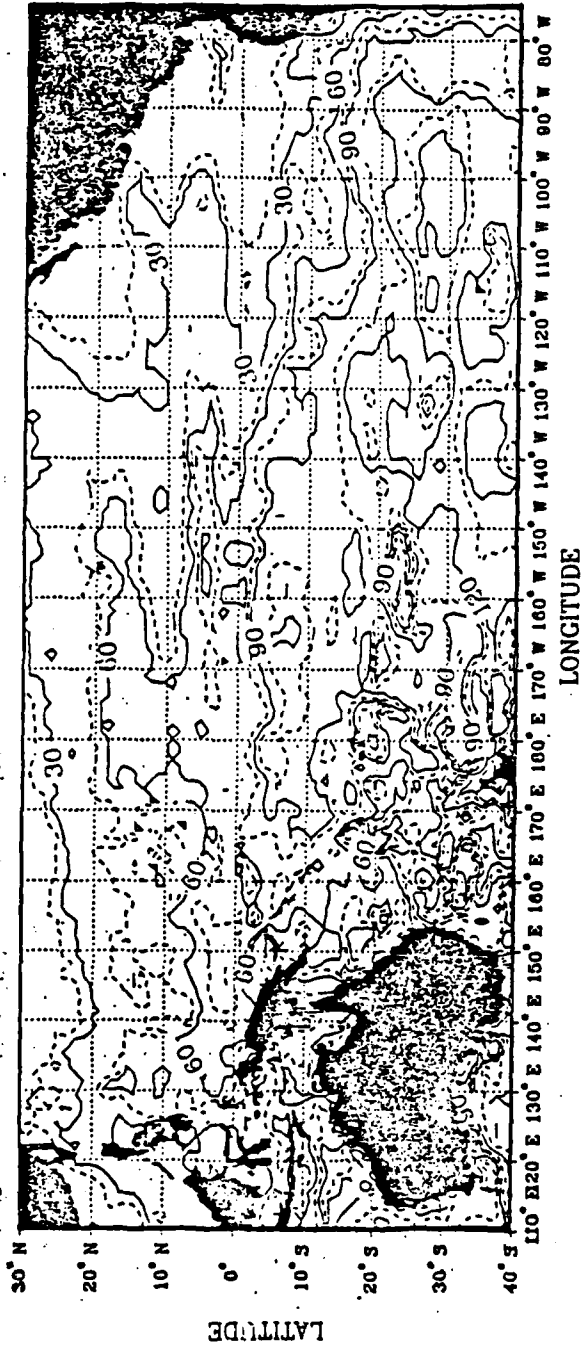


Fig. B.8 August Mixed Layer Depth.

SEPTEMBER
MIXED LAYER DEPTH
(METERS)

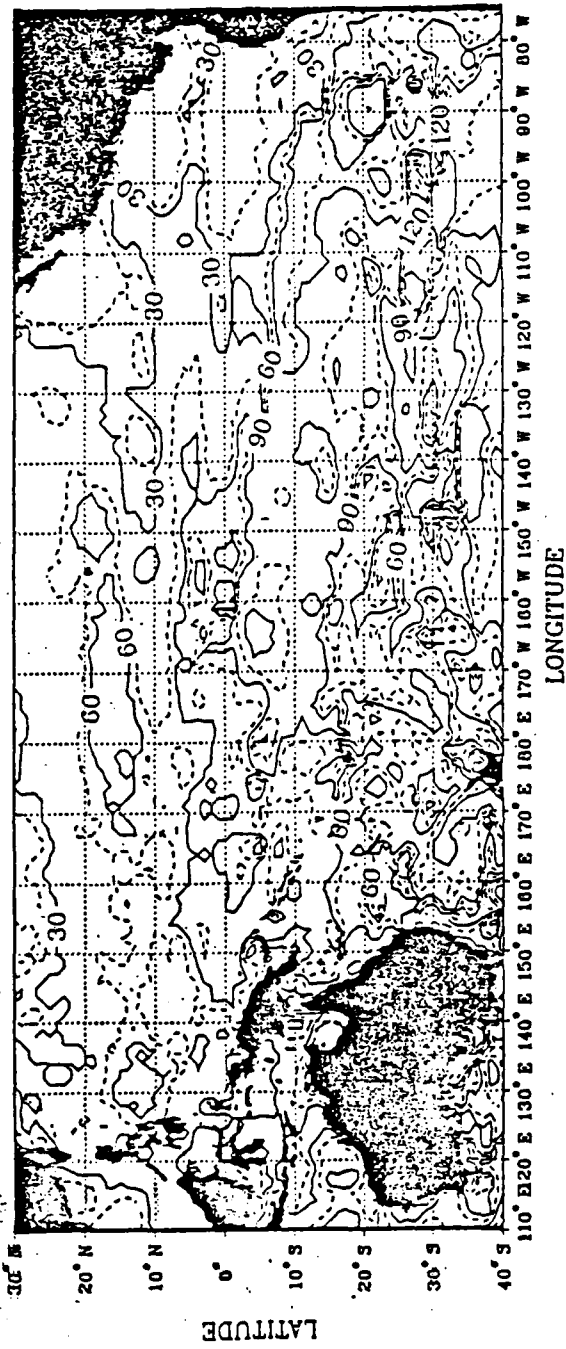


Fig. B.9 September Mixed Layer Depth.

OCTOBER
MIXED LAYER DEPTH
(METERS)

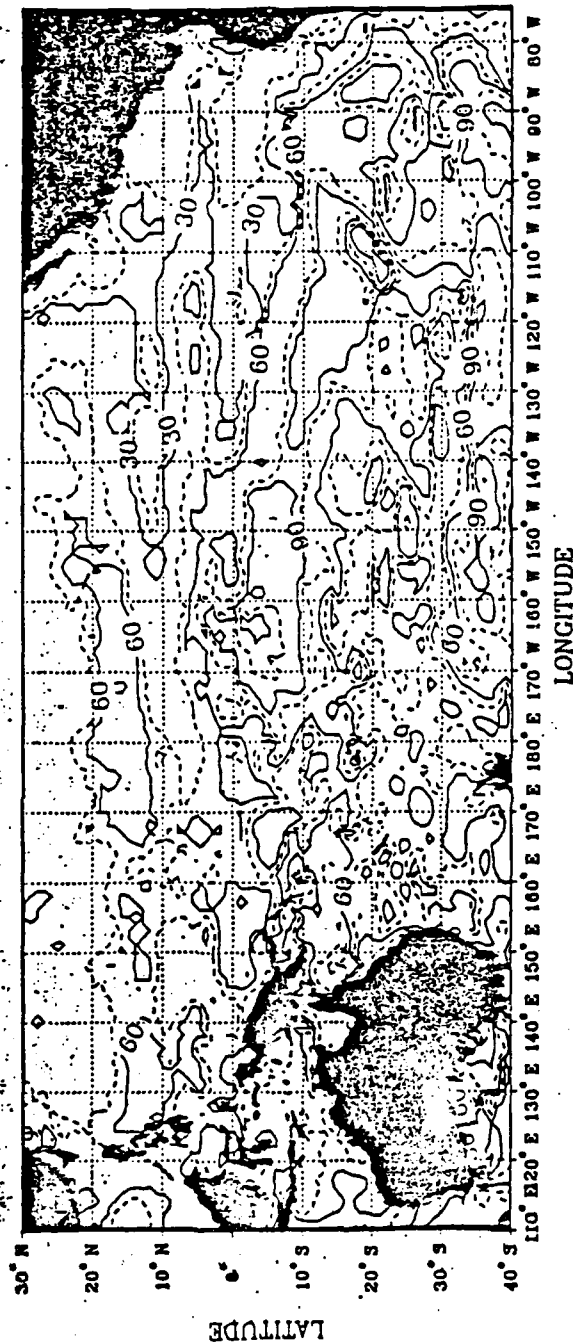


Fig. B.10 October Mixed Layer Depth.

NOVEMBER
MIXED LAYER DEPTH
(METERS)

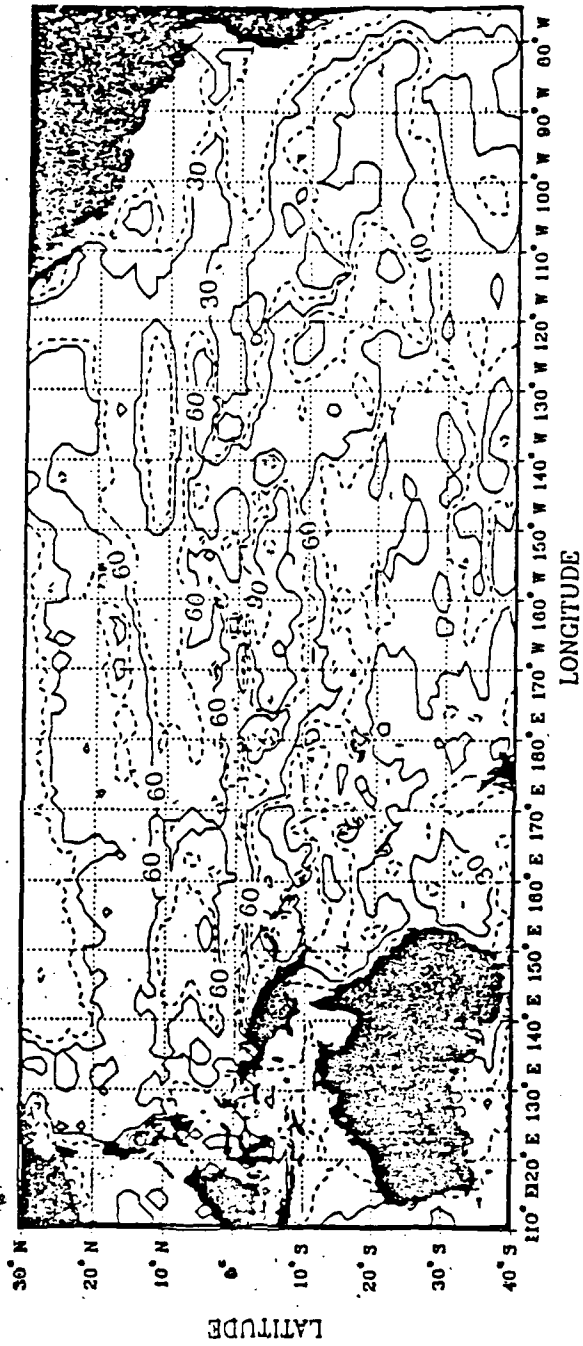


Fig. B.11 November Mixed Layer Depth.

DECEMBER
MIXED LAYER DEPTH
(METERS)

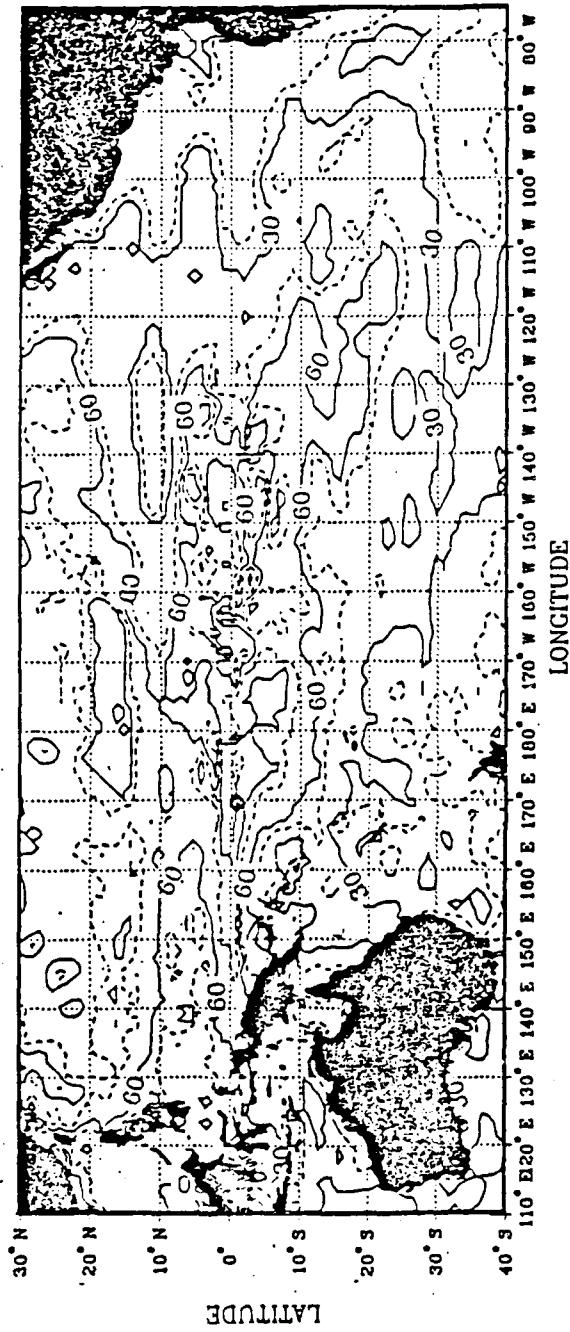


Fig. B.12 December Mixed Layer Depth.

APPENDIX C

ENHANCEMENT OF DEEPENING AND SHALLOWING OF MLD

The theory that a strong enhancement of mixed layer cooling and deepening can result from upwelling between the heating and cooling seasons (Muller, Garwood, and Garner, 1983) is tested in the composite diagram, Figs. C.1,C.2,C.3. In figure C.2 a, the clear areas (non-cross-hatched) are those areas where upwelling is indicated from Figs. 3.21. Downwelling is indicated by the cross-hatched areas. The lines containing the star symbol are the lines of zero net surface heating indicating a transition between surface heating and cooling. In Fig. C.2 b, the corresponding field of mixed layer depth contains areas of probable enhancement of deepening or shallowing that are indicated within an ellipse. The mixed layer depth contour contained within the ellipse occurs over a transitional zone and shows an indication of enhanced deepening or shallowing by its shape. That is to say, there is an obvious protrusion of the contour line. In the Western Pacific Ocean (Fig. C.1), enhanced deepening and shallowing is not as prevalent as it is in the Eastern Pacific Ocean, where upwelling and downwelling may be much stronger. These results tend to verify the theory presented in Muller, Garwood, and Garner (1983) using climatological data on a seasonal time scale.

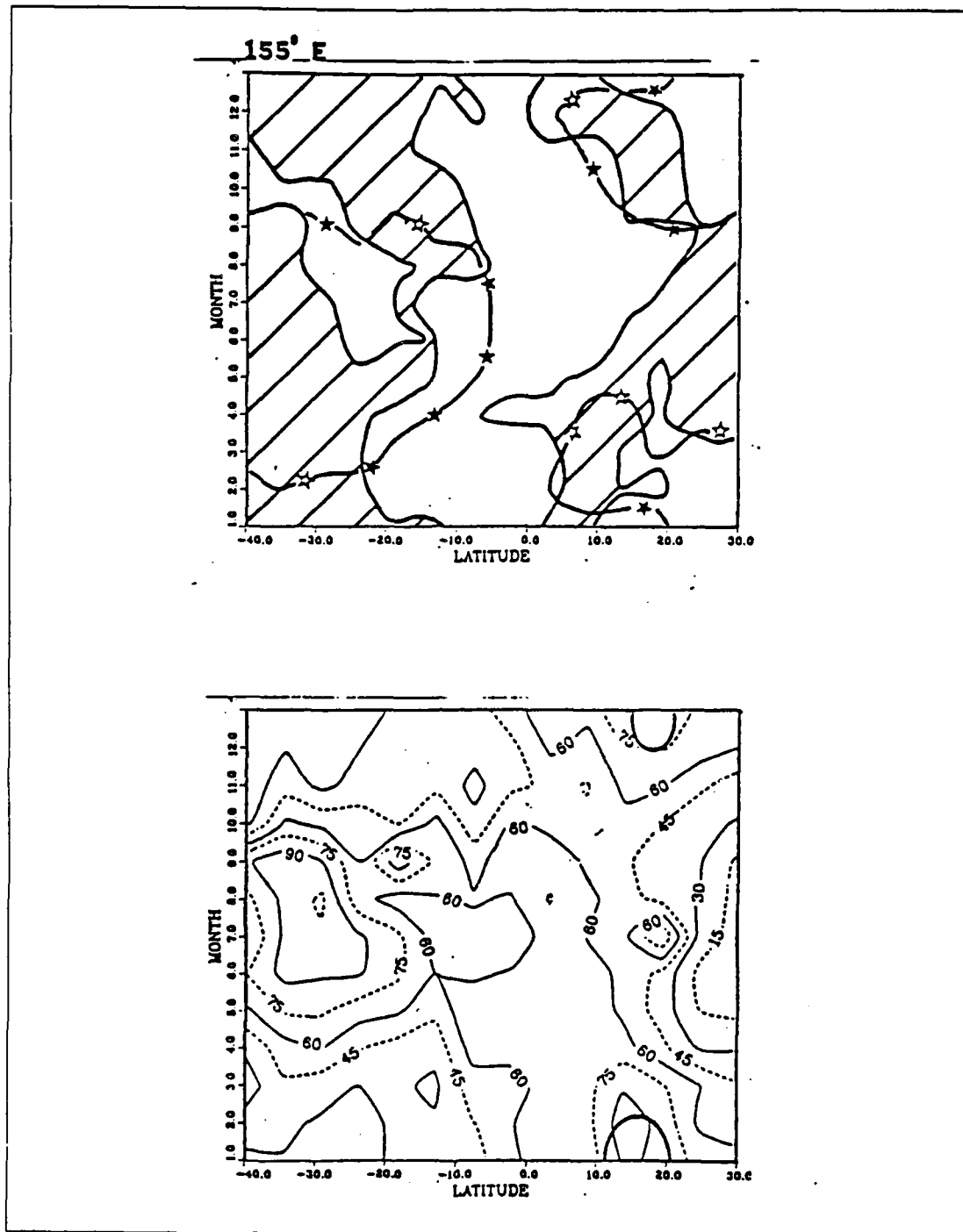


Fig. C.1 (a) Areas of Upwelling and Downwelling and Lines of Zero Surface Heat Flux (b) and Enhanced Deepening and Shallowing at 155°E.

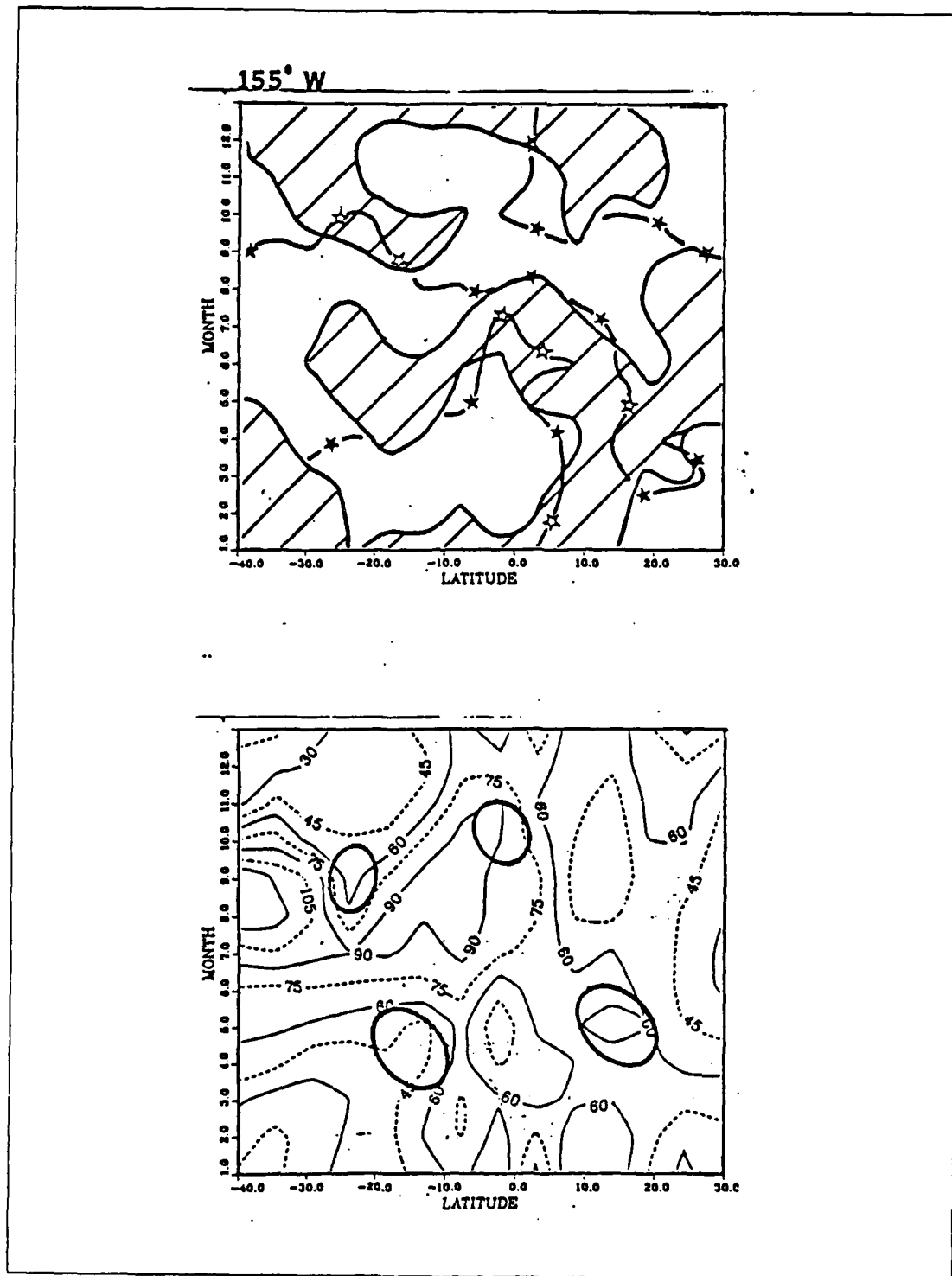


Fig. C.2 Same as Fig. C.1 but at 155° W..

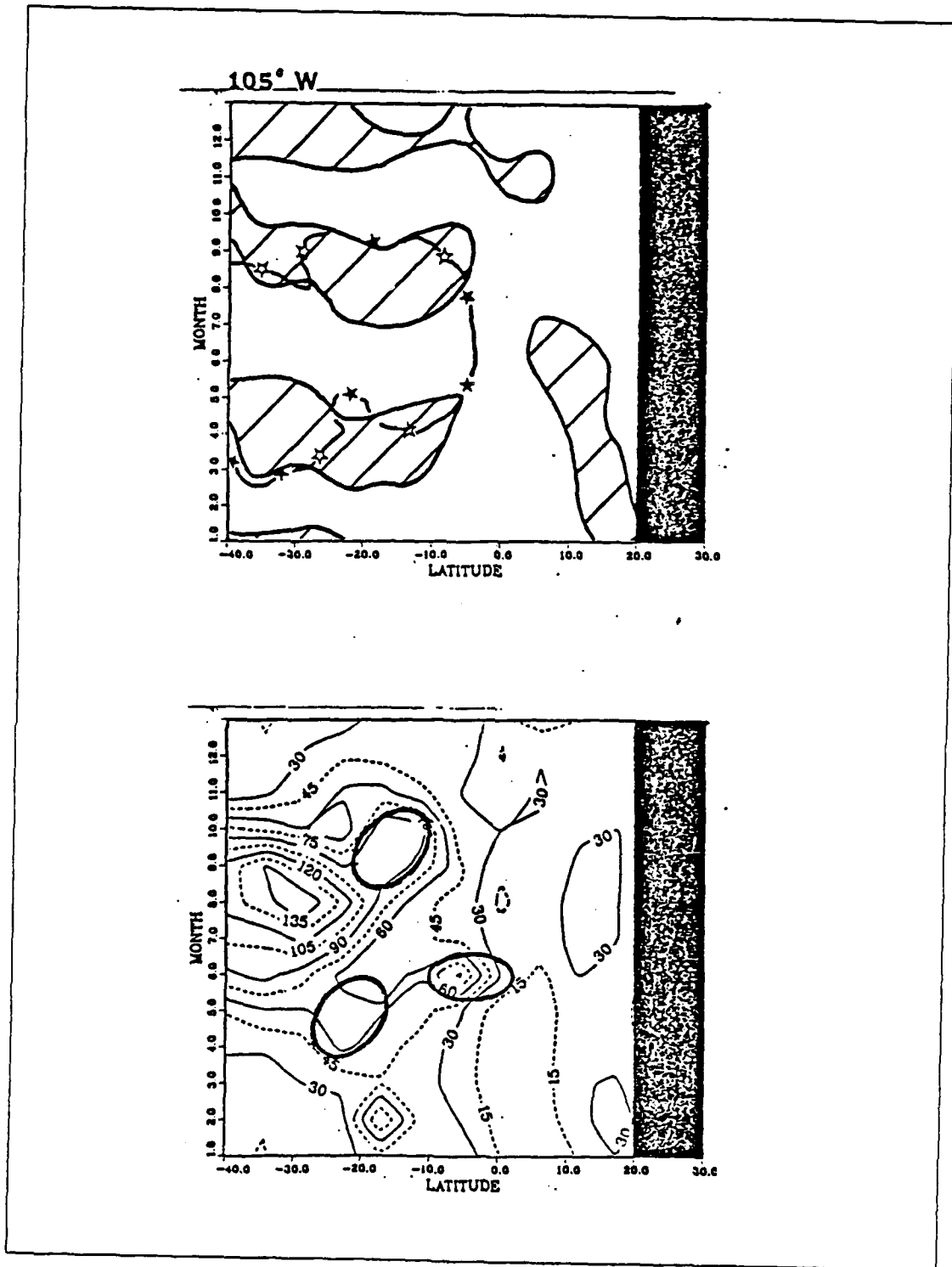


Fig. C.3 Same as Fig. C.1 but at 105°W..

APPENDIX D

MODIFIED MIXING SCALE

The one-dimensional model of Kraus and Turner is very heavily dependent upon the role of vertical advection, $W(z=-h)$, to prevent open ended mixing of the entire water column on an annual or greater time scale. In Garwood (1977), the full TKE budget was utilized to model the mixed layer with certain special considerations. Garwood proposed a bulk layer model in which the rate of entrainment was based on the total average turbulent kinetic energy in the mixed layer, and on the relative distribution of this energy among three kinetic energy component equations. In particular, the redistribution of TKE into the vertical direction is critical for the occurrence of mixing. In addition, the time scale for viscous dissipation of TKE depends on planetary rotation. The conclusion from Garwood (1977) was that these special considerations allow a cyclical steady state solution for seasonally varying heat fluxes since dissipation increases with mixed layer depth.

Both the pressure redistribution terms and the rotational stress terms in each of the component equations of the TKE budget vanish in summation. In Garwood (1977) the importance of the pressure redistribution terms in the transformation of horizontal TKE to vertical TKE was proposed as an important energy source for the process of entrainment. The rotational stress term, within which the Reynolds stresses interact with the northerly component of planetary rotation, is now believed to be an important redistribution term within the total TKE budget, as examined in Garwood, *et. al* (1985 a and b). The direction of turbulent kinetic energy exchange depends upon the sign of the east-west component of wind stress. Vertical mixing and MLD are reduced for a westerly wind regime, while easterly winds increase vertical mixing and MLD. When this theory is applied in the equatorial Pacific Ocean the westward deepening of the equatorial thermocline is effectively simulated.

Because of these results a new modified diagnostic equation for the equilibrium mixed layer depth is taken from Garwood (1985 a and b). The modified mixing scale $L(\Phi)$ in equation D.3 is computed by dividing the Obukhov length (L) by the additional factors in equation D.1. The northward component of planetary rotation is represented by Ω_y and the zonal wind stress represented by τ_x . The surface buoyancy flux B_o is computed in equation D.2.

$$\Phi = (\Omega_y \tau_x) / (\rho_o B_o) \quad (\text{eqn D.1})$$

$$B_o = \alpha g(Q_o / (\rho C_p)) \quad (\text{eqn D.2})$$

$$L(\Phi) = L / [1 + (12.7) \Phi] \quad (\text{eqn D.3})$$

The contoured fields of the modified mixing scale (Figs. D.1 and D.2) are noisier than the corresponding Obukhov length fields (presented in Chapter III). This is believed to be due to the zonal wind stress value used in computing the modifying factor. The zonal wind stress component was computed using a variable drag coefficient that was highly dependent upon the stability of the air just above the surface. Comparison of this zonal wind stress with one derived from hand calculation, using a constant drag coefficient showed the Weare zonal component to be too small and highly variable. This additional source of error and variance, given the high degree of the same in surface heat flux and wind speed, has produced inconclusive results in the fields of the modified mixing scale.

155 E
MODIFIED MIXING SCALE
(METERS)

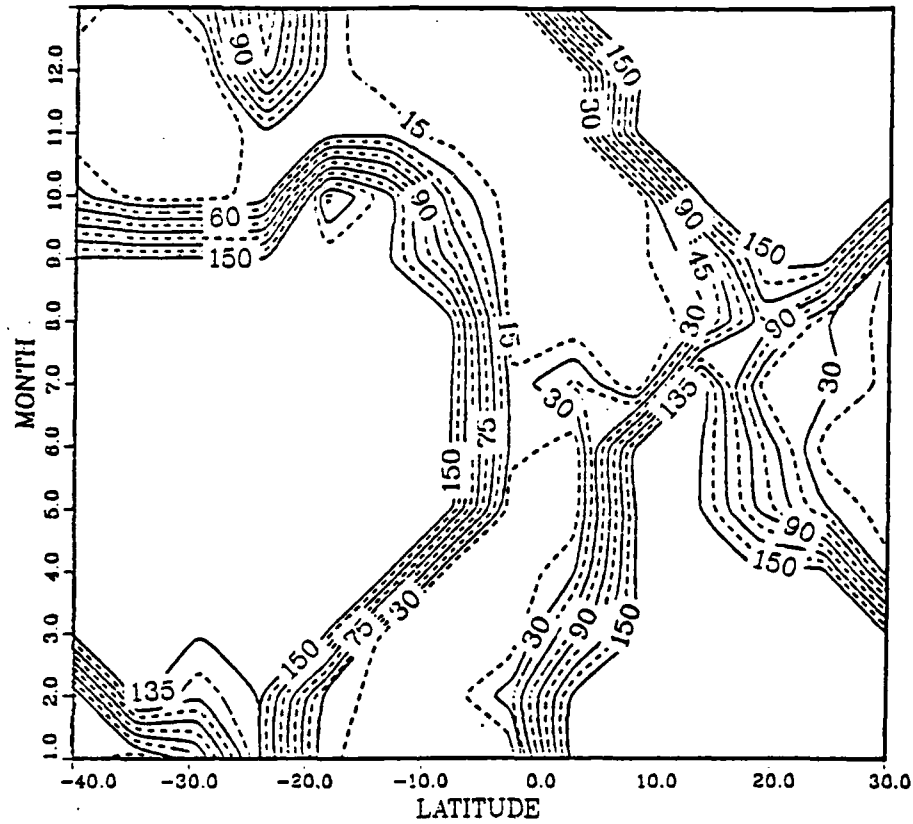


Fig. D.1 Modified Mixing Scale at 155 °E.

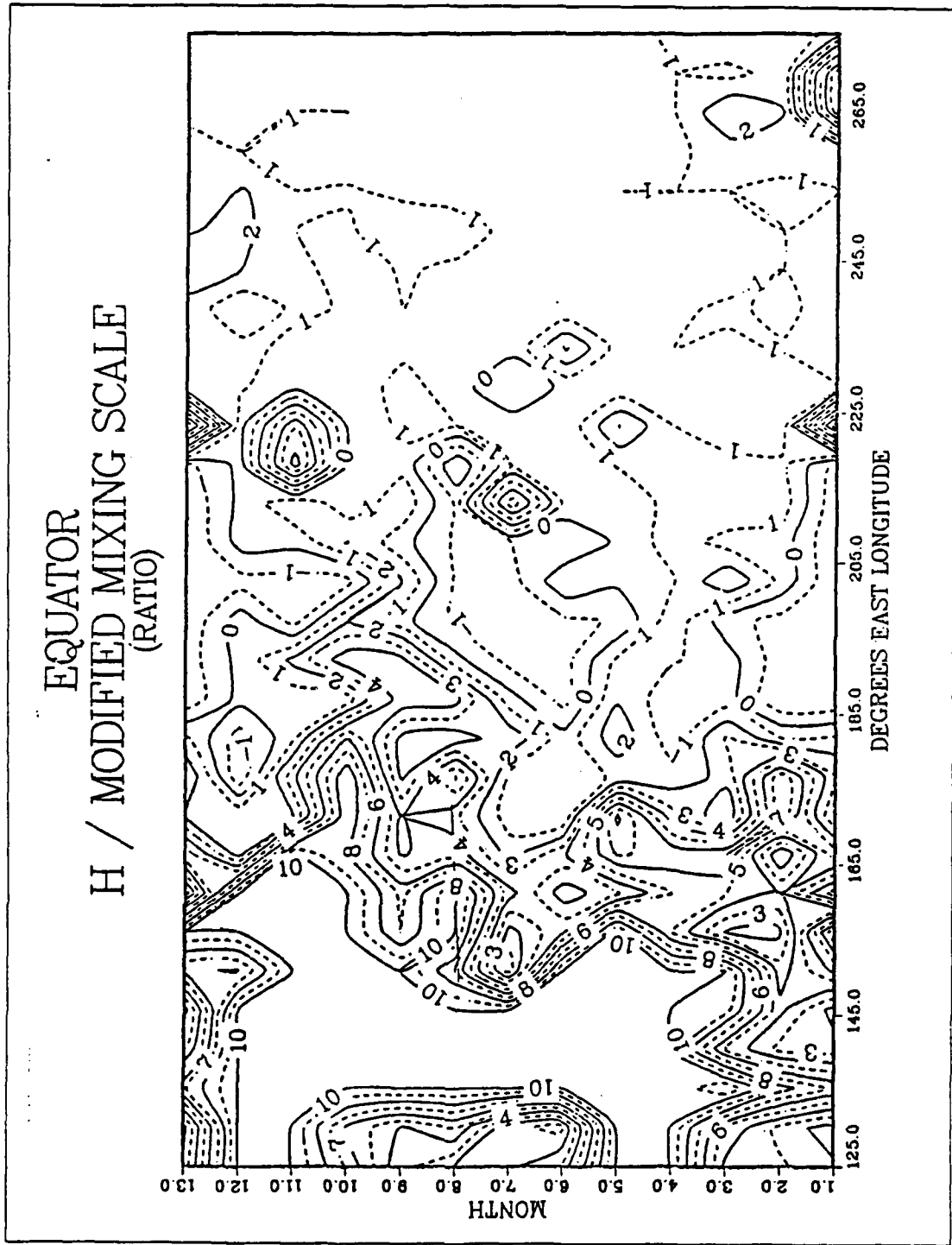


Fig. D.2 Ratio of Mixed Layer Depth and Modified Mixing Scale at the Equator.

LIST OF REFERENCES

- Bathan, K.H., 1972: On the Seasonal Changes in the Depth of the Mixed Layer in the North Pacific Ocean. *Journal of Geographical Research*, 77, No. 36, 7138-7149.
- Bialek, E.L., 1966: *Handbook of Oceanographic Tables (SP-68)*, U.S. Naval Oceanographic Office Special Publication, Naval Oceanographic Office, Washington D.C., 130 pp.
- Colburn, J.G., 1975: *The Thermal Structure of the Indian Ocean*. University of Hawaii Press, Honolulu, HI., 173 pp.
- Elsberry, R.L., and N.T. Camp, 1978: Oceanic Thermal Response to Strong Atmospheric Forcing. 1, Characteristics of forcing events. *Journal of Physical Oceanography*, 8, 206-214.
- Garwood, R.W., Jr., 1977: An Oceanic Mixed Layer Model Capable of Simulating Cyclic States. *Journal of Physical Oceanography*, 7, 455-468.
- Garwood, R.W., Jr., P.C. Gallacher and P. Muller, 1985: Wind Direction and Equilibrium Mixed Layer Depth: General Theory. *Journal of Physical Oceanography*, 15, 1332-1338.
- Garwood, R.W., Jr., P. Muller and P.C. Gallacher, 1985: Wind Direction and Equilibrium Mixed Layer Depth in the Tropical Pacific. *Journal of Physical Oceanography*, 15, 1332-1338.
- Gill, A.E., 1982: *Atmospheric Ocean Dynamics*. Academic Press, Inc., London, England, 662 pp.
- Kraus, E.B., and J.S. Turner, 1967: A One-dimensional Model of the Seasonal Thermocline II. The General Theory and Its Consequences. *Tellus*, XIX, 1, 98-105.
- Levitus, S., 1982: *Climatological Atlas of the World*. NOAA Professional Paper Number 13, U.S. Government Printing Office, 173 pp.
- Muller, P., R.W. Garwood and J.P. Garner, 1984: Effect of Vertical Advection on the Dynamics of the Oceanic Surface Mixed Layer. *Annales Geographicae*, 2, 387-398.

- Pickard, G.L. and W.J. Emery, 1982: *Descriptive Physical Oceanography: An Introduction*. Pergamon Press, 249 pp.
- Robinson, M.K., 1976: *Atlas of North Pacific Ocean Monthly Mean Temperatures and Mean Salinities of the Surface Layer*. U.S. Naval Oceanographic Office Reference Publication 2, Naval Oceanographic Office, Washington D.C., 173 pp.
- Weare, B.C., P.T. Strub and M.D. Samuel, 1980: *Marine Climate Atlas of the Tropical Pacific Ocean*. University of California Press, Davis, California, 147 pp.
- Weare, B.C., P.T. Strub and M.D. Samuel, 1981: Annual Mean Surface Heat Fluxes in the Tropical Pacific Ocean. *Journal of Physical Oceanography*, 11, 705-717.
- Wyrski, K., 1971: *Oceanographic Atlas of the International Indian Ocean Expedition*. National Science Foundation, NSF-IOE-1, Washington, D.C., 74 pp.
- Wyrski, K., 1981: An Estimate of Equatorial Upwelling in the Pacific. *Journal of Physical Oceanography*, 11, 1205-1214.
- Wyrski, K., and G. Meyers, 1976: The Trade Wind Field Over the Pacific Ocean. *Journal of Applied Meteorology*, 15, 698-704.

INITIAL DISTRIBUTION LIST

	No. Copies
1. Defense Technical Information Center Cameron Station Alexandria, VA 22304-6145	2
2. Library, Code 0142 Naval Postgraduate School Monterey, CA 93943-5100	2
3. R. W. Garwood, Jr. (Code 68Gd) Department of Oceanography Naval Postgraduate School Monterey, CA 93943-5100	1
4. M. L. Batteen (Code 68Bv) Department of Oceanography Naval Postgraduate School Monterey, CA 93943-5100	1
5. Chairman (Code 68Co) Department of Oceanography Naval Postgraduate School Monterey, CA 93943-5100	1
6. LT. Harry J. Ries, Jr., USN 314 Main Street Hulmeville, PA 19047	2
7. Prof. Peter Muller Department of Oceanography University of Hawaii Honolulu, HI	1
8. Department of Oceanography Dalhousie University Halifax, N.S., Canada B3H 4J1	1
9. Prof. Roger Lukas Department of Oceanography University of Hawaii Honolulu, HI	1

- | | | |
|-----|---|---|
| 10. | Director Naval Oceanography Division
Naval Observatory
34th and Massachusetts Avenue NW
Washington, DC 20390 | 1 |
| 11. | Commander
Naval Oceanography Command
NSTL Station
Bay St. Louis, MS 39522 | 1 |
| 12. | Commanding Officer
Naval Oceanographic Office
NSTL Station
Bay St. Louis, MS 39522 | 1 |
| 13. | Commanding Officer
Fleet Numerical Oceanography Center
Monterey, CA 93940 | 1 |
| 14. | Commanding Officer
Naval Ocean Research and Development
Activity
NSTL Station
Bay St. Louis, MS 39522 | 1 |
| 15. | Commanding Officer
Naval Environmental Prediction
Research Facility
Monterey, CA 92940 | 1 |
| 16. | Chairman, Oceanography Department
U. S. Naval Academy
Annapolis, MD 21402 | 1 |
| 17. | Office of Naval Research (Code 420)
Attn: Dr. T. Curtin
Dr. D. Evans
800 N. Quincy Street
Arlington, VA 22217 | 2 |
| 18. | Scientific Liaison Office
Office of Naval Research
Scripps Institution of Oceanography
La Jolla, CA 92037 | 1 |
| 19. | Library
Scripps Institution of Oceanography
P.O. Box 2367
La Jolla, CA 92037 | 1 |

20. Library 1
Department of Oceanography
University of Washington
Seattle, WA 98105
21. Library 1
CICESE
P.O. Box 4803
San Ysidro, CA 92073
22. Library 1
School of Oceanography
Oregon State University
Corvallis, OR 97331
23. Commander 1
Oceanographic Systems Pacific
Box 1390
Pearl Harbor, HI 96860
24. Chief, Ocean Services Division 1
National Oceanic and Atmospheric
Administration
8060 Thirteenth Street
Silver Spring, MD 20910
25. Department of Oceanography 1
University of British Columbia
Vancouver, B.C. Canada
V6T 1W5
26. Library 1
Bedford Institute of Oceanography
P.O. Box 1006
Dartmouth, N.S., Canada
B2Y 4A2